

Synthetic and Mechanistic Studies with  
Biologically Active Macrocyclic Peptides

Thomas M. Wood

Thomas Melvin Wood

PhD Thesis

Utrecht University

The work described in this thesis was financially supported by the NWO  
Future Medicines Grant.

Cover Design: Thomas Melvin Wood & Liubov Yakovlieva

**Printed by: Ridderprint**

**Synthetic and Mechanistic Studies with Biologically Active  
Macrocyclic Peptides**

**Synthetische en Mechanistische Studies met Biologisch  
Actieve Macrocyclische Peptiden**

(met en samenvatting in het Nederlands)

**Proefschrift**

ter verkrijging van de graad van doctor aan de Universiteit Utrecht op  
gezag van de rector magnificus, Prof. Dr. H.R.B.M. Kummeling, ingevolge  
het besluit van het college voor promoties in het openbaar te verdedigen op  
woensdag 22 december 2021 des middags te 4.15 uur

door

**Thomas Melvin Wood**

Geboren op 12 november 1992 te Ogden, Utah, Verenigde Staten van  
Amerika

**Promotoren:**

Prof. Dr. N.I. Martin

Prof. Dr. R.J. Pieters

Dit proefschrift werd (mede) mogelijk gemaakt met financiële steun van  
NWO: Future Medicines.

“A journey will have pain and failure.  
It is not only the steps forward that we much accept.  
It is the stumbles.  
The trials.  
The knowledge that we will fail.  
But if we stop, if we accept the person we are when we  
fall, the journey ends.  
That failure becomes our destination.  
To love the journey is to accept no such end.  
I have found, through painful experience, that the most  
important step a person can take is always the next one.”

- Brandon Sanderson, “Oathbringer”



## Table of contents

<b>Chapter 1</b> .....	1
Introduction to cyclic lipopeptide antibiotics	
<b>Chapter 2</b> .....	27
Structure-activity studies and high-resolution crystal structures of laspartomycin analogues	
<b>Chapter 3</b> .....	51
Contribution of achiral residues in laspartomycin	
<b>Chapter 4</b> .....	63
Chemoenzymatic preparation of macrocyclic peptides with activity against Gram-negative pathogens	
<b>Chapter 5</b> .....	85
Design of $\beta$ -hairpin peptides to study substrate recognition of EarP rhamnosyltransferase	
<b>Chapter 6</b> .....	113
Summary and outlook	
Nederlandse samenvatting.....	117
Popular summaries.....	121
List of Publications.....	123
<i>Curriculum vitae</i> .....	125
Acknowledgments.....	126





# Chapter 1

## Introduction to cyclic lipopeptide antibiotics

*To push back the growing tide of antibacterial resistance the discovery and development of new antibiotics is a must. In recent years the calcium dependent lipopeptide antibiotics (CDAs) have emerged as a potential source of new antibacterial agents rich in structural and mechanistic diversity. All CDAs share a common lipidated cyclic peptide motif containing amino acid side chains that specifically chelate calcium. It is only in the calcium bound state that the CDAs achieve their potent antibacterial activities. Interestingly, despite their common structural features, the mechanisms by which different CDAs target bacteria can vary dramatically. This review provides both a historic context for the CDAs while also addressing the state of the art with regards to their discovery, optimization, and antibacterial mechanisms.*

Published in: Wood, T.M.; Martin, N.I. *Med. Chem. Commun.* **2019**, 10, 643-646

## 1.1 Introduction

The rapid emergence and onset of drug-resistant bacteria is now considered one of the most urgent global threats to human health.<sup>1</sup> In 2017 the Centers for Disease Control and prevention (CDC) revealed that more than 2 million people acquire an antibiotic-resistant infection per year which leads to at least 23,000 deaths in the US alone.<sup>2</sup> The pernicious increase in the incidence of multi-drug resistant (MDR) Gram-negative bacteria that are resistant to carbapenems<sup>3,4</sup> and colistin<sup>5,6</sup> in Enterobacteriaceae is considered a top priority by the CDC. The same holds true for infections caused by Gram-positive pathogens as exemplified by the infamous hospital bacteria methicillin-resistant *Staphylococcus aureus* (MRSA)<sup>7,8</sup> and vancomycin-resistant enterococci (VRE).<sup>9</sup> These developments have seen a steady decline in the availability of clinically approved antibiotics that are effective at combating MDR pathogens, leading some to speculate that the antibiotic era is coming to an end.<sup>10,11</sup> During the so-called golden age of antibiotic discovery (1940s-1960s) a myriad of powerful and structurally unique antibiotics were discovered and brought to the clinic, including: sulfonamides,  $\beta$ -lactams, aminoglycosides, glycopeptides, macrolides, tetracyclines, chloramphenicol, lincosamides, quinolones and streptogramins.<sup>12</sup> However, the decades that followed (1970s-2000s) are now known as the “discovery void” with only two new classes of antibiotics being discovered in this period as the pipeline of readily available antibiotics from nature dried up.<sup>13</sup> Notably, the calcium-dependent lipopeptide antibiotic daptomycin is one of a rare number of first in class antibiotics to have entered the market since the year 2000.<sup>14,15</sup>

In this chapter a comprehensive summary of the calcium-dependent lipopeptide class of antibiotics (CDAs), with a primary focus on their structural features, antibacterial mechanisms and clinical potential is described. As the only currently clinically approved CDA, daptomycin (Fig. 1) is a special and representative case. First discovered by researchers at Eli Lilly in 1983, daptomycin was later shepherded through clinical development by Cubist pharmaceuticals, gaining approval as cubicin in 2003 for the treatment of skin infections caused by Gram-positive bacteria and later in 2006 for bloodstream (bacteraemia) infections caused by MRSA.<sup>15,16</sup> Industrially, daptomycin is produced by the fermentation of *Streptomyces roseosporus* supplemented with decanoic acid to favour

production of the compound containing the desired C10-fatty acid.<sup>16,17</sup> In the years 2006-2014 annual sales of daptomycin reached 1 billion dollars making it a rare example of a blockbuster antibiotic drug. Based on these strong sales figures, Merck acquired Cubist in 2014 for a sum of 9.5 billion USD. As of 2016 daptomycin is off patent and various generic versions are now available.<sup>18</sup>

While daptomycin is the most renowned CDA, there are several other cyclic lipo(depsi)peptides of the same family that display potent antibacterial activity. These include a number of depsipeptides produced by *Streptomyces coelicolor* A(3)<sup>218</sup> and A 54145 produced by *Streptomyces fradiaei*.<sup>19</sup> Other CDAs include the amphomycin,<sup>20</sup> friulimicin,<sup>21</sup> and laspartomycin/glycinocin<sup>22,23</sup> classes which are also produced by various other streptomycetes.<sup>24</sup> As illustrated by the structure of daptomycin (Fig. 1) nearly all CDAs share the same positioning of constituent D-amino or achiral amino acids in addition to a highly conserved Asp-X-Asp-Gly motif.<sup>25</sup> This Asp-X-Asp-Gly sequence is imperative for calcium binding, which is needed for achieving full antibacterial activity as in the absence of calcium, the activity of the CDAs is significantly reduced.<sup>25</sup>

The structure of all CDAs consists of two main components: a cyclic peptide macrocycle and a long-chain fatty acid tail which is linked to the peptide core. In nature CDAs are produced by nonribosomal peptide synthetases (NRPSs). Several excellent previous reviews provide in-depth information regarding the biosynthetic pathways and the specific enzymes involved in CDA production.<sup>24,25</sup>

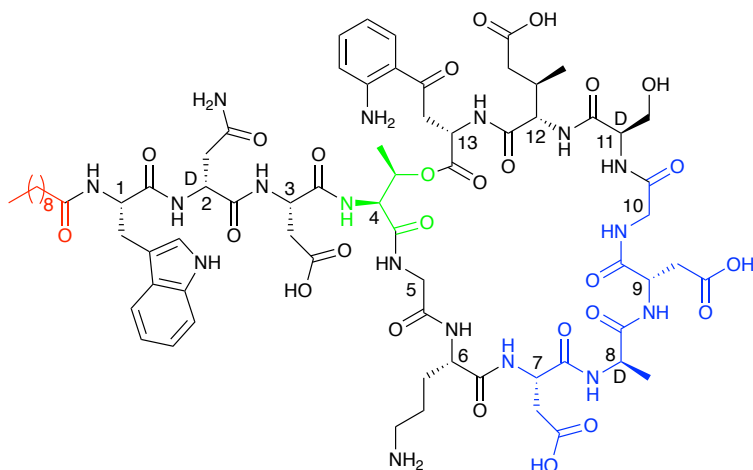


**Figure 1.** Structure of daptomycin indicating N-terminal lipid in red and in blue the calcium binding motifs. The peptide macrocycles are formed biosynthetically *via* cyclization of the C-terminal residue with the side chain of Thr4 (linkages shown in green).

## 1.2 Clinically used CDAs and compounds in advanced development

Daptomycin is the only clinically approved CDA and is primarily prescribed for the treatment of serious Gram-positive infections. The dosing of daptomycin is based on individual body weight and shows a concentration-dependent mode of action.<sup>15</sup> Produced industrially by fermentation of the actinomycete *Streptomyces roseosporus*, daptomycin is formed as member of the so-called A21978C complex of structurally related CDAs (Fig. 2). All members of the A21978C complex consist of the same 13 amino acid peptide and are exemplified by their ten-membered ring which is achieved by macro-lactonization between Thr4 and Kyn13.<sup>16</sup> Other unique D- and non-proteinogenic amino acids present include: D-Asn2, D-Ala4, ornithine (Orn6), D-Ser11 and 3-methylglutamic acid (MeGlu12).<sup>25</sup> The CDAs of the A21978C complex differ only in their aliphatic lipid tails and Figure 2 illustrates this structural variation. Interestingly, daptomycin was initially identified as a minor component of the A21978C complex but demonstrated superior biological activity when compared with the other

members of the complex.<sup>26</sup> This led to an optimization of the production process whereby addition of exogenous decanoic acid to fermentation of *S. roseosporus* results in an increased production of daptomycin.<sup>27</sup>

Despite its clinical importance, the exact working mechanism by which daptomycin kills bacteria has not yet been fully elucidated. Over the past decade numerous studies and experiments have tried to pinpoint its mechanism of action resulting in various models, including blockage of essential cell wall precursors, membrane pore formation and oligomerization in membranes.<sup>28-30</sup> After more than a decade of use in the clinic, reports are now emerging of daptomycin resistance in strains of both *E. faecium*<sup>31</sup> and MRSA.<sup>32</sup> Resistance to daptomycin stems from mutation in several bacterial genes. These genes generally activate the pathogen's defences to cell wall damage and stress as the bacterial cell attempts to prevent daptomycin from reaching the cytoplasmic membrane. Mutations in such genes can in turn result in increased MIC.<sup>33</sup> Notably, clinical isolates from patients failing to respond to daptomycin therapy have shown frequent accumulation of *mprF* point mutations in *S. aureus*.<sup>34</sup>

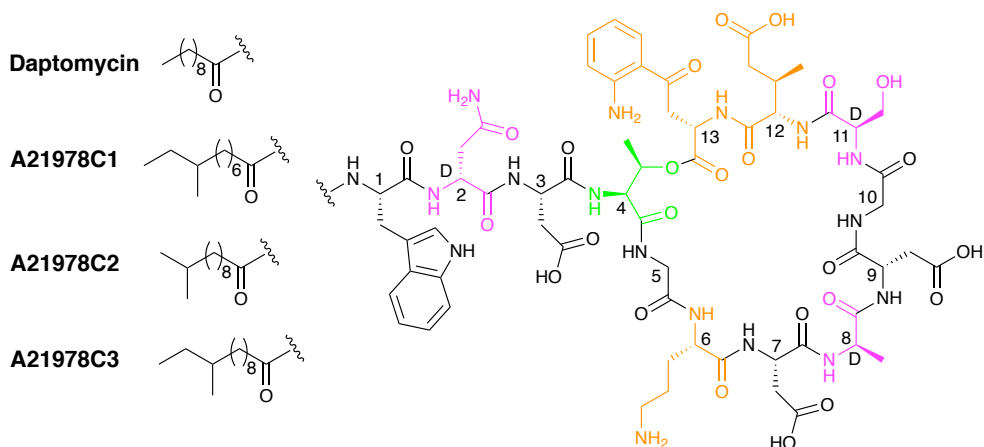
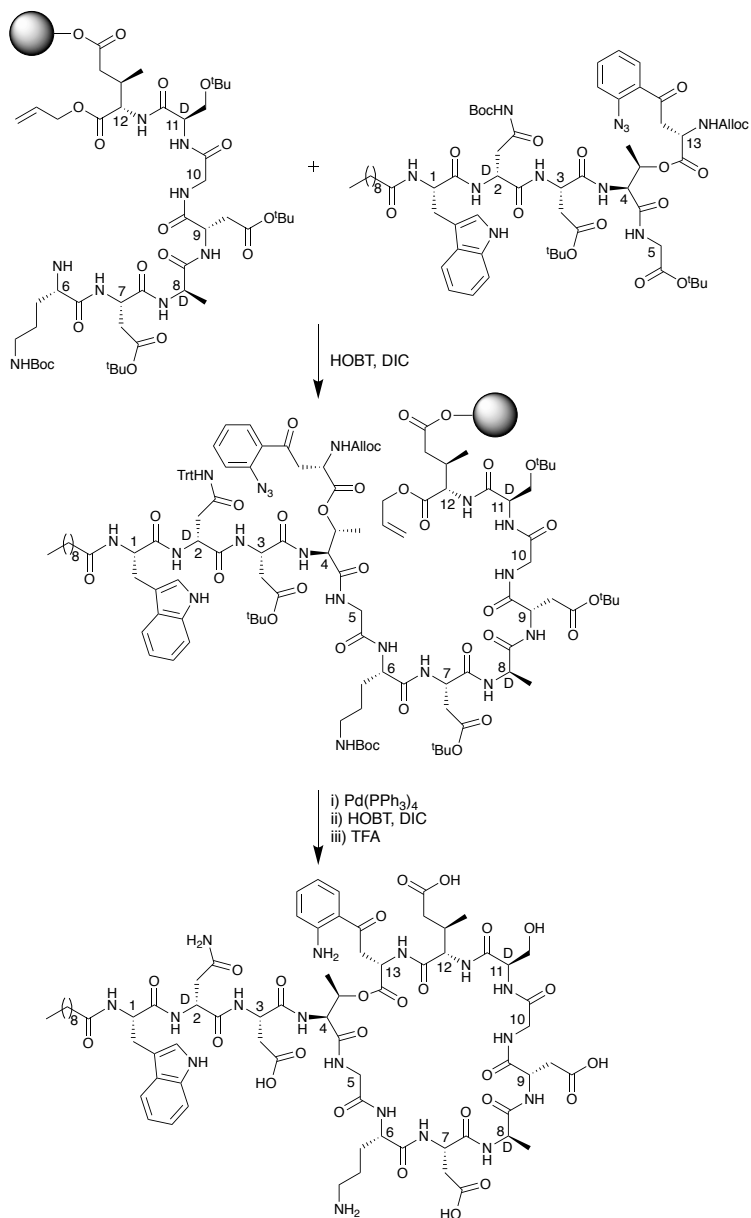
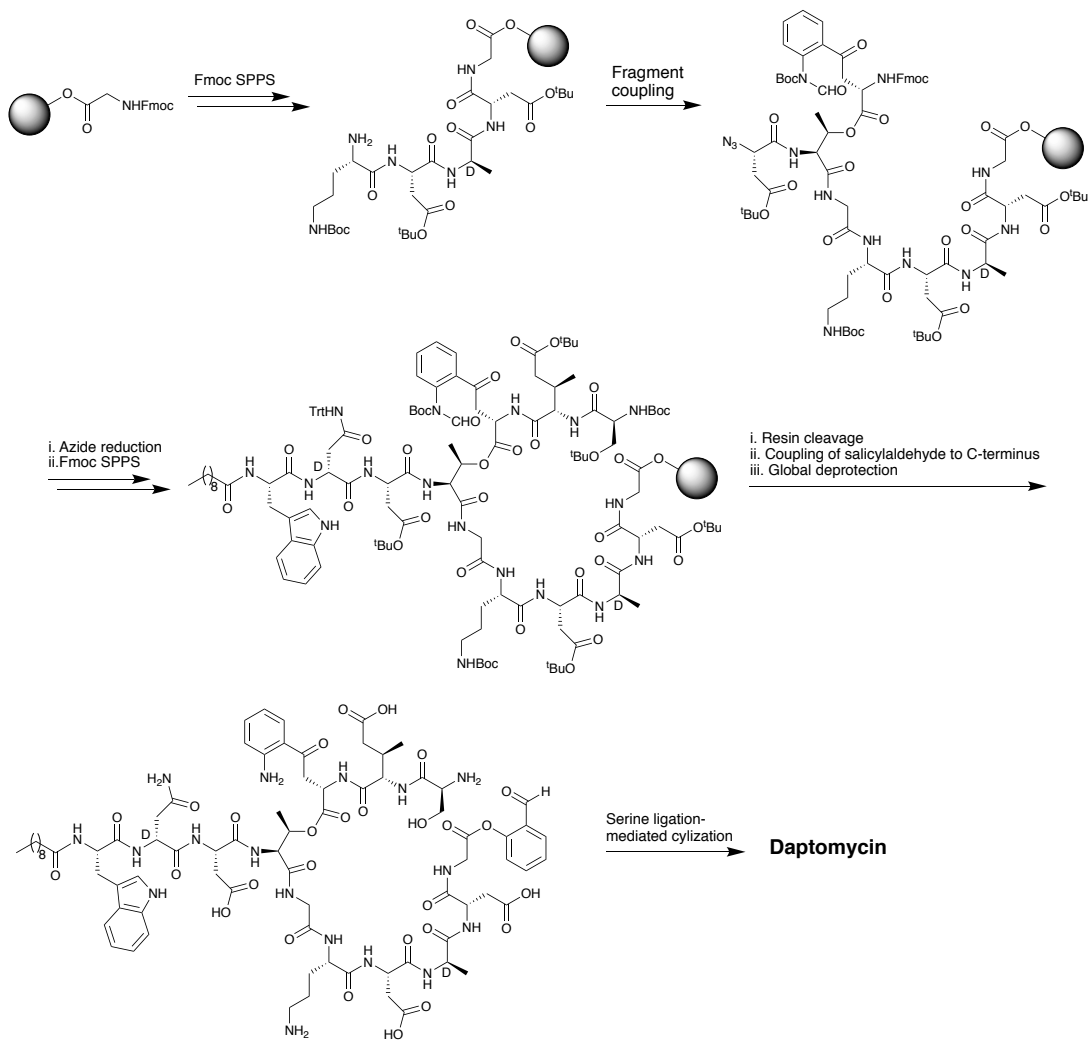


**Figure 2.** Structures of the A21978C family; the macro-lactonization site is shaded in green, D-amino acids in purple and non-proteinogenic amino acids in orange.

The first total chemical synthesis of daptomycin was achieved by researchers at Cubist Pharmaceuticals in 2006 and appears only in the patent literature.<sup>35</sup> The cubist team employed a convergent approach (Scheme 1) wherein one peptide fragment containing the synthetically challenging ester linkage between Thr4 and Kyn13 was coupled to a second resin bound peptide fragment attached to a solid support *via* the side chain of MeGlu12. Prudent use of alloc and allyl ester protecting groups and temporary azide masking of the aniline nitrogen of the kynurine unit in the coupled fragment enabled the subsequent simultaneous deprotection/reduction of the resin bound intermediate using palladium catalysis. Following on-resin cyclization and cleavage/deprotection daptomycin was isolated in moderate yield. A second total synthesis of daptomycin was reported by the group of Li in 2013 who employed a similar convergent route combining solid- and solution-phase approaches with a chemoselective serine ligation providing the key cyclization step of the macrocycle (Scheme 2).<sup>36,37</sup> Also notable in the Li synthesis was the practical introduction of an appropriately protected kynurine by ozonolysis of the corresponding N-Boc-protected Trp.



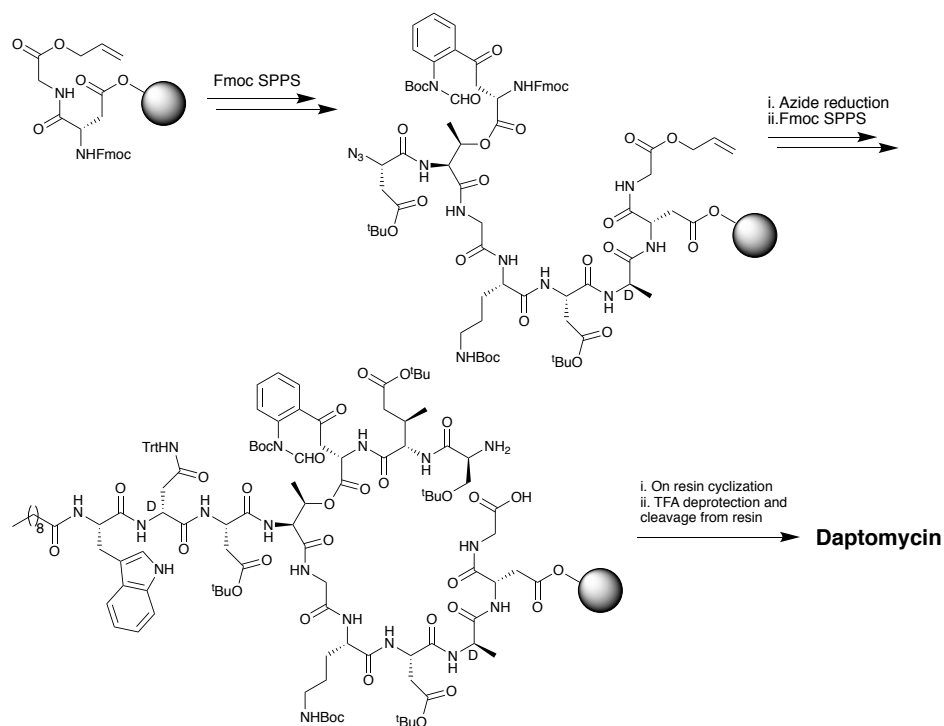
**Scheme 1.** SPPS approach used by Cubist team to achieve the first total synthesis of daptomycin.



**Scheme 2.** Serine ligation route used by Li and coworkers in synthesizing daptomycin.



Judicious use of azide chemistry also provided the requisite orthogonality for elaboration of the resin bound peptide. More recently, Taylor and coworkers described an elegant approach to synthesizing daptomycin entirely on solid support enabling the rapid synthesis of other daptomycin analogues (Scheme 3).<sup>38,39</sup> To enable the total SPPS approach Taylor's group employed an elegant protecting group strategy, including a number of azide masked amino acid building blocks, as well as optimized Fmoc deprotection conditions to protect the sensitive ester linkage.



**Scheme 3.** Entirely SPPS approach used by the Taylor group in the synthesis of daptomycin.

Semisynthetic approaches have also been used to produce daptomycin analogues with improved MIC profiles compared to that of the parent compound.<sup>40</sup> Structure-activity relationship studies on the fatty acid tail revealed several critical factors for antimicrobial activity: lipophilicity,

chain length and the location of key aromatic functionalities.<sup>40,41</sup> The acyl tail is crucial for binding to the bacterial cell membrane and calcium-dependent insertion.<sup>42</sup> One such semisynthetic analogue thus developed is surotomycin (Fig. 3) which differs from daptomycin only in the structure of its lipid tail. In surotomycin the lipid tail contains a conjugated substituted alkene and an aromatic moiety that was found to give enhanced activity against *C. difficile*. To date, two registered Phase III clinical studies have been completed with surotomycin.<sup>43,44</sup> Both were randomized, double blind, multi-center, global studies in adult patients with *C. difficile*-associated diarrhoea. In these studies, the efficacy of surotomycin was compared to that of vancomycin for 10-day treatment regimens. At their conclusion these trials revealed that while surotomycin was generally well tolerated, it did not meet the primary efficacy endpoint of noninferiority compared to that of vancomycin. It also failed to meet the secondary endpoints, *i.e.* superiority over vancomycin and sustained clinical response at the end of the trial.

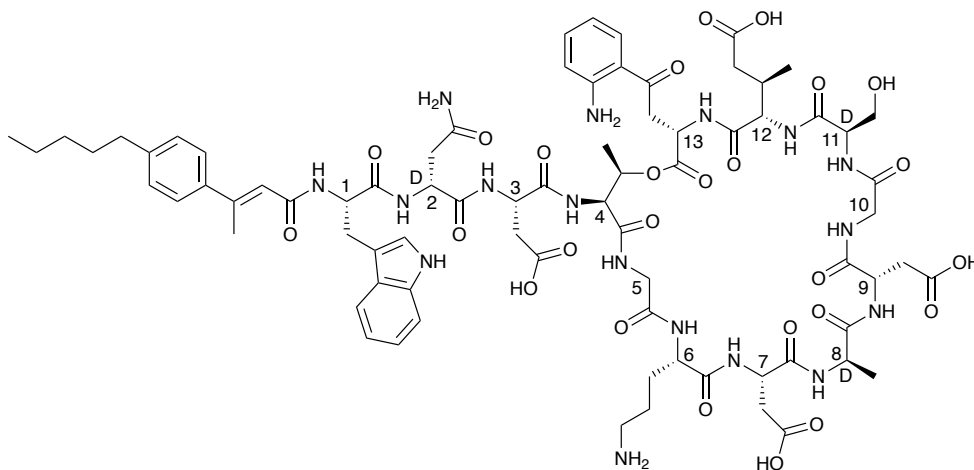


**Figure 3.** Structure of surotomycin. This semisynthetic analogue of daptomycin bears an unnatural lipid tail imparting potent activity against *C. difficile*.

The lipodepsipeptides daptomycin and surotomycin are not the only CDAs to have been taken to clinical trials. Two others, amphomycin and friulimycin (Fig. 4), both belonging to a structurally distinct lipopeptide sub class of CDAs, have been evaluated as human therapeutics. Discovered

in the 1950s, amphomycin was the first CDA reported in the literature.<sup>20</sup> In the years following, a myriad of similar or identical compounds have been reported under different names, which has led to significant confusion in the nomenclature associated with the class.<sup>24,25,45,46</sup> The reader is referred to a comprehensive 2005 review by Baltz and coworkers that serves to clarify much of the ambiguity associated with this group of CDAs.<sup>21,24</sup> Typically these lipopeptides are subdivided into three subclasses, the amphomycins, the friulimicins and the laspartomycins. As indicated in Figure 4, there is a logical convention used in the naming of the various friulimicins as A, B, C, or D depending on the lipid tail. We respectively propose to apply the same convention in the nomenclature used for describing the structurally similar amphomycin class of CDA (see Figure 4 for proposed nomenclature). The amphomycins and the friulimicins are identical apart from the exocyclic Asp residue found in the amphomycin class, which in the friulimicins is instead an Asn. Variation in the lipid chains is responsible for additional diversity.

The amphomycins and friulimicins both share the same macrocyclic peptide consisting of 10 amino acids with cyclization between the diamminobutyrate (Dab) at position 2 and Pro11. Several D- and nonproteinogenic amino acids, such as *L*-threo and *D*-allo-2,3-Dab, D-pipicolic acid (D-Pip) as well as *L*-threo-3-methyl-aspartate (MeAsp), are found at positions 2, 9, 3 and 4 in the peptide core respectively. Four main fatty acid tails are found throughout these compounds, consisting of either 13, 14 or 15 carbon atoms in total. The lipids commonly bear iso or anteiso branching groups at their terminal ends and all contain an unsaturated double bond between carbon three and four.

As is common to nearly all the CDAs, the amphomycin, friulimicin and laspartomycin lipopeptides contain the same Asp-X-Asp-Gly calcium binding motif as daptomycin. Despite this structural similarity, several investigations have revealed that the amphomycins, friulimicins, and laspartomycins operate *via* a mechanism different than that of daptomycin. Early studies with amphomycin indicated that it interferes with the first membrane associated step of bacterial cell wall biosynthesis by disrupting the transfer of the soluble UDP cell wall precursor to the phospholipid membrane anchor undecaprenyl phosphate (C<sub>55</sub>-P).<sup>47</sup> More recent studies

have revealed that members of this class of CDA form tight complexes with C<sub>55</sub>-P as a major driver of their antibacterial mechanisms.<sup>48,49</sup>

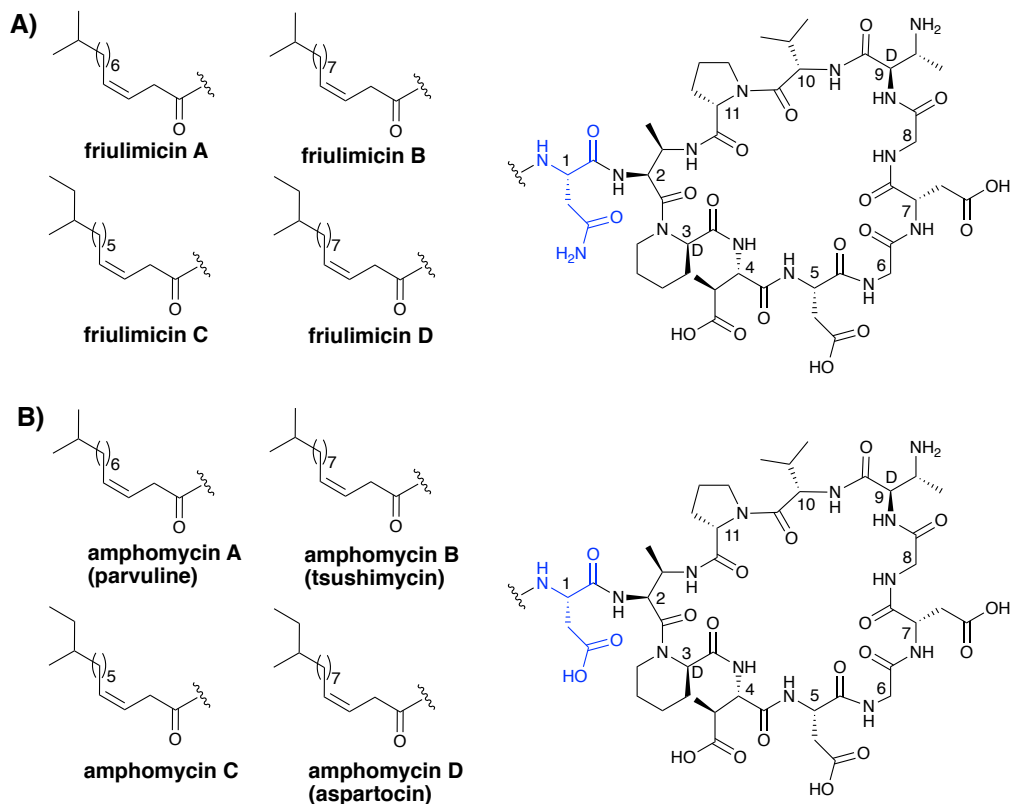


**Figure 4.** Structures of the (A) friulimicin and (B) amphomycin families of CDA. Indicated in brackets are the carious other names that have historically been assigned to these structures.

As stated above, both amphomycin and friulimicin have been investigated as possible leads for antibiotic drug development. To this end a semisynthetic analogue of amphomycin, MX-2401 (Fig. 5), was recently brought to clinical trials by BioWest Therapeutics Inc. for the treatment of serious Gram-positive infections.<sup>50,51</sup> Compared to amphomycin, MX-2401 is rapidly bactericidal and was shown to be effective in several infections models with potent activity against VRSA, VRE and MRSA.<sup>48,49</sup> Recent

NMR studies demonstrated that *S. aureus* cells treated with MX-2401 exhibit a thinning of the cell wall, a decrease in D-alanine linked teichoic acids, and a reduction in peptidoglycan cross-linking.<sup>52</sup> Although MX-2401 reached late stage preclinical development it has never been tested in human patients in a clinical setting. By comparison, in 2007 MerLion Pharmaceuticals initiated Phase I clinical trial studies with friulimicin B. However, the trial was terminated soon thereafter due to unfavourable pharmacokinetics.

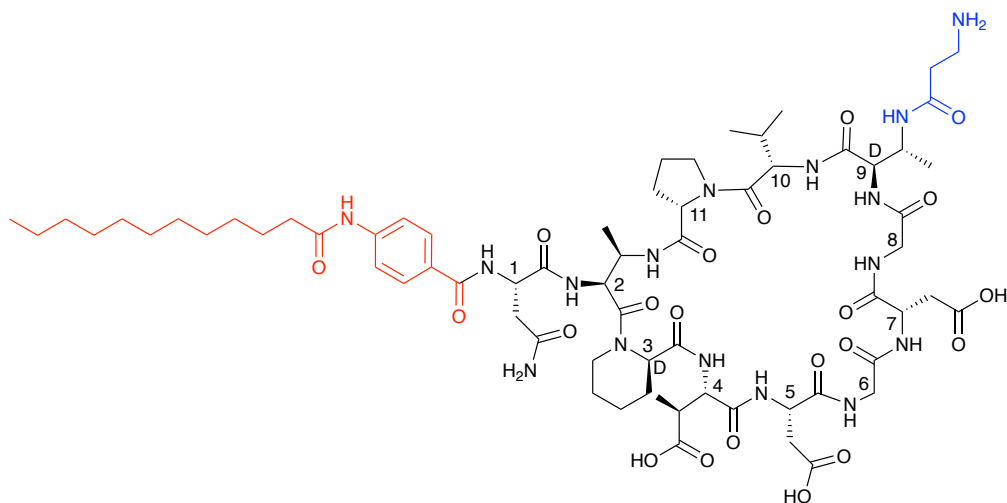


**Figure 5.** Structure of the semisynthetic amphomycin analogue MX-2401. Highlighted in red is the 4-(dodecanamido) benzoic acid lipid tail and in blue the modified Dab9.

### 1.3 The A54145 and CDA classes

A54145 is a lipodepsipeptide like daptomycin and the A21978 family but is much more structurally complex (Fig. 6). The A54145 group is produced by *Streptomyces fradiae* and shows antibacterial activity against various strains of *Staphylococcus aureus*, *Staphylococcus epidermidis*, *Clostridium*, *Streptococcus*, and *Enterococci*.<sup>19,53</sup> The lipid tails of the A54145 family are fully saturated and often terminate with iso or anteiso branching patterns.<sup>19</sup>

The structural complexity of the A54145 group is found in their peptide sequences. Seven of the thirteen component amino acids are nonproteinogenic including three D-amino acids. Six of the seven unique amino acids (D-Glu2, 3-hydroxy-L-asparagine (hAsn3), sarcosine (Sar5), D-Lys8, 3-methoxyAsp (MeO-Asp9) and D-Asn11) are found in all members of the A54145 family. In addition, a MeGlu residue is found at position 12 in four of the known A54145 peptides and position 13 is either an Ile or a Val giving rise to additional structural variation.<sup>53,54</sup> A54145 is homologous to daptomycin and permeabilizes the cell membrane of Gram-positive bacteria in a similar fashion. As for daptomycin, membrane permeabilization depends on the presence of calcium and phosphatidylglycerol and leads to the formation of oligomeric membrane pores that consist of six-eight individual subunits.<sup>55,56</sup>

In 1983 a new class of calcium dependent antibiotics produced by *Streptomyces coelicolor* was discovered and given the general family name CDA which subsequently led to some confusion in the field.<sup>18</sup> These CDAs from *S. coelicolor* were later structurally characterized and found to belong to the same class of lipodepsipeptides as daptomycin and the A54145 family (Fig. 7).<sup>57</sup> However, unlike daptomycin and the A54145s, in the so named CDA group the exocyclic motif consist of a single amino acid (Ser) and the fatty acid acyl tail is exclusively found to be 2,3-epoxy-hexanoyl.<sup>57,58</sup> A high degree of structural variation is found within the macrocycles of the CDA peptides. Most notable is the D-hydroxy asparagine at position 9, in which the beta-hydroxyl is phosphorylated in CDA1 and CDA2. Two additional D-amino acids, D-Trp and D-4-hydroxyphenylglycine, are found at positions 3 and 6 respectively. Position 10 is either a Glu or 3-methyl-Glu. Another unique site of structural variation is found in the side chain of Trp-11: in CDA2a, CDA3a, ACD4a and CDAfa, Trp-11 is dehydrogenated to Z-2,3-dehydrotryptophan ( $\Delta$ Trp).<sup>58</sup>

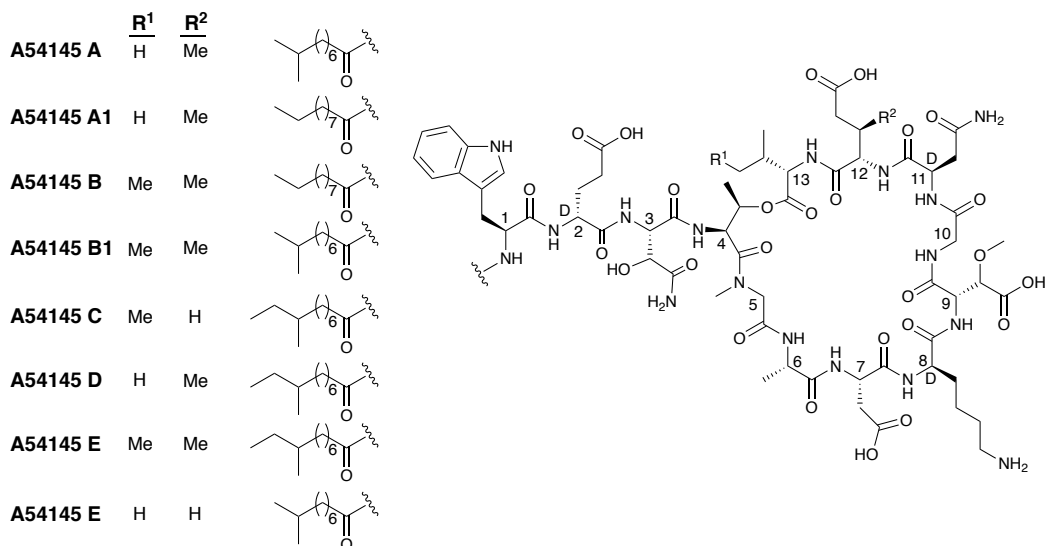


Figure 6. Structures of A54145 class of CDAs.

CDAx	R <sup>1</sup>	R <sup>2</sup>	R <sup>3</sup>	R <sup>4</sup>
CDA1b	OH	PO <sub>3</sub> H <sub>2</sub>	H	H,H
CDA2a	OH	PO <sub>3</sub> H <sub>2</sub>	CH <sub>3</sub>	π-bond
CDA2b	OH	PO <sub>3</sub> H <sub>2</sub>	CH <sub>3</sub>	H,H
CDA3a	OH	PO <sub>3</sub> H <sub>2</sub>	H	π-bond
CDA3b	OH	H	H	H,H
CDA4a	OH	H	CH <sub>3</sub>	π-bond
CDA4b	OH	H	CH <sub>3</sub>	H,H
CDA2d	H	PO <sub>3</sub> H <sub>2</sub>	CH <sub>3</sub>	H,H
CDAfa	F	PO <sub>3</sub> H <sub>2</sub>	CH <sub>3</sub>	π-bond
CDAfb	F	PO <sub>3</sub> H <sub>2</sub>	CH <sub>3</sub>	H,H

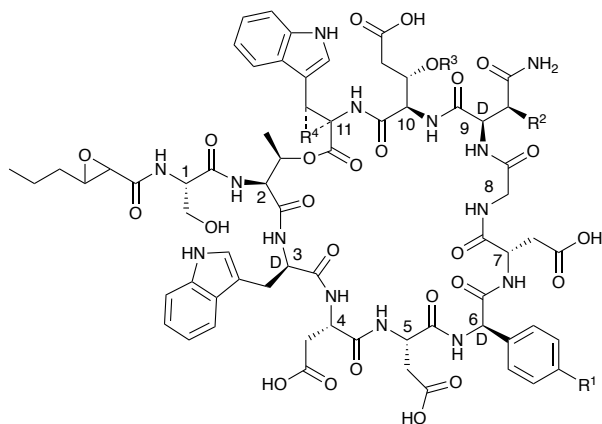
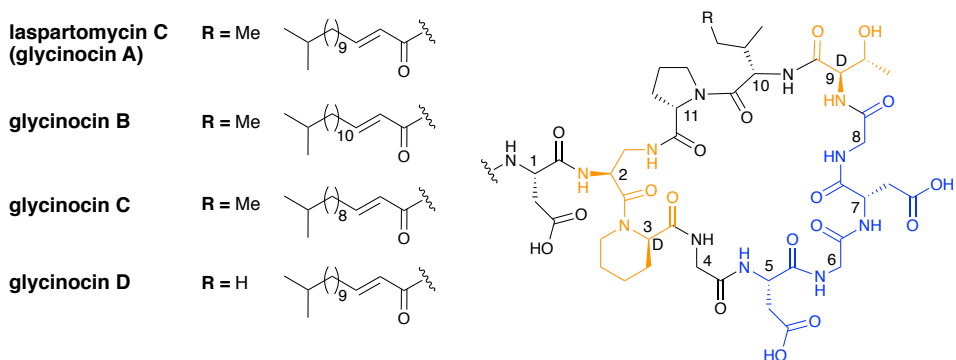


Figure 7. Structural diversity among the CDA class.

## 1.4 Emerging insights and recent developments

Recent studies conducted both in the Payne group<sup>59</sup> as well as our own<sup>60</sup> have focused on the synthesis and mechanism of action of the laspartomycin family of the CDAs. The laspartomycins belong to the same sub-family as the amphomycins/friulimicins and the first laspartomycin to be reported was isolated from *Streptomyces viridochromogense* in 1968.<sup>22</sup> Due to the analytical constraints of the time, a full chemical characterization was not reported until 2007 when advanced purification techniques and spectroscopic methods led to the structure elucidation of the major component, laspartomycin C.<sup>23</sup> Somewhat parallel to this work, investigations aimed at identifying the active antibiotic components in the fermentation broth of an unidentified terrestrial *Actinomycetes* species led to the discovery of the so-called glycinocin family of the CDAs.<sup>61</sup> The glycinocins were subsequently shown to be largely identical to the laspartomycins with the dominant glycinocin A sharing the exact same structure as laspartomycin C (Fig. 8). Among the other glycinocins characterized, glycinocin B and C have the same peptide core as laspartomycin C and only differ in the length of their fatty acid, with the lipids both consisting of iso branching at the terminal end. Glycinocin D has the same lipid tail as laspartomycin C however, in place of an Ile at position 10, it contains Val (as for the amphomycins and friulimicins).<sup>61</sup> Unlike the amphomycins and friulimicins, in both the laspartomycin and glycinocin classes, a diaminopropionic acid residue (Dap2) facilitates macrolactamization rather than 2S,3R-diaminobutyrate (Dab2). Other differences include D-allo-Thr9 in place of 2R,3R-D-Dab9, and a simple Gly at position 4 instead of non-proteinogenic MeAsp4. Furthermore, the fatty acid of the laspartomycin/glycinocin family is 2,3-unsaturated and has E geometry versus the 3,4-unsaturation with Z geometry observed in the amphomycin and friulimicin families. Laspartomycin C shows antibacterial activity against a variety of Gram-positive pathogens including MRSA, VRE and VRSA.<sup>22,62</sup> To further examine its potential as an antibiotic lead compound, a number of semisynthetic laspartomycin variants have been reported by incorporating a number of different lipid tails.<sup>62</sup> These studies revealed that both the length and saturation of the lipid tail is essential for full activity.

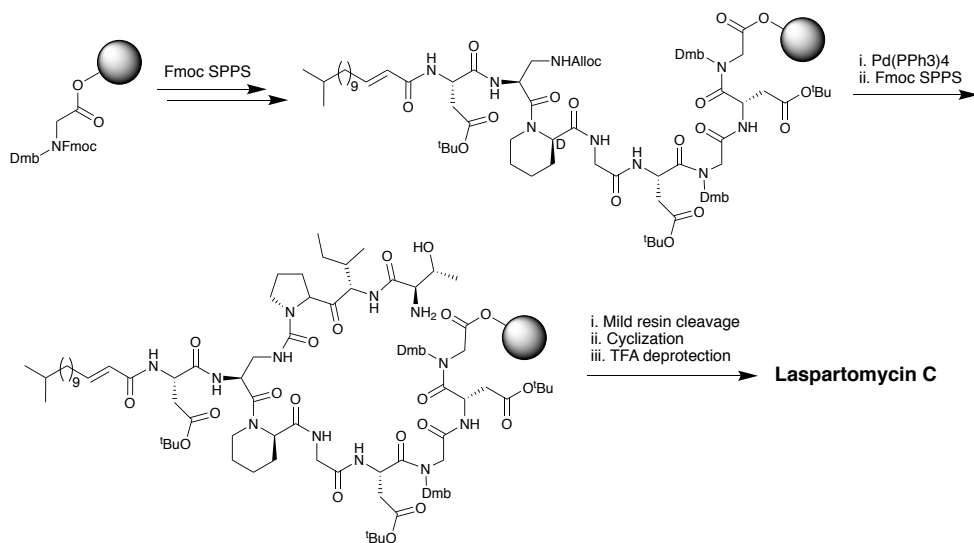




**Figure 8.** Laspartomycin C and the glycinocin A-D family. Highlighted in blue is the conserved Asp-X-Asp-Gly  $\text{Ca}^{2+}$  binding motif and highlighted in orange are nonproteinogenic amino acids.

While laspartomycin C shares many structural similarities with the amphomycins and friulimicins the mechanistic details of its antibacterial mode of action remained unknown until recently elucidated by our group in 2016.<sup>60</sup> In doing so we also developed a convenient combined solid- and solution-phase approach for the synthesis of laspartomycin C and structural analogues (Scheme 4). Notably, our synthesis of laspartomycin C represents only the second CDA to be prepared *via* total synthesis. Soon thereafter Payne and coworkers reported a similar approach to the synthesis of glycinocins A-C and variants thereof.<sup>63</sup> Using our synthetic laspartomycin we demonstrated that it specifically and tightly binds undecaprenyl phosphate ( $\text{C}_{55}\text{-P}$ ) a bacterial phospholipid essential for cell wall synthesis. Using isothermal titration calorimetry, we quantified  $\text{C}_{55}\text{-P}$  binding laspartomycin with a remarkably low nanomolar  $K_d$  value. Following up on this work and in a collaboration with the Janssen group we recently solved the crystal structure of laspartomycin C bound to a more soluble truncated analogue of  $\text{C}_{55}\text{-P}$ , geranyl phosphate ( $\text{C}_{10}\text{-P}$ ).<sup>64</sup> The structure reveals a basic unit comprised of a 1:2:1 laspartomycin C/ $\text{Ca}^{2+}$ / $\text{C}_{10}\text{-P}$  stoichiometry (Fig. 9). The structure also suggests that a dimeric species may be biologically relevant wherein two laspartomycin C fatty acid side chains and two  $\text{C}_{10}\text{-P}$  tails orientated perpendicular to a hydrophobic plane.

The phosphate head groups are then sequestered within the core of laspartomycin C dimer which lies slightly embedded in the bacterial membrane. While a previous crystal structure of tsushimycin (amphomycin B according to the nomenclature proposed in Fig. 4) provided insight into calcium binding,<sup>65</sup> our laspartomycin C structure represents the first structure of a CDA bound to both calcium and its truncated biomolecular target.



**Scheme 4.** Combined solution- and solid-phase approach used by our group in the first total synthesis of laspartomycin C.

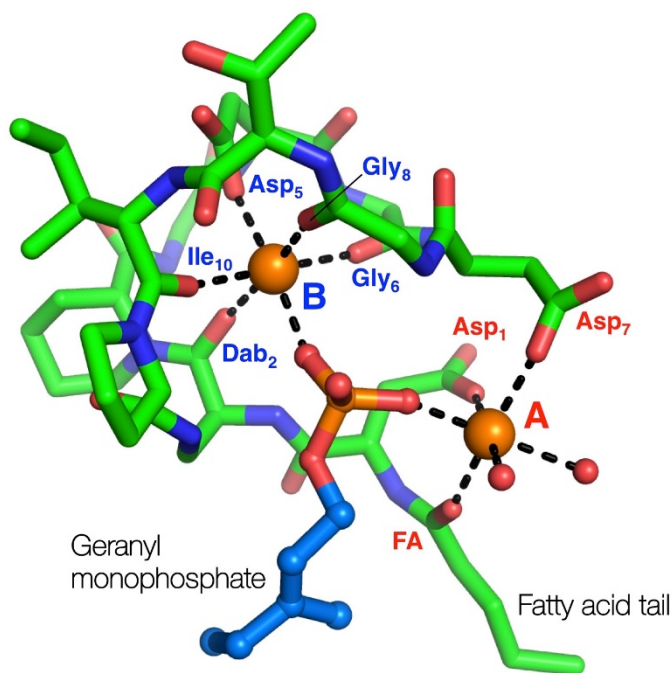


**Figure 9.** Crystal structure of laspartomycin C (green stick representation) bound to two bound Ca<sup>2+</sup> ions (orange spheres) and the geranyl phosphate ligand coordinated by the Ca<sup>2+</sup> ions. The two Ca<sup>2+</sup> ions are labelled A (red) and B (blue) with the interacting parts of laspartomycin C responsible for the chelation of the Ca<sup>2+</sup> ions also indicated.

Advancements in the field of next-generation sequencing technologies have shed new light on microbial genomes as a potentially rich source for novel antibiotics. In a recent report from the Moore group, a transformation-associated recombination cloning technique was used to clone, refactor, and express a silent biosynthetic pathway to yield two CDAs named taromycin A and taromycin B (Fig. 10).<sup>66,67</sup> While taromycin is structurally similar to daptomycin it also contains two chlorinated amino acids, namely a 6-chloro-tryptophan at position 1 and a 4-chloro-kynuenine at position 13. While these chlorinated amino acids are not found in any

other CDAs, they do not seem to offer a significant advantage as the activity of taromycin does not match or surpass that of daptomycin.

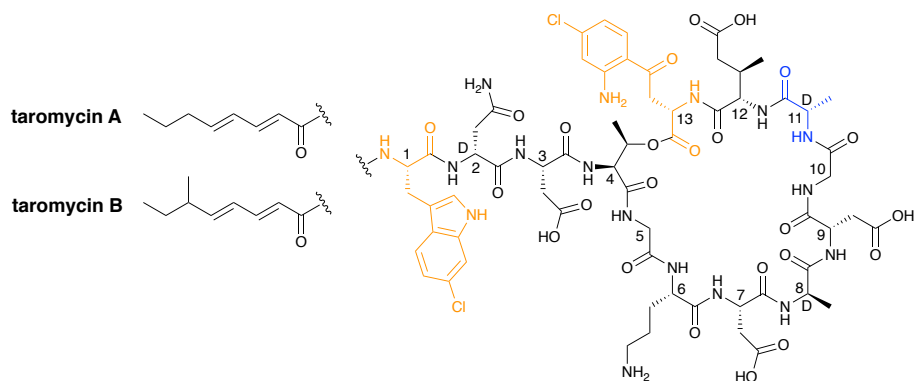


**Figure 10.** Taromycin A and B. Highlighted in orange are the chlorinated amino acids 6-chloro-tryptophan and 4-chloro-kynurenine. The taromycin family has a D-alanine in place of the D-serine found in daptomycin (highlighted in blue).

In another demonstration of the power of microbial genome mining, Brady and co-workers recently reported an entirely new class of CDAs, termed the malacidins (Fig. 11A).<sup>68</sup> The malacidins are unique among the CDAs in that they lack the canonical Asp-X-Asp-Gly calcium binding motif which is instead replaced by the tri-peptide  $\beta$ -hydroxy-Asp-Asp-Gly. This change results in the malacidins having a nine amino acid peptide macrocycle rather than the ten amino acid macrocycle found in all other CDAs. Despite this difference, the malacidins demonstrate a strong calcium dependence for their antibacterial activity. Also, of note is the unique mechanism of action of the malacidins. Unlike the other CDAs, that act by membrane disruption (daptomycin, A54145, CDA) or by binding C<sub>55</sub>-P to inhibit cell-wall biosynthesis (amphomycins, friulimicins, laspartomycins), the malacidins inhibit bacterial cell-wall biosynthesis by binding to lipid II.<sup>68</sup> The activity of the malacidins are on par with that of daptomycin, with MICs of 0.2-0.8  $\mu\text{g}/\text{mL}$  against MRSA and 0.8-2.0  $\mu\text{g}/\text{mL}$  against VRE. Malacidin's *in vivo* activity was also assessed in a rat cutaneous wound model where it successfully cleared MRSA infection.

Very recently, the Brady group reported another new member of the CDA family which they also identified using genome mining approaches and named the cadasides (Fig. 11B).<sup>69</sup> Similar to the malacidins, the cadasides contain a nine amino macrocycle however, unlike the malacidins, the cycle is closed *via* an ester linkage to yield a depsipeptide. Also, of note, while the malacidin lipid tail bears an E, Z unsaturation pattern, that of the cadasides contains the reversed Z, E geometry. The cadasides also lack the canonical calcium binding Asp-X-Asp-Gly motif found in other CDAs but do contain a  $\beta$ -hydroxy-Asp and a  $\gamma$ -hydroxy-Glu within their macrocycle. It is tempting to speculate that one or both of these hydroxylated amino acids may play a role in calcium binding. However, this hypothesis remains to be investigated experimentally. While metagenomic based antibiotic discovery is still in its infancy it may prove to be a useful tool in discovering new CDAs that are hidden in so-called cryptic gene clusters.

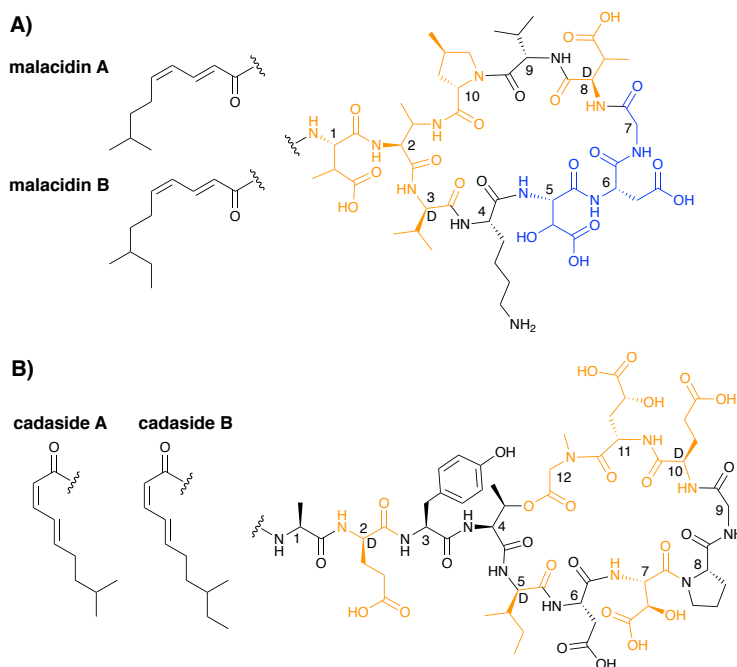


**Figure 11.** Structures of A) the malacidins and B) the cadasides. Highlighted in orange are the nonproteinogenic amino acids and highlighted in blue is the presumed  $\text{Ca}^{2+}$  binding motif for the malacidins.

## 1.5 The future of CDAs

The spread of multi-drug resistant bacteria remains a concern and presents a serious threat to modern healthcare. While the first CDA was reported in the early 1950s, it was the approval of daptomycin in 2003 that brought this unique class of antibiotics into the spotlight. Enabled by advances in screening and synthetic chemistry, the past decade has witnessed a burst of activity in the field. With now over 40 unique CDAs reported, their structural diversity continues to provide opportunity for discovery. Of particular note is the growing appreciation that the different members of the CDA superfamily utilize a diverse range of antibacterial mechanisms. A more complete understanding of these different mechanisms, supported by structural insights, will be key to establishing a more complete structure-activity relationships for the various CDAs. Such information is in turn expected to inform the design of optimized CDAs accessible *via* synthetic means. While daptomycin remains the only clinically used CDA, the many advances and increasing interest in this compound class suggest there is good reason to expect additional family members to enter the clinic in the years to come.

## 1.6 Scope and outline of this thesis

This thesis describes research concerned with the design, synthesis and biological evaluation of cyclic peptides that target infectious diseases.

**Chapter 2** describes the design and synthesis of cyclic peptides related to Laspartomycin C. A small library of lipopeptides were synthesized and tested for their activity. In collaboration with the group of Bert Janssen (Utrecht University) high-resolution crystal structures were obtained for two compounds. Interestingly, the results show that a high-ordered crystal arrangement is formed, this higher-ordered arrangement is driven by various amino acids not present in the parent compound but found in the amphomycin/friulimicin class.

**Chapter 3** builds upon the results described in Chapter 2. To further understand the amino acids that play a key role in the activity of Laspartomycin C three achiral amino acids (Gly) were substituted with the bulkier 2-aminoisobutyric acid (Aib) counterpart. These findings led to the

discovery that position eight in Laspartomycin is crucial for activity as it is part of the calcium binding motif. The other two positions were much more amenable to change and further substituted for either a L- or D-Alanine. While overall activity increased when going from Aib to either L- or D-alanine it was found that there was an eight-fold difference in activity between L- and D-alanine at position six (with D-alanine being more active). Position six is always a D-amino acid in the broader CDA family, with Laspartomycin C being the only one that contains a Gly at that position.

**Chapter 4** reports a fast and convenient synthetic route to obtaining bicyclic peptides that are active against Gram-negative pathogens. Specifically, this synthesis route uses a chemoenzymatic approach to generate large quantities of polymyxin E nona-peptide (PMEN). This PMEN can be covalently linked to the second  $\beta$ -hairpin peptide macrocycle. These peptides bind to the newly reported BamA complex in Gram-negative pathogens and even demonstrate potent activity against MCR-1 pathogens.

**Chapter 5** focuses on the design and synthesis of  $\beta$ -hairpin peptide macrocycles that can be recognized by the newly discovered bacterial enzyme EarP. EarP transfers a rhamnose to a specific arginine residue in its acceptor protein EF-P. The *in vitro* rhamnosyltransferase activity of EF-P is abolished when presented with linear substrate peptide (derived from EF-P). However, the enzyme readily glycosylates the same sequence in a cyclized  $\beta$ -hairpin mimic. This was done in collaboration with the group of Marthe Walvoort (University of Groningen). Using detailed NMR studies, it was established that the active peptide substrates all share some degree of  $\beta$ -hairpin formation.

## References

1. J. O'Neill, *Rev. Antimicrob. Resist.*, **2014**, 1-16.
2. CDCD, US Dep. Heal. Hum. Serv.
3. P. E. Waterman, P. McGann, E. Snesrud, R. J. Clifford, Y. I. Kwak, I. P. Munoz-Urbizo, J. Tabora-Castellanos, M. Milillo, L. Preston, R. Aviles, D. E. Sutter and E. P. Lesho, *Antimicrob. Agents Chemother.*, **2013**, 57, 4584-4586.
4. K. H. M. E. Tehrani and N. I. Martin, *Med. Chem Commun.*, **2018**, 9, 1439-1456.
5. Y. Wang, R. Zhang, J. Li, Z. Wu, W. Yin, S. Schwarz, J. M. Tyrrell, Y. Zheng, S. Wang, Z. Shen, Z. Liu, J. Liu, L. Lei, M. Li, Q. Zhang, C. Wu, Q. Zhang, Y. Wu, T. R. Walsh and J. Shen, *Nat. Microbiol.*, **2017**, 2, 1-7
6. X. Zhang, B. Zhang, Y. Guo, J. Wang, P. Zhao, J. Liu and K. He, *Int. J. Food Microbiol.*, **2019**, 291, 87-90.
7. H. F. Chambers and F. R. DeLeo, *Nat. Rev. Microbiol.*, 2009, 7, 629-641.
8. N. Pourramezan, S. Ohadian Moghadam and M. R. Pourmand, *New Microbes New Infect.*, **2019**, 27, 29-35.
9. E. Tacconelli and M. A. Cataldo, *Int. J. Antimicrob. Agents*, **2008**, 31, 99-106.
10. J. Davies, *Can. J. Infect. Dis. Med. Microbiol.*, **2006**, 17, 287-290.
11. C. L. Ventola, *Pharmacy and Therapeutics.*, **2015**, 40, 277-283.
12. R. Aminov, *Biochem. Pharmacol.*, **2017**, 133, 4-19.
13. M. N. Gwynn, A. Portnoy, S. F. Rittenhouse and D. J. Payne, *Ann. N. Y. Acad. Sci.*, **2010**, 1213, 5-19.
14. A. E. Muller and I. C. Gyssens, *Kucers Use Antibiot. A Clin. Rev. Antibacterial, Antifung. Antiparasit. Antivir. Drugs*, Seventh Ed., **2017**, 2, 866-907.
15. R. Sauer mann, M. Rothenburger, W. Graninger and C. Joukhar, *Pharmacology*, **2008**, 81, 79-91.
16. M. Debono, M. Barnhart, C. Carrell, J. L. Occolowitz, B. Abbott, D. Fukuda, L. Hamil and J. Hoffmann, *J. Antibiot. (Tokyo)*, **1986**, 6, 761-777.
17. M. A. Mchenney, T. J. Hosted, B. S. Dehoff, P. R. Rostek and R. H. Baltz, *J. Bacteriol.*, **1998**, 180, 143-151.
18. J. H. Lakey, E. J. Lea, B. A. Rudd, H. M. Wright and D. A. Hopwood, *J. Gen. Microbiol*, **1983**, 129, 3565-3573.
19. F. P. M. and D. M. B. L.D. Boeck, H.R. Papiska, R.W. Wetzal, J.S. Mynderse, D.S. Fukuda, *J. Antibiot. (Tokyo)*, **1989**, XLIII, 587-593.
20. I. R. Heinemann, B. Kaplan, M. A. Muir, R. D. Hooper, *Antibiot, Chemother.*, **1953**, 3, 1239-1242.
21. W. Aretz, J. Meiwes, G. Seibert, G. Vobis and J. Wink, *J. Antibiot. (Tokyo)*, **2000**, 53, 807-15.
22. H. Naganawa, M. Hamada, K. Maeda, Y. Okami, T. Takeuchi and H. Umezawa, *J. Antibiot. (Tokyo)*, **1968**, XXI, 55-62.
23. D. B. Borders, R. A. Leese, H. Jarolmen, N. D. Francis, A. A. Fantini, T. Falla, J. C. Fiddes and A. Aumelas, *J. Nat. Prod.*, **2007**, 70, 443-446.
24. R. H. Baltz, V. Miao, S. K. Wrigley and V. Miao, *Nat. Prod. Rep.*, **2005**, 717-741.
25. M. Strieker and M. A. Marahiel, *ChemBioChem*, **2009**, 10, 607-616.
26. M. Debono, B. J. Abbott, R. M. Molloy, D. S. Fukuda, A. H. Hunt, V. M. Daupert, F. T. Counter, J. L. Ott, C. B. Carrell, L. C. Howard, L. D. Boeck and R. L. Hamill, *J. Antibiot. (Tokyo)*, **1988**, XLI, 1093-1105.



27. F. M. Huber, R. L. Pieper, A. J. Tietz, A. D. Division and E. Lilly, J. Biotechnol. **1988**, 7, 283–292.
28. A. Müller, M. Wenzel, H. Strahl, F. Grein, T. N. V Saaki and B. Kohl, Proc. Natl. Acad. Sci. U. S. A., **2016**.
29. S. D. Taylor and M. Palmer, Bioorg. Med. Chem., **2016**, 24, 6253–6268.
30. J. Zhang, W. R. P. Scott, F. Gabel, M. Wu, R. Desmond, J. Bae, G. Zaccai, W. R. Algar and S. K. Straus, BBA - Proteins Proteomics, **2017**, 1865, 1490–1499.
31. J. P. Quinn, K. Lolans, R. A. Weinstein and M. K. Hayden, Antimicrob. Agents Chemother., **2005**, 49, 1664–1665.
32. F. M. Marty, W. W. Yeh, C. B. Wennersten, L. Venkataraman, E. Albano, E. P. Alyea, H. S. Gold, L. R. Baden and S. K. Pillai, Antimicrob. Agents. Chemother., **2006**, 44, 595–597.
33. T. J. Foster, FEMS Microbiol. Rev., **2017**, 430–449.
34. A. S. Bayer, N. N. Mishra, L. Chen, B. N. Kreiswirth, A. Rubio and S. Yang, Antimicrob. Agents. Chemother., **2015**, 59, 4930–4937.
35. Y. Z. A.D. Christopher, R.H. Baltz, B. Paul, C.G. Marie-Francoise, D. Sascha, HE. Xiaowei, V. Kulkarni, C. Leitheiser, V.P.W. Miao, K.T. Nguyen, I.B. Parr, D. Ritz, WO Pat, 2006110185A2, **2006**.
36. H. Y. Lam, Y. Zhang, H. Liu, J. Xu, C. T. T. Wong, C. Xu and X. Li, J. Am. Chem. Soc., **2013**, 135, 6272–6279.
37. C. L. Lee, H. Y. Lam and X. Li, Nat. Prod. Rep., **2015**, 1274–1279.
38. C. R. Lohani, R. Taylor, M. Palmer and S. D. Taylor, Org. Lett., **2015**, 17, 748–751.
39. G. Barnawi, M. Noden, R. Taylor, C. Lohani, D. Beriashvili, M. Palmer and S. D. Taylor, PeptideScience, **2017**, 2, 1-9
40. N. Yin, J. Li, Y. He, P. Herradura, A. Pearson, M. F. Mesleh, C. T. Mascio, K. Howland, J. Steenbergen, G. M. Thorne, D. Citron, A. D. G. Van Praagh, L. I. Mortin, D. Keith, J. Silverman and C. Metcalf, J. Med. Chem., **2015**, 58, 5137–5142.
41. V. Knight, C. Carmela, M. Laurent and J. Silverman, J. Ind. Microbiol. Biotechnol., **2016**, 43, 195–204.
42. T. A. Mukhtar, T. Patel, K. Koteva, N. Waglechner, D. W. Hughes, G. D. Wright and G. De Pascale, Antimicrob. Agents Chemother., **2012**, 757–764.
43. V. Boix, R. N. Fedorak, K. M. Mullane, Y. Pesant, U. Stoutenburgh, M. Jin, A. Adedoyin, L. Chesnel, D. Guris, K. B. Larson and Y. Murata, Open Forum Infect. Dis., **2017**, 4, 1–8.
44. P. Daley, T. Louie, J. E. Lutz, S. Khanna, U. Stoutenburgh, M. Jin, A. Adedoyin, L. Chesnel, D. Guris, K. B. Larson and Y. Murata, J. Antimicrob. Chemother., **2017**, 72, 3462–3470.
45. H. O. Jun-Ichi Shoji, Shuichi Kozuka, Saburo Okamoto, Ryuji Sakazaki, J. Antibiot. (Tokyo), **1968**, XXI, 439–443.
46. A. P. Tyurin, V. A. Alferova, A. S. Paramonov, M. V. Shuvalov, I. A. Malanicheva, N. E. Grammatikova, P. N. Soloyev, S. Liu, C. Sun, I. A. Prokhorenko, T. A. Efimenko, L. P. Terekhova, O. V. Efremenkova, Z. O. Shenkarev and V. A. Korshun, Med. Chem. Commun., **2018**, 9, 667–675.
47. S. M. and S. O. Haruo Tanaka, Ruiko Oiwa, Biochem. Biophys. Res. Commun., **1979**, 86, 902–908.
48. E. Rubinchik, T. Schneider, M. Elliott, W. R. P. Scott, J. Pan, C. Anklin, H. Yang, D. Dugourd, A. M??ller, K. Gries, S. K. Straus, H. G. Sahl and R. E. W. Hancock, Antimicrob. Agents Chemother., **2011**, 55, 2743–2754.

49. T. Schneider, K. Gries, M. Josten, I. Wiedemann, S. Pelzer, H. Labischinski and H. G. Sahl, *Antimicrob. Agents Chemother.*, **2009**, 53, 1610–1618.
50. D. Dugourd, H. Yang, M. Elliott, R. Siu, J. J. Clement, S. K. Straus, R. E. W. Hancock and E. Rubinchik, *Antimicrob. Agents Chemother.*, **2011**, 55, 3720–3728.
51. W. A. Craig, D. R. Andes and T. Stamstad, *Antimicrob. Agents Chemother.*, **2010**, 54, 5092–5098.
52. M. Singh, J. Chang, L. Coffman and S. J. Kim, *Nat. Publ. Gr.*, **2016**, 1–9.
53. V. Miao, Æ. R. Brost, Æ. J. Chapple and K. S. Æ. Marie-franc, *J. Ind. Microbiol. Biotechnol.*, **2006**, 129–140.
54. F. T. Counter, N. E. Allen, D. S. Fukuda, J. N. Hobbs, J. Ott, P. W. Ensminger, J. S. Mynderse, D. A. Preston, C. Y. E. Wu, T. Lilly and E. Lilly, *J. Antibiot. (Tokyo)*, **1990**, 616–622.
55. R. Taylor, K. Butt, B. Scott, T. Zhang, J. K. Muraih, E. Mintzer, S. Taylor and M. Palmer, *BBA - Biomembr.*, **2016**, 1858, 1999–2005.
56. T. Zhang, S. D. Taylor, M. Palmer and J. Duhamel, *Biophys*, **2016**, 111, 1267–1277.
57. C. Kempter, D. Kaiser, S. Haag, G. Nicholson, V. Gnau, T. Walk, K. H. Gierling, H. Decker, H. Zahner, G. Jung and J. W. Metzger, *Angew. Chemie. Int. Ed.*, **1997**, 42, 498–501.
58. Z. Hojati, C. Milne, B. Harvey, L. Gordon, M. Borg, F. Flett, B. Wilkinson, P. J. Sidebottom, B. A. M. Rudd, M. A. Hayes, C. P. Smith and J. Micklefield, *Chem. Biol.*, **2002**, 9, 1175–1187.
59. L. Corcilius, N. T. Elias, J. L. Ochoa, R. G. Linington and R. J. Payne, *J. Org. Chem.*, **2017**, 82, 12778–12785.
60. L. H. J. Kleijn, S. F. Oppedijk, P. T Hart, R. M. Van Harten, L. A. Martin-Visscher, J. Kemmink, E. Breukink and N. I. Martin, *J. Med. Chem.*, **2016**, 59, 3569–3574.
61. G. T. C. F. Kong, *J. Antibiot. (Tokyo)*, **2003**, 56, 557–564.
62. W. V Curran, R. A. Leese, H. Jarolmen, D. B. Borders, D. Dugourd, Y. Chen and D. R. Cameron, *J. Nat. prod*, **2007**, 70, 447–450.
63. L. Corcilius, D. Y. Liu, J. L. Ochoa, R. G. Linington and R. J. Payne, *Org. Biomol. Chem.*, **2018**, 16, 5310–5320.
64. L. H. J. Kleijn, H. C. Vlieg, T. M. Wood, J. Sastre Toraño, B. J. C. Janssen and N. I. Martin, *Angew. Chemie. Int. Ed.*, **2017**, 56, 16546–16549.
65. G. Bunkóczi, L. Vértesy and G. M. Sheldrick, *Acta Crystallogr. Sect. D Biol. Crystallogr.*, **2005**, 61, 1160–1164.
66. K. Yamanaka, K. A. Reynolds, R. D. Kersten, K. S. Ryan, D. J. Gonzalez and B. S. Nizet, Victor Dorrestein, Pieter C, Moore, *Proc. Natl. Acad. Sci. U. S. A.*, **2014**, 111, 1957–1962.
67. K. A. Reynolds, H. Luhavaya, J. Li, S. Dahesh, V. Nizet, K. Yamanaka and B. S. Moore, *J. Antibiot. (Tokyo)*, **2018**, 71, 333–338.
68. B. M. Hover, S. H. Kim, M. Katz, Z. Charlop-Powers, J. G. Owen, M. A. Ternei, J. Maniko, A. B. Estrela, H. Molina, S. Park, D. S. Perlin and S. F. Brady, *Nat. Microbiol.*, **2018**, 3, 415–422.
69. C. Wu, Z. Shang, C. Lemetre, M. A. Ternei, S. F. Brady, C. Wu, Z. Shang, C. Lemetre, M. A. Ternei and S. F. Brady, *J. Am. Chem. Soc.*, **2019**.

# Chapter 2

Structure-activity studies and high-resolution crystal structures provide new mechanistic insights into the C<sub>55</sub>-P targeting family of calcium-dependent lipopeptide antibiotics

*Key to addressing the threat of antibiotic resistance is the discovery and development of new antibiotics that operate by unexploited modes of action. The calcium-dependent lipopeptide antibiotics (CDAs) are an important emerging class of natural products that provides a source of new antibiotic agents rich in structural and mechanistic diversity. Notable in this regard is laspartomycin C, a CDA that specifically targets the bacterial cell wall precursor undecaprenyl pyrophosphate (C<sub>55</sub>-P). In this study we describe the design and synthesis of new laspartomycin C variants with enhanced antibacterial activities. High-resolution crystal structures reveal a unique crystal packing that governs the interaction of these lipopeptides with C<sub>55</sub>-P and provide an explanation for the observed activity enhancement.*

**Collaboration statement:** *The contents of this chapter are the result of a collaboration with the group of Bert Janssen (Utrecht University). All peptide synthesis and biological evaluation was performed by T. Wood. All crystal structure analysis was done by collaborators.*

Accepted for publication in ACS Central Science after minor revisions: †Wood, T.M.; ‡Zeronian, M.R.; Abedian, H.K.; Johnson, A.V.; Pearce, N.M.; Lutz, M.; Kemmink, J.; Seirnsma, T.; Hamoen, L.W.; Janssen, B.J.C.; Martin, N.I.

†Indicates equal contribution.

## 2.1 Introduction

The rapid emergence of multidrug resistant bacteria presents a growing threat to human health and is considered a top priority of the World Health Organization.<sup>1</sup> The most effective way to address this threat is to identify antibiotics that operate by unique, unexploited mechanisms.<sup>2</sup> While the so-called “golden age” of antibiotic discovery spanning the 1940s-1960s delivered a plethora of life-saving drugs, in the subsequent 50 years only two new antibiotic classes operating with truly novel modes of action have been introduced.<sup>3</sup> Among these is the macrocyclic lipopeptide daptomycin, the preeminent calcium-dependent antibiotic (CDA), which entered the clinic as a first-in-class agent in 2004.<sup>4,5</sup> Despite its clinical success, daptomycin’s precise mechanism of action remains a topic of continued investigation.<sup>6-9</sup> By comparison, the mode of action of other structurally similar CDAs like laspartomycin C, friulimicin B, and amphomycin (Fig. 1) are more fully understood.<sup>10-13</sup> These CDAs specifically target the unique bacterial phospholipid undecaprenyl phosphate ( $C_{55}\text{-P}$ ). In bacteria,  $C_{55}\text{-P}$  plays an essential role as a lipid carrier in cell wall biosynthesis.<sup>14</sup> Specifically, on the inner surface of the bacterial membrane, the enzyme MraY couples  $C_{55}\text{-P}$  with UDP-MurNAC-pentapeptide to form lipid I. The membrane anchored lipid I is next converted to lipid II by action of MurG. Lipid II is then flipped to the periplasm where the disaccharide-pentapeptide motif is incorporated into the growing peptidoglycan layer and the phospholipid carrier is released, first as the pyrophosphate ( $C_{55}\text{-PP}$ ) which is subsequently converted to  $C_{55}\text{-P}$  by action of the phosphatase UppP/BacA.<sup>15,16</sup> For another cycle to begin,  $C_{55}\text{-P}$  must first be flipped back to the cytoplasm where it can again be used as a membrane anchor for peptidoglycan synthesis. Compounds capable of binding to and sequestering  $C_{55}\text{-P}$  on the outer surface of the bacterial membrane therefore have the capacity to function as antibacterial agents. Notably, while  $C_{55}\text{-P}$  plays a central role in peptidoglycan synthesis, to date there are no clinically approved antibiotics that operate by directly binding  $C_{55}\text{-P}$ .

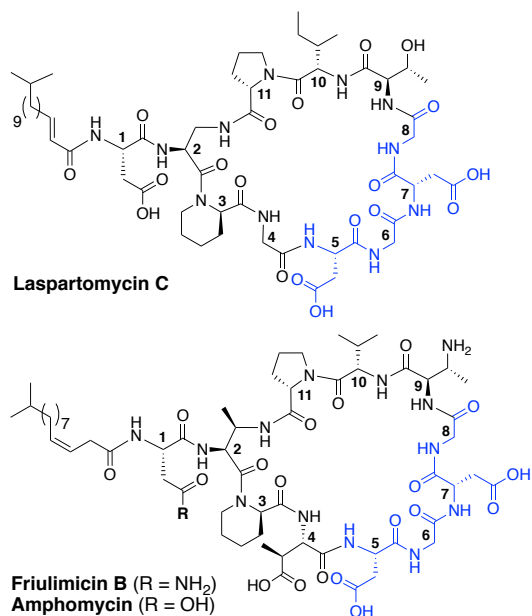


**Figure 1.** Structures of laspartomycin C, friulimicin B, and amphomycin. Highlighted in blue is the Asp-X-Asp-Gly calcium binding motif conserved throughout the CDAs. Laspartomycin C differs from friulimicin B and amphomycin at positions 2, 4, 9, and 10.

To date, more than 40 structurally distinct CDAs have been reported with varying antibacterial activities and mechanisms of action.<sup>17</sup> A number of structural features are common among the CDAs, including specifically positioned D-amino acids and the highly conserved Asp-X-Asp-Gly motif, essential for binding of calcium (Fig. 1).<sup>18</sup> Apart from the recently reported malacidins,<sup>19,20</sup> all CDAs contain 10 amino acids in their macrocycle. An interesting sub-class of CDAs are those wherein the peptide macrocycle is closed by a lactam linkage, a group comprised of laspartomycin C, friulimicin B, and amphomycin (Fig. 1). Considering their structural similarities, it is perhaps not surprising that all three share the same target (C<sub>55</sub>-P) as part of their antibacterial mechanisms. There are, however, a number of subtle structural features that distinguish laspartomycin C from the friulimicins/amphomycins. For example, the length and geometry of the N-terminal lipid in laspartomycin C differs

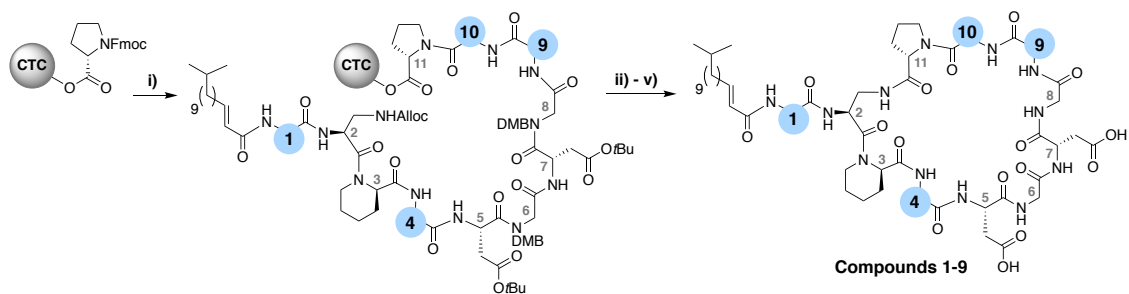
slightly from that found in friulimicin B and amphomycin. In addition, while both laspartomycin C and amphomycin contain an Asp residue at position 1, in friulimicin B this is Asn. A more notable difference is observed within the peptide macrocycles of these CDAs. Laspartomycin C contains diamino-propionic acid (Dap), Gly, D-allo-Thr, and Ile at positions 2, 4, 9, and 10 respectively whereas in the friulimicin/amphomycin class the same positions are filled by (2S, 3R)-diamino-butyric acid, (2S, 3S)-3-methyl-Asp, (2R, 3R)-diamino-butyric acid, and Val respectively (Fig. 1).

Previous findings from our group revealed that for laspartomycin C the sidechains of residues 4, 9, and 10 are not directly involved in coordinating the C<sub>55</sub>-P phosphate head group or the bridging calcium ions.<sup>12</sup> This knowledge, coupled with the structural differences between the laspartomycin and friulimicin/amphomycin class, prompted us to investigate the impact of introducing structural features present in friulimicin/amphomycin into the laspartomycin C macrocycle. Specifically, the introduction of residues containing carboxylate and amino side chains at positions 4 and 9, respectively were first investigated providing analogues with rather diminished activity. Surprising, however, was the subsequent finding that in the same series, the additional substitution of Ile<sup>10</sup> in laspartomycin C for Val (as in the friulimicin/amphomycin class) resulted in a significant enhancement of antibacterial activity. This subtle effect, wherein antibacterial activity is strongly dependent upon the absence of a single methyl group in the side chain of the residue at position 10, was subsequently investigated and explained by high-resolution X-ray crystal structures of the new lipopeptide variants in complexation with C<sub>55</sub>-P and Ca<sup>2+</sup>. Notably, these findings provide key new insights into the mechanism of action of the friulimicin/amphomycin class of CDAs and the subtle differences with that of the laspartomycin family. In addition, a series of live-cell imaging studies were also performed that shed new light on the effects that C<sub>55</sub>-P targeting CDAs have on bacterial cell growth and division.

## 2.2 Results and Discussion

To evaluate the impact of introducing amino acids specific to the friulimicins/amphomycin class into laspartomycin C we applied a robust synthetic route wherein the linear peptide precursor, including the N-

terminal lipid, was first assembled on solid support using the acid sensitive 2-chlorotrityl resin (Scheme 1).<sup>11,21,22</sup> Notably, Gly residues at positions 6 and 8 were incorporated using the corresponding Fmoc-DMB-Gly building block to avoid aspartamide formation. On resin removal of the alloc group on the Dap<sup>2</sup> side chain was followed by mild acid cleavage to yield the protected peptide intermediate. Formation of the macrocycle was achieved by treatment with BOP/DIPEA under at high dilution, after which global deprotection and RP-HPLC purification provided lipopeptides **1-9**. The first structural variation explored involved the swapping of the exocyclic Asp<sup>1</sup> found in laspartomycin C for Asn<sup>1</sup> as in friulimicin B. This analogue (**2**) showed no appreciable difference in minimum inhibitory concentration (MIC) when compared to laspartomycin C (Table 1). This is not surprising as this exocyclic amino acid is also the only difference between the amphomycin and friulimicin class of CDAs which are reported to have similar activities.<sup>11,13</sup> We next focused our attention to the differing amino acids contained within the peptide macrocycles of the laspartomycin and friulimicins/amphomycin classes. To this end compounds **3-5** were prepared to assess the contribution of the acidic and basic residues unique to positions 4 and 9 in the amphomycin/friulimicin class. Interestingly, these new variants bearing either Asp<sup>4</sup> or D-Dap<sup>9</sup>, or both substitutions, demonstrated severely reduced antibacterial activities relative to laspartomycin C and friulimicin B. Compound **6** was next synthesized to probe the role of Val<sup>10</sup> present in the amphomycin/friulimicin class compared to the slightly bulkier Ile residue found at the same position in laspartomycin C. Somewhat surprisingly, the subtle substitution of Val for Ile at position 10 led to a significant enhancement in the antibacterial activity of lipopeptide **6** relative to compound **5**. In the presence of 10 mM Ca<sup>2+</sup>, **6** was found to exhibit an MIC of 1 µg/mL against MRSA, an activity on par/ slightly better than that measured for both laspartomycin C and friulimicin B. Given the potent activity observed for **6**, analogue **7**, bearing Asn at position 1, was also prepared and found to also demonstrate a similarly enhanced antibacterial activity. Our findings with compounds **6** and **7** indicate that the potent antibacterial activity exhibited by these more friulimicin/amphomycin-like analogues is the product of a combined effect dependent on an acidic side chain at AA<sup>4</sup>, a basic side chain at AA<sup>9</sup>, and a slightly less bulky side chain in AA<sup>10</sup>.



**Scheme 1:** i) Fmoc SPPS; ii) Pd[PPh<sub>3</sub>]<sub>4</sub>, PhSiH<sub>3</sub>, CH<sub>2</sub>Cl<sub>2</sub>, 1h; iii) HFIP, CH<sub>2</sub>Cl<sub>2</sub>, 1h; (v) BOP, DIPEA, CH<sub>2</sub>Cl<sub>2</sub>, 16h; v) TFA, TIS, H<sub>2</sub>O, 1h.

**Table 1.** MIC<sup>a</sup> values for laspartomycin C, compounds **2-9**, and friulimicin B

Compound	AA <sup>1</sup>	AA <sup>4</sup>	AA <sup>9</sup>	AA <sup>10</sup>	0	[Ca <sup>2+</sup> ] (mM)		
						2.5	5	10
<b>1</b> (Laspc)	L-Asp	Gly	D- <i>allo</i> -Thr	L-Ile	>128	8	4	2
<b>2</b>	L-Asn	Gly	D- <i>allo</i> -Thr	L-Ile	>128	8	4	4
<b>3</b>	L-Asp	L-Asp	D- <i>allo</i> -Thr	L-Ile	>128	64	32	16
<b>4</b>	L-Asp	Gly	D-Dap	L-Ile	>128	16	8	4
<b>5</b>	L-Asp	L-Asp	D-Dap	L-Ile	>128	32	16	8
<b>6</b>	L-Asp	L-Asp	D-Dap	L-Val	>128	<b>4</b>	<b>2</b>	<b>1</b>
<b>7</b>	L-Asn	L-Asp	D-Dap	L-Val	>128	<b>4</b>	<b>4</b>	<b>2</b>
<b>8</b>	L-Asp	L-Asp	D- <i>allo</i> -Thr	L-Val	>128	8	4	4
<b>9</b>	L-Asp	Gly	D-Dap	L-Val	>128	32	16	8
Friulimicin B <sup>b</sup>	L-Asn	MeAsp	D-Dab	L-Val	>128	4	2	1-2

<sup>a</sup>Minimum inhibitory concentration reported in µg/mL against MRSA USA 300 at calcium concentration indicated.

<sup>b</sup>Natural product.

This reasoning was further probed by the preparation of analogues **8** and **9** wherein the acidic and basic residues at positions 4 and 9 were independently exchanged for the uncharged Gly and D-*allo*-Thr residues found in laspartomycin C. The reduced activity measured for these compounds further confirms a role for both the acidic and basic residues at positions 4 and 9, in combination with the optimized sterics of Val<sup>10</sup>, in achieving full antibacterial effect.



## 2.3 Mechanistic and crystallographic studies

The pronounced increase in antibacterial activity observed upon substituting Ile<sup>10</sup> in analogue **5** for Val<sup>10</sup> as in compounds **6** and **7** led us to further investigate the underlying mechanism responsible for this effect. To do so we first examined the ability of these compounds to interfere with bacterial cell wall synthesis. Specifically, an assay was used that detects accumulation of the cell wall precursor UDP-MurNAc pentapeptide in response to cell-wall targeting antibiotics. As the last soluble precursor in the lipid II cycle, UDP-MurNAc pentapeptide serves as a convenient diagnostic for compounds that disrupt cell wall synthesis. Interestingly, compound **5**, while exhibiting reduced antibacterial activity, was still found to elicit an accumulation effect similar to that of the more active compound **6** (Supplementary Fig. S1).

To gain molecular level insights into the differences in activity observed for compounds **6** and **7** relative to **5**, all three were taken forward for crystal structure determination in collaboration with the group of Bert Janssen (Utrecht University). In doing so the lipopeptides were incubated with C<sub>10</sub>-P, a more soluble analogue of C<sub>55</sub>-P, in buffers containing Ca<sup>2+</sup>. Under these conditions, compounds **5** and **7** gave crystals of sufficient quality for structural analysis, diffracting to a resolution of 1.04 Å and 1.14 Å, respectively. The structures of the complexes obtained for both **5** and **7** with C<sub>10</sub>-P and Ca<sup>2+</sup> share many similarities with the structure previously reported for the laspartomycin C complex.<sup>12</sup> As illustrated in Figure 2A, the complex itself consists of one lipopeptide molecule, one geranyl phosphate ligand, and two calcium ions which play key roles both in establishing the conformation of the peptide as well as mediating binding of the phosphate head group. Notable interactions observed in the complex include hydrogen bonds formed between the C<sub>10</sub> phosphate group and the backbone and side chain amides of Dap<sup>2</sup> as well as the backbone amide of Gly<sup>8</sup>. Each calcium ion also provides an interaction with the phosphate moiety. Of the two calcium ions in the complex, one is more centrally coordinated *via* multiple interactions with the lipopeptide including four backbone carbonyls (Dap<sup>2</sup>, Gly<sup>6</sup>, Gly<sup>8</sup>, Ile/Val<sup>10</sup>) and one aspartic acid side chain (Asp<sup>5</sup>). The peripheral Ca<sup>2+</sup> is bound *via* interactions with the side chains of Asp/Asn<sup>1</sup> and Asp<sup>7</sup> and the N-terminal fatty acid carbonyl group along with one water molecule.

Collectively, these interactions cause the lipopeptides to adopt a saddle-shaped fold wherein the cavity created envelops the C<sub>10</sub>-P phosphate head group and the two calcium ions. As also observed for laspartomycin C, the complexes formed by both compounds **5** and **7** with C<sub>10</sub>-P and Ca<sup>2+</sup> organize as dimers stabilized by several intermolecular interactions. As shown in Figure 2B, dimerization is largely driven by hydrogen bonding interactions between the D-Dap<sup>9</sup> backbone amide one lipopeptide molecule and the Asp<sup>7</sup> side chain carboxylate of the other. Additional indirect hydrogen bonding interactions are mediated by interaction of the D-Dap<sup>9</sup> backbone carbonyl and the water molecules coordinated by the peripheral Ca<sup>2+</sup> of the other ternary unit. In this dimer complex, the two C<sub>10</sub>-P phosphate head groups are fully coordinated and completely sequestered from the solvent. Notable, however, was the finding that the differing side chains at positions 4, 9, and 10 in compounds **5** and **7** induce and stabilize a unique, higher-ordered assembly not observed for laspartomycin C.

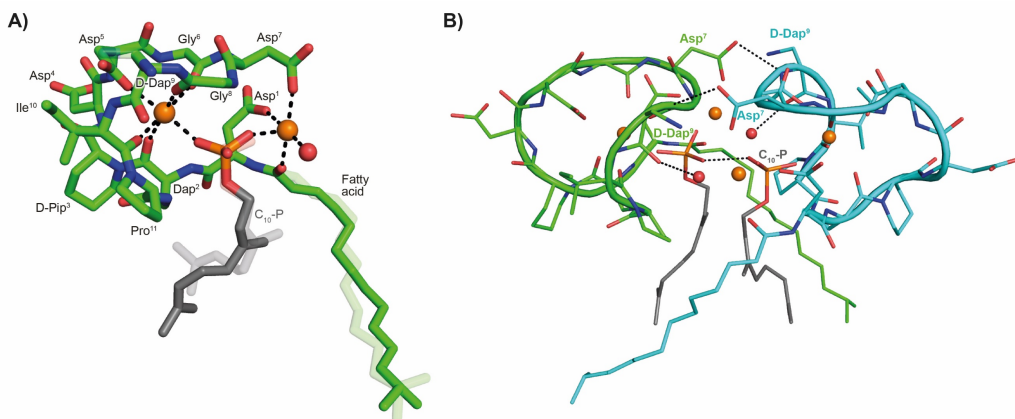


**Figure 2.** **A)** Structure of the ternary complex with lipopeptide **5** (green stick representation), two bound Ca<sup>2+</sup> ions (orange spheres), a bound water molecule (red sphere), and the C<sub>10</sub>-P ligand (lipid in grey). Major and minor conformations of the D-Dap<sup>9</sup> side chain, the C<sub>10</sub>-P lipid and the lipopeptide fatty acid tail are shown in the structure (indicated with dark and light colouring respectively). **B)** Lipopeptide **5** adopts a saddle-shaped conformation when complexed with two Ca<sup>2+</sup> ions and C<sub>10</sub>-P that forms a dimer in the crystal. Crystallographic studies performed by Matthieu Zeronian (PhD candidate in the group of Bert Janssen).

As noted above, the amphomycin/friulimicin class of lipopeptide antibiotics differs from the laspartomycin class at positions 4, 9, and 10. Compounds **5**, **6**, and **7** were generated to specifically probe the roles played by the side chains of these different amino acids. The crystal structures obtained with **5** and **7** indeed reveal that the presence of Asp<sup>4</sup> and D-Dap<sup>9</sup> result in additional inter-dimer interactions not possible for laspartomycin C. Particularly striking was the finding that when coordinated with C<sub>10</sub>-P and Ca<sup>2+</sup>, lipopeptides **5** and **7** both formed higher-ordered complexes that are not observed for laspartomycin under the same conditions (Fig. 3A). Specifically, interactions between Asp<sup>4</sup> and D-Dap<sup>9</sup> in **5** and **7** serve to stabilize this higher-ordered arrangement wherein the sidechain carboxylate and backbone carbonyl of one Asp<sup>4</sup> residue in one dimer interacts with the amino side chain of a D-Dap<sup>9</sup> residue in an adjacent dimer (Fig. 3B). Furthermore, the same Asp<sup>4</sup> also interacts with the proximal calcium coordinated by the second dimer further stabilizing this arrangement. Interestingly, the dimer of dimers thus formed is precisely oriented so as to make the same interactions with the Asp<sup>4</sup> and D-Dap<sup>9</sup> sidechains of a third dimer to generate a trimer of dimers. This repeating “trimer of dimers” motif is not observed in the crystal packing formed by laspartomycin C in complex with C<sub>10</sub>-P and Ca<sup>2+</sup> as it lacks the Asp<sup>4</sup> and D-Dap<sup>9</sup> required to do so. Also different from laspartomycin C is the finding that lipopeptides **5** and **7** form alternating layers in the crystal, with a peptide macrocycle layer inducing a strong packing in cis (within the same layer), sandwiched by a hydrophobic layer constituted of lipids (geranyl phosphate and the peptide N-terminal lipid) and by a hydrophilic layer composed of water molecules, both inducing a weak packing in trans.

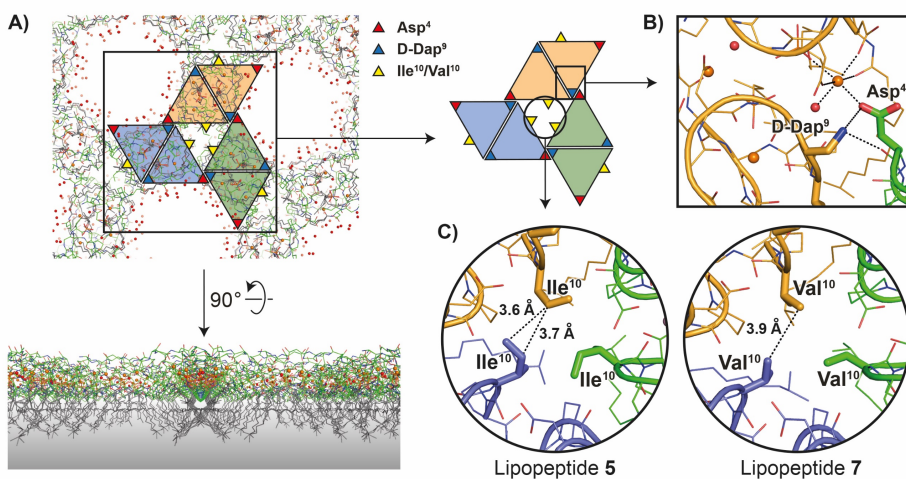


**Figure 3.** A) crystal packing of lipopeptides 5 and 7 adopt higher-ordered structures not observed with laspartomycin C. In this arrangement the lipids of both the lipopeptides and C<sub>10</sub>-P are oriented in the same direction while the peptide macrocycles interact to form a repeating trimer of dimers motif. A proposed orientation of the multimeric assembly in the bacterial membrane (indicated with a grey gradient) is shown. B) Interactions between the D-Dap<sup>9</sup> and Asp<sup>4</sup> residues present in lipopeptides 5 and 7 but absent in laspartomycin C. C) The presence of a hydrophobic core formed at the center of the trimer of dimers motif suggests that the sidechain of Val<sup>10</sup> present in the biologically more active lipopeptide 7 more optimally suits the steric requirements of this motif *vs.* the slightly bulkier Ile<sup>10</sup> in lipopeptide 5. For clarity only major conformations are shown.

The higher-ordered trimer of dimers motif formed by both 5 and 7 in complex with C<sub>10</sub>-P and Ca<sup>2+</sup> also points to an explanation for the notable enhancement in the biological activity of lipopeptides 6 and 7 relative to 5. As described above, the peptide macrocycles of 6 and 7 contain a Val residue at position 10 while in lipopeptide 5 the same position is filled by a slightly bulkier Ile residue. This subtle structural difference results in an 8-fold increase in the activity for 6 and 7 relative to 5. Careful inspection of the trimer of dimers formed by both peptides 5 and 7 reveals a hydrophobic pocket at center of the trimer where the sidechains of Val<sup>10</sup>/Ile<sup>10</sup> meet (Fig. 3C). This finding suggests that the Val<sup>10</sup> sidechain in compounds 6 and 7 (and as found naturally in the amphomycin/friulimycin class) allows for optimal packing of the trimer, enhancing the interaction with the C<sub>55</sub>-P bacterial target, and drives the antibiotic activity observed. By comparison,

the slightly bulkier Ile<sup>10</sup> sidechain in compound **5** may impinge upon the precise steric requirements of the hydrophobic pocket formed at the trimer interface and in doing so destabilize the interaction with C<sub>55</sub>-P resulting in reduced antibacterial activity. Taken together, these findings provide new insight into the mechanism of action of amphomycin/friulimycin class of calcium dependent antibiotics and how they compare to the laspartomycin family.

## 2.4 Live cell imaging

To gain additional insights into the impact of these lipopeptide antibiotics on live bacteria, laspartomycin C, lipopeptide **6**, and daptomycin were evaluated in a set of comprehensive mode-of-action studies conducted using the model organism *Bacillus subtilis* and imaged using fluorescence light microscopy.<sup>8, 23</sup> These studies were performed in collaboration with the group of prof. Leendert Hamoen (University of Amsterdam) and reveal that laspartomycin C and **6** both interfere with bacterial membrane integrity by delocalizing key membrane proteins and/or interfering with lipid organization in a manner that is distinct from that observed for daptomycin. An extensive bacterial cytological profiling study previously showed that daptomycin causes the clustering of 'fluid lipids', *i.e.* lipids with short, branched or unsaturated fatty acyl chains, into large aggregates, lowering the membrane fluidity outside these aggregates.<sup>8</sup> This has a severe effect on the binding of peripheral membrane proteins with essential functions, including the *N*-acetylglucosamine transferase MurG responsible for the last synthesis step of the peptidoglycan precursor lipid II. To further compare the effect of laspartomycin C with that of daptomycin, we performed bacterial cytological profiling using a broad set of *B. subtilis* reporter strains expressing GFP-tagged proteins involved in DNA replication (DNA polymerase subunit PolC), transcription (RNA polymerase subunit RpoC), translation (ribosome subunit RpsB), ATP synthesis (F1F0-ATPase subunit AtpA), cell division (FtsZ), cell wall synthesis coordination (MreB), cell division regulation (MinD) and peptidoglycan synthesis (MurG). The reporters MreB, MinD and MurG are all peripheral membrane proteins. Cells were incubated with the lipopeptide antibiotics at 2xMIC and observed by fluorescent light

microscopy after 10 min and 30 min incubation. The reporter strains indicated that neither DNA, RNA and protein synthesis, nor cell division and the localization of F1F0-ATPase ATP were affected by laspartomycin C or compound 6 (Fig. 4), findings that are in keeping with those previously observed for daptomycin.<sup>8</sup> Likewise, the delocalization of MreB by laspartomycin C and compound 6 is similar to the effect seen with daptomycin.<sup>8</sup> A notable difference, however, was the finding that the localization of MinD was unaffected by laspartomycin C and 6, whereas this protein rapidly detaches from the membrane when treated with daptomycin. Another clear difference is the delocalization of MurG, which detaches from the cell membrane in the presence of daptomycin, whereas laspartomycin C and compound 6 appear to dissolve the large MurG clusters so that the protein diffuses along the cell membrane (Fig. 4).

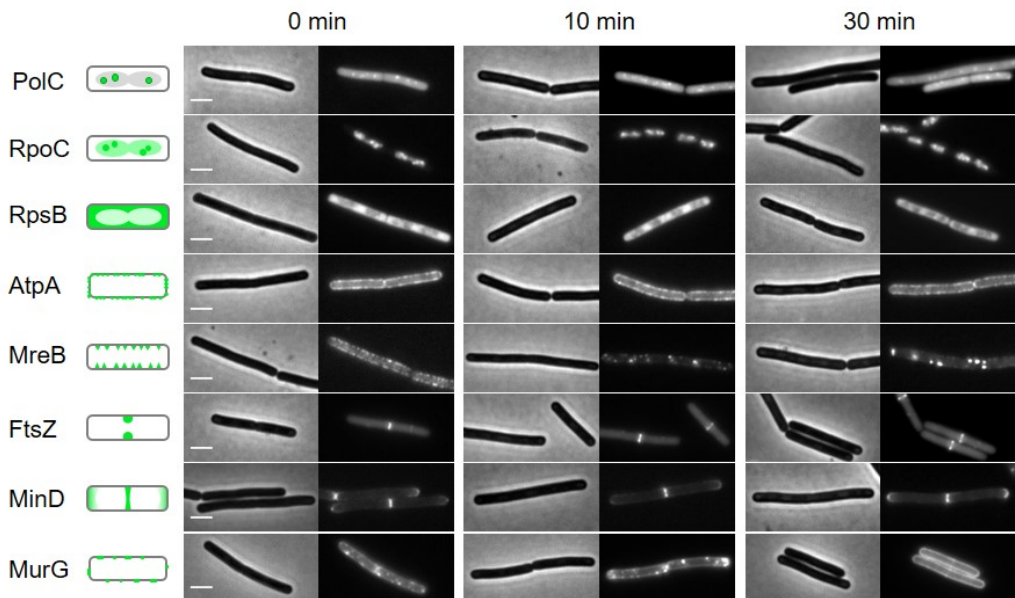


**Figure 4.** Bacterial cytological profiling analysis of Laspartomycin C. The GFP-tagged marker proteins represent the following cellular activities: DNA polymerization (PolC), RNA polymerization (RpoC), protein synthesis (RpsB), F<sub>0</sub>F<sub>1</sub> ATPase (AtpA), lateral cell wall synthesis regulation (MreB), cell division regulation (FtsZ), cell division regulation (MinD) and peptidoglycan precursor synthesis (MurG). Left panels schematically show the normal localization patterns of the different GFP fusions. Strains were grown in LB medium supplemented with 2 mM CaCl<sub>2</sub> at 30 °C. 2xMIC concentration was added (0 min) and samples for microscopy were taken after 10- and 30-min incubation, respectively. Scale bars indicate 2  $\mu$ m.

The differences observed for laspartomycin C and lipopeptide **6** *vs* daptomycin may be explained by the multifaceted mechanism of action attributed to daptomycin. Recent investigations have revealed that in the presence of phosphatidylglycerol, daptomycin can interact with C<sub>55</sub>-P, C<sub>55</sub>-PP, and the peptidoglycan precursor lipid II.<sup>9</sup> As a result, the insertion of daptomycin in the cell membrane not only affects lipid II synthesis, but also causes a dramatic rearrangement of lipids in the cell membrane resulting in the detachment of peripheral membrane proteins, including MinD and MurG.<sup>8</sup> Conversely, the binding of laspartomycin C to C<sub>55</sub>-P is not facilitated by phosphatidylglycerol or any other phospholipids<sup>11</sup> and is therefore likely to more specifically interfere with lipid II synthesis and not

with the distribution of other phospholipids in the membrane. However, the activity of proteins that rely on the C<sub>55</sub>-P precursor, including MurG and MreB, will still be affected, explaining the dissolution of MurG clusters and the delocalization of MreB observed in our studies. This rationale is also in line with a recent report revealing MreB membrane association to be dependent on the presence of lipid-linked peptidoglycan precursors and that when such precursors are depleted, MreB filaments disassemble and peptidoglycan synthesis is disrupted.<sup>24</sup>

## 2.5 Further insights into position 10 of laspartomycin C and amphotomycin B

The SAR and structural studies described in the previous sections of this chapter revealed that the hydrophobic amino acid at position 10 of the friulimicin/amphotomycin class sits at an interface where three molecules come together. Notably, a substitution from an Ile<sup>10</sup> to a Val<sup>10</sup> improved activity by roughly eight-fold. Given this pronounced effect we synthesized and evaluated of new series of analogues containing different hydrophobic amino acids, with various branching patterns, at position 10 in the laspartomycin and amphotomycin class of lipopeptides (Fig 5).

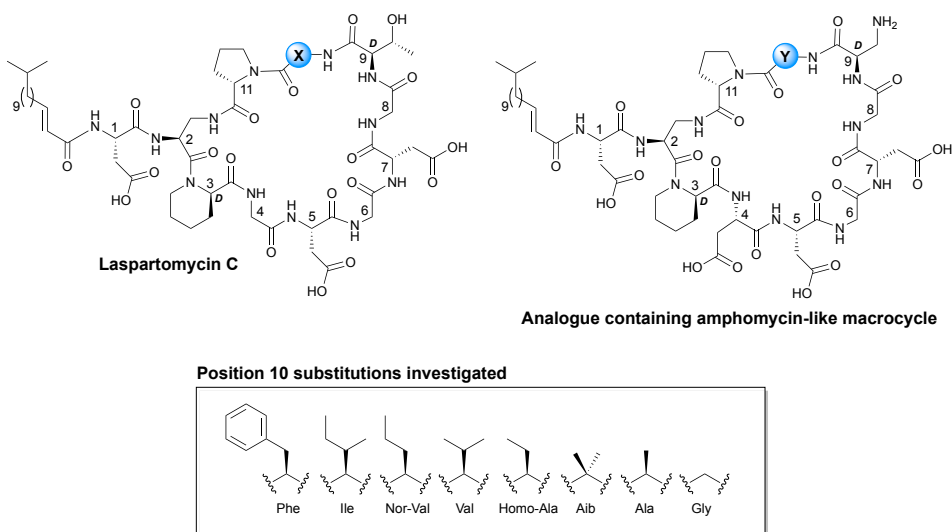


**Figure 5.** Various amino acids used to explore the effects of substitution at position 10.



To assess the contribution of hydrophobic amino acids at position 10, analogues **1-16** were prepared. The antimicrobial activity of all analogues was tested in a serial dilution assay employing a clinically relevant strain of Methicillin-resistant *Staphylococcus aureus* (MRSA) (Table 1). In the laspartomycin C class of analogues (**1-8**) the parent compound performed the best. When the chain length and branching pattern starts to decrease there is roughly a two-fold reduction in activity each time. The same is true for when a Phe is substituted in, the activity drops about four-fold. The other set of amphomycin analogues (**9-16**) show a similar pattern as well, albeit a bit more dramatic. The parent compound amphomycin which naturally has a Val at position 10 is the most active compound. It is known that a Val sits at the interface and is the most tolerated amino acid. When either increasing or decreasing chain length and branching pattern, a precipitous drop off in activity is observed. In laspartomycin's case it was a two-fold reduction in activity whereas with amphomycin it is an eight-fold drop off in activity. This could arise from the fact that laspartomycin C does not form a higher order structure where position 10 sits at the interface, while in the case of amphomycin/friulimycin it does. Both a Gly and Aib substitution at position 10 is not tolerated at all and compounds are devoid of activity.

**Table 1.** MIC values for laspartomycin C, analogues **2-9**, amphomycin B and analogues **10-16**

Compound	[Ca <sup>2+</sup> ]			
	0	2.5	5	10
<b>1 (LaspC)</b>	>128	8	4	2
<b>2 (Val)</b>	>128	8	8	4
<b>3 (Nor-Val)</b>	>128	16	16	8
<b>4 (Homo-Ala)</b>	>128	32	16	16
<b>5 (Ala)</b>	>128	64	32	16
<b>6 (Gly)</b>	>128	>128	>128	>128
<b>7 (Aib)</b>	>128	>128	>128	>128
<b>8 (Phe)</b>	>128	16	8	8
<b>9 (ampho)</b>	>128	4	2	1
<b>10 (Ile)</b>	>128	32	16	8
<b>11 (Nor-Val)</b>	>128	64	32	16
<b>12 (Homo-Ala)</b>	>128	32	16	8
<b>13 (Ala)</b>	>128	>128	>128	64
<b>14 (Gly)</b>	>128	>128	>128	>128
<b>15 (Aib)</b>	>128	>128	>128	>128
<b>16 (Phe)</b>	>128	>128	64	32

<sup>a</sup>Minimum inhibitory concentration reported in  $\mu\text{g/mL}$  against MRSA USA 300 at calcium concentration indicated.

## 2.6 Conclusion

In summary, several novel laspartomycin C variants were synthesized to probe the effects associated with structural differences specific to the friulimicin/amphomycin class of CDAs. The antibacterial activities measured, and the high-resolution crystal structures obtained for these lipopeptide antibiotics reveal a previously unknown interplay between the side chains of residues at positions 4, 9, and 10 in the peptide macrocycle. Interestingly, the amino acid side chains present at these positions in the friulimicin/amphomycin class contribute to the formation of higher-order assemblies when in complex with Ca<sup>2+</sup> and the bacterial target, an effect not seen for the other well-characterized C<sub>55</sub>-P binding CDA laspartomycin C. In addition, live cell imaging studies reveal subtle differences in the activity of laspartomycin C and daptomycin. Compared to daptomycin, laspartomycin C and the other C<sub>55</sub>-P targeting lipopeptides here studied appear to have a more narrowly defined range of cellular targets.

Particularly notable is the ability of laspartomycin C to dissolve large clusters of MurG along the cell membrane, an effect not seen in daptomycin. Taken together, our results provide new insights into the mechanisms of action associated with the C<sub>55</sub>-P-targeting subfamily of CDAs and expand our current understanding of this promising class of lipopeptide antibiotics.

## 2.6 Experimental

### 2.6.1 Reagents and General Methods

All reagents employed were of American Chemical Society (ACS) grade or finer and were used without further purification unless otherwise stated. D-amino acids and 2-chlorotrityl resin was obtained from Iris Biotech GmbH, Egg PG and 0:6 PA was obtained from INstruChemie BV. C<sub>10</sub>-P lithium salt was obtained from Sigma Aldrich and lyophilized from warm <sup>t</sup>BuOH:H<sub>2</sub>O (1:1) to obtain a white powder with increased aqueous solubility.

### 2.6.2 Instrumentation for Compound Characterization

2D NMR experiments were performed on a 850 MHz instrument. HSQC, TOCSY and NOESY spectra were recorded for all peptides (5 mM in DMSO-d<sub>6</sub>) and the parent compound laspartomycin C matched previous recorded spectra reported by our group.

HRMS analysis was performed on a Shimadzu Nexera X2 UHPLC system with a Waters Acquity HSS C18 column (2.1 × 100 mm, 1.8 μm) at 30 °C and equipped with a diode array detector. The following solvent system, at a flow rate of 0.5 mL/min, was used: solvent A, 0.1 % formic acid in water; solvent B, 0.1 % formic acid in acetonitrile. Gradient elution was as follows: 95:5 (A/B) for 1 min, 95:5 to 15:85 (A/B) over 6 min, 15:85 to 0:100 (A/B) over 1 min, 0:100 (A/B) for 3 min, then reversion back to 95:5 (A/B) for 3 min. This system was connected to a Shimadzu 9030 QTOF mass spectrometer (ESI ionisation) calibrated internally with Agilent's API-TOF reference mass solution kit (5.0 mM purine, 100.0 mM ammonium trifluoroacetate and 2.5 mM hexakis(1H,1H,3H-tetrafluoropropoxy)phosphazine) diluted to achieve a mass count of 10000.

Purity of the peptides was confirmed to be ≥ 95% by analytical RP-HPLC using a Shimadzu Prominence-i LC-2030 system with a Dr. Maisch ReproSil Gold 120 C18 column (4.6 × 250 mm, 5 μm) at 30 °C and equipped with a UV detector monitoring at 214 nm. The following solvent system, at a flow rate of 1 mL/min, was used: solvent A, 0.1 % TFA in water/acetonitrile, 95/5; solvent B, 0.1 % TFA in water/acetonitrile, 5/95. Gradient elution was as follows: 95:5 (A/B) for 2 min, 95:5 to 0:100 (A/B) over 55 min, 0:100 (A/B) for 2 min, then reversion back to 95:5 (A/B) over 1 min, 95:5 (A/B) for 2 min.

The compounds were purified *via* preparative HPLC using a BESTA-Technik system with a Dr. Maisch Reprosil Gold 120 C18 column (25 × 250 mm, 10 μm) and equipped with a ECOM Flash UV detector monitoring at 214 nm. The following solvent system, at a flow rate of 12 mL/min, was used: solvent A, 0.1 % TFA in water/acetonitrile 95/5; solvent B, 0.1 % TFA in water/acetonitrile 5/95. Gradient elution was as follows: 95:5 (A/B) for 2 min, 95:5 to 0:100 (A/B) over 55 min, 0:100 (A/B) for 2 min, then reversion back to 95:5 (A/B) over 1 min, 95:5 (A/B) for 2 min.

### 2.6.3 Solid Phase Peptide Synthesis

Chlorotrityl resin (5.0 g, 1.60 mmol/g) was loaded with Fmoc-Pro-OH. Resin loading was determined to be 0.41-0.62 mmol.g<sup>-1</sup>. Linear peptide encompassing Pro11 to Asp1 were assembled manually *via* standard Fmoc solid-phase peptide synthesis (SPPS) (resin bound AA:Fmoc-AA:BOP:DiPEA, 1:4:4:8 molar eq.) on a 0.1 mmol scale. DMF was used as solvent and Fmoc deprotections were carried out with piperidine:DMF (1:4 v:v). Amino acid side chains were protected as follows: tBu for Asp, Alloc for DAP, and DMB for Gly<sup>6</sup> and Gly<sup>8</sup>. D-allo-Thr was introduced without side chain protection. Following coupling and Fmoc deprotection of Asp<sup>1</sup>, N-terminal acylation was achieved by coupling (E)-13-methyltetradec-2-enoic acid using the same coupling conditions used for SPPS. The resin-bound, Alloc protected intermediate was next washed with CH<sub>2</sub>Cl<sub>2</sub> and treated with Pd(PPh<sub>3</sub>)<sub>4</sub> (30mg, 0.03 mmol) and PhSiH<sub>3</sub> (0.30 mL, 3.0 mmol) in CH<sub>2</sub>Cl<sub>2</sub> (*ca.* 7 mL) under argon for 1 hour. The resin was subsequently washed with CH<sub>2</sub>Cl<sub>2</sub> (5×10 mL), followed by a solution of diethyldithiocarbamic acid trihydrate sodium salt (5 mg mL<sup>-1</sup> in DMF, 5×10 mL), and DMF (5×10 mL). The resin was treated with (CF<sub>3</sub>)<sub>2</sub>CHOH:CH<sub>2</sub>Cl<sub>2</sub> (1:4, 10 mL) for 1 hour and rinsed with additional (CF<sub>3</sub>)<sub>2</sub>CHOH:CH<sub>2</sub>Cl<sub>2</sub> and CH<sub>2</sub>Cl<sub>2</sub>. The combined washings were then evaporated to yield the linear protected peptide with free C- and N-termini. The residue was dissolved in CH<sub>2</sub>Cl<sub>2</sub> (150 mL) and treated with BOP (0.22 g, 0.5 mmol) and DiPEA (0.17 mL, 1.0 mmol) and the solution was stirred overnight after which TLC indicated complete cyclization. The reaction mixture was concentrated and directly treated with TFA:TIS:H<sub>2</sub>O (95:2.5:2.5, 10 mL) for 90 minutes. The reaction mixture was added to MTBE:hexanes (1:1) and the resulting precipitate washed once more with MTBE:hexanes (1:1). The crude cyclic

peptide was lyophilized from <sup>t</sup>BuOH:H<sub>2</sub>O (1:1) and purified with reverse phase HPLC. Pure fractions were pooled and lyophilized to yield the desired cyclic lipopeptide products in >95% purity as white powders, typically in 10-45 mg quantities (4.2-30 % yield based on resin loading).

#### 2.6.4 Antibacterial Assays

Minimum inhibitory concentrations (MICs) were determined by broth microdilution according to CLSI guidelines.<sup>25</sup> Blood agar plates were inoculated with glycerol stocks of MRSA and *S. simulans* 22 followed by incubation for 16 hours at 37 °C and 30 °C respectively. Cation adjusted Mueller-Hinton broth (MHB) containing 10 mg L<sup>-1</sup> Mg<sup>2+</sup> was inoculated with individual colonies of MRSA and *S. simulans* and incubated for 16 hours at 220 RPM. The peptides were dissolved in MHB (10 mg L<sup>-1</sup> Mg<sup>2+</sup>) and serially diluted on polypropylene microtiter plates with a volume of 50 µL per well. Inoculated MHB (2x10<sup>5</sup> CFU.mL<sup>-1</sup>) containing 10 mg L<sup>-1</sup> Mg<sup>2+</sup> and varying concentrations of Ca<sup>2+</sup> was added to reach a total volume of 100 µL per well. The microtiter plates were sealed with an adhesive membrane and after 16 hours of incubation at 37 °C or 30 °C and 220 RPM the wells were visually inspected for bacterial growth. All reported MIC values result from three or more measurements.

#### 2.6.5 UDP-MurNAc-pentapeptide Accumulation Assay

MRSA USA 300 was grown until OD<sub>600</sub> = 0.5 in TSB supplemented with CaCl<sub>2</sub> (5.0 mM). Chloramphenicol (130 µg mL<sup>-1</sup>) was added and after incubation for 15 minutes at 37 °C, the culture was divided in 5 mL aliquots. Antibiotics were added at 10xMIC and one aliquot remained untreated. After 60 minutes, cells were separated from the medium and extracted with boiling d-H<sub>2</sub>O (1 mL) for 15 minutes. The suspensions were spun down and the supernatant was lyophilized. The resulting material was analyzed by HPLC applying a gradient from 100% eluent A (50 mM NaHCO<sub>3</sub>:5 mM Et<sub>3</sub>N, pH = 8.3) to 75% eluent A over 15 minutes using a C18 column (eluent B: MeOH). Formation of UDP-MurNAc-pentapeptide was confirmed by comparison with authentic material by HPLC, and LC-MS analysis

applying the same gradient with an adjusted eluent A (50 mM  $\text{NH}_4\text{HCO}_3$ :5 mM Et3N, pH = 8.3).

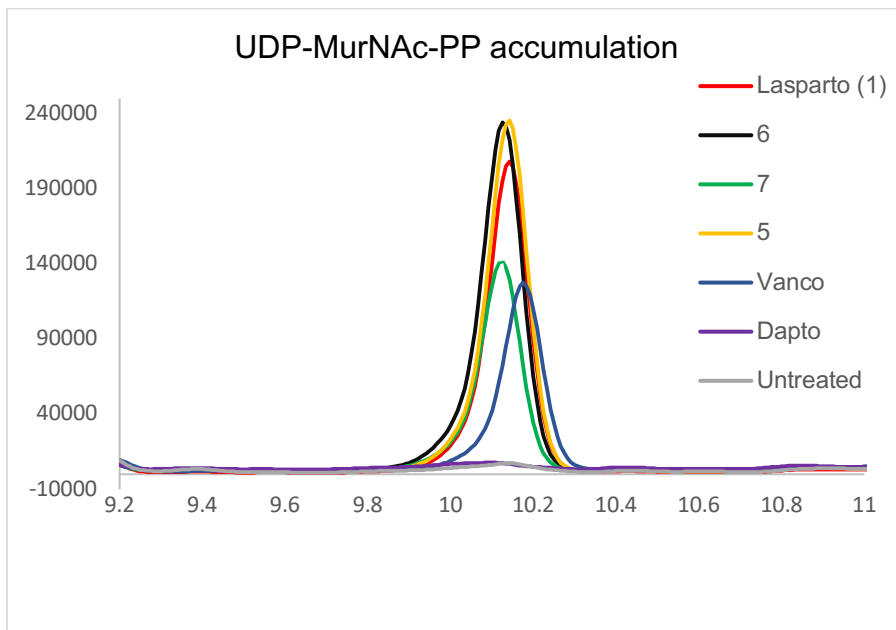


**Figure S1.** Analytical HPLC trace (zoom) for UDP-MurNac-pentapeptide accumulation assay. Treatment of MRSA USA 300 with **1**, **5-7** results in accumulation of UDP-MurNac-pentapeptide, an effect not observed with daptomycin. Vancomycin taken along as a control.

### 2.6.6 Crystallization and data collection

Lipopeptide **5** or **7** was solubilized in 5 mM HEPES pH 7.5, 10 mM  $\text{CaCl}_2$  and mixed 1:2 with  $\text{C}_{10}\text{-P}$ , to achieve a final concentration of 7.2 mM : 14.4 mM in presence of 10 % v/v PEG 200. Crystals were obtained by sitting drop vapour diffusion at 18 °C, by mixing 150 nL of the peptide solution with 150 nL of the reservoir solution, composed of 0.2 M sodium formate and 40 % v/v MPD for lipopeptide **5**, or 0.2 M cadmium chloride and 40 % v/v MPD for lipopeptide **7**, both supplemented by 10 % v/v PEG 200. Crystals were harvested without additional cryoprotectant and flash-cooled in liquid nitrogen. Datasets were collected at 100 K at the Diamond Light Source beamline I04-1 (lipopeptide **5**) or I04 (lipopeptide **7**).

### 2.6.7 Structure solution and refinement

The dataset of lipopeptide 5 was processed in the DIALS pipeline<sup>26</sup>, whereas autoPROC<sup>27</sup> was used for lipopeptide 7. The crystal of lipopeptide 7 was initially indexed in a hexagonal setting but based on the merging R-values the true symmetry appeared to be Primitive monoclinic with  $\beta = 120^\circ$ . The reflection file was therefore re-indexed accordingly, and parameters for pseudo-merohedral twinning were included in the structure refinement. Additional anisotropic correction was done for the datasets of both analogues in STARANISO.<sup>27</sup> Structures were solved by molecular replacement using PHASER,<sup>28</sup> and one copy (lipopeptide 5) or one dimer (lipopeptide 7) of laspartomycin C in complex with geranyl phosphate (PDB: 5O0Z)<sup>29</sup> was used as a search model. Models were manually improved in Coot,<sup>30</sup> refinement was performed using REFMAC<sup>31</sup> and Molprobity<sup>32</sup> was used for validation. Structures of lipopeptides 5 and 7 in complex with  $\text{Ca}^{2+}$  and  $\text{C}_{10}\text{-P}$  were deposited to the Protein Data Bank under the accession codes 7AG5 and 7ANY, respectively.

### 2.6.8 Bacterial cytological profiling

*B. subtilis* reporter strains were aerobically grown at 30 °C in LB supplemented with 2 mM  $\text{CaCl}_2$  and antibiotic (5  $\mu\text{g}/\text{ml}$  chloramphenicol or 100  $\mu\text{g}/\text{ml}$  spectinomycin). Overnight cultures were diluted 100x without antibiotics and GFP-fusion protein expression induced with xylose. At an  $\text{OD}_{600}$  of approximately 0.4 the cultures were diluted 10x in the same medium. At  $\text{OD}_{600}$  0.2-0.3 150  $\mu\text{l}$  cells were incubated with 12.5  $\mu\text{g}/\text{ml}$  laspartomycin C, 5  $\mu\text{g}/\text{ml}$  lipopeptide 6, or 2  $\mu\text{g}/\text{ml}$  lipopeptide 6. After 10 and 30 minutes 0.5  $\mu\text{l}$  cells were immobilized on microscope slides covered with a 1% agarose film and imaged immediately.

Fluorescence microscopy was carried out using a Zeiss Axiovert 200M equipped with a Zeiss Neofluar 100x/1.30 Oil Ph3 objective, a Lambda S light source (Shutter Instruments), a Photometrics Coolnap HQ2 camera, and Metamorph 6 software (Molecular Devices). Images were analyzed using ImageJ (National Institutes of Health) v.1.52a.



## References

- 1 P. Beyer, S. Paulin, *Bull. World Health Organ.* **2020**, 98, 151.
- 2 M. F. Chellat, L. Raguz, R. Riedl, *Angew. Chemie - Int. Ed.* **2016**, 55, 6600–6626.
- 3 M. N. Gwynn, A. Portnoy, S. F. Rittenhouse, D. J. Payne, *Ann. N. Y. Acad. Sci.* **2010**, 1213, 5–19.
- 4 R. Sauermaun, M. Rothenburger, W. Graninger, C. Joukhadar, *Pharmacology* **2008**, 81, 79–91.
- 5 R. M. Humphries, S. Pollett, G. Sakoulas, *Clin. Microbiol. Rev.* **2013**, 26, 759–780.
- 6 P. 't Hart, L. H. J. Kleijn, G. de Bruin, S. F. Oppedijk, J. Kemmink, N. I. Martin, *Org. Biomol. Chem.* **2014**, 12, 913–8.
- 7 S. D. Taylor, M. Palmer, *Bioorganic Med. Chem.* 2016, 24, 6253–6268.
- 8 A. Müller, M. Wenzel, H. Strahl, F. Grein, T. N. V Saaki, B. Kohl, *Proc. Natl. Acad. Sci. USA.* **2016**, 113, E7077-E7086.
- 9 F. Grein, A. Müller, K. M. Scherer, X. Liu, K. C. Ludwig, A. Klöckner, M. Strach, H. G. Sahl, U. Kubitscheck, T. Schneider, *Nat. Commun.* **2020**, 11, 1–11.
- 10 T. Schneider, K. Gries, M. Josten, I. Wiedemann, S. Pelzer, H. Labischinski, H. G. Sahl, *Antimicrob. Agents Chemother.* **2009**, 53, 1610–1618.
- 11 L. H. J. Kleijn, S. F. Oppedijk, P. T Hart, R. M. Van Harten, L. A. Martin-Visscher, J. Kemmink, E. Breukink, N. I. Martin, *J. Med. Chem.* **2016**, 59, 3569–3574.
- 12 L. H. J. Kleijn, H. C. Vlieg, T. M. Wood, J. Sastre Torano, B. J. C. Janssen, N. I. Martin, *Angew. Chemie - Int. Ed.* **2017**, 56, 16546–16549.
- 13 A. Diehl, T. M. Wood, S. Gebhard, N. I. Martin, G. Fritz, *Antibiotics* **2020**, 9, 1–16.
- 14 G. Manat, S. Roure, R. Auger, A. Bouhss, H. Barreteau, D. Mengin-Lecreulx, T. Touzé, *Microb. Drug Resist.* **2014**, 20, 199–214.
- 15 M. El Ghachi, N. Howe, C. Y. Huang, V. Olieric, R. Warshamanage, T. Touzé, D. Weichert, P. J. Stansfeld, M. Wang, F. Kerff, et al., *Nat. Commun.* **2018**, 9, 1–13.
- 16 S. D. Workman, L. J. Worrall, N. C. J. Strynadka, *Nat. Commun.* **2018**, 9, 765–776
- 17 T. M. Wood, N. I. Martin, *Medchemcomm* **2019**, 10, 634–646.
- 18 M. Strieker, M. A. Marahiel, *ChemBioChem* **2009**, 10, 607–616.
- 19 B. M. Hover, S. H. Kim, M. Katz, Z. Charlop-Powers, J. G. Owen, M. A. Ternei, J. Maniko, A. B. Estrela, H. Molina, S. Park, et al., *Nat. Microbiol.* **2018**, 3, 415–422.
- 20 Z. Sun, Z. Shang, N. Forelli, K. H. L. Po, S. Chen, S. F. Brady, X. Li, *Angew. Chemie - Int. Ed.* **2020**, 59, 19868–19872.
- 21 L. Corcilius, N. T. Elias, J. L. Ochoa, R. G. Linington, R. J. Payne, *J. Org. Chem.* **2017**, 82, 12778–12785.
- 22 T. M. Wood, K. Bertheussen, N. I. Martin, *Org. Biomol. Chem.* **2020**, 18, 514–517
- 23 M. Wenzel, M. P. Dekker, B. Wang, M. J. Burggraaf, W. Bitter, J. R. T. van Weering, L. W. Hamoen, *Commun. Biol.* **2021**, 4, 1–13.
- 24 K. Schirmer, Y. J. Eun, M. Dion, Y. Luo, J. D. Helmann, E. C. Garner, S. Walker, *Nat. Chem. Biol.* **2015**, 11, 38–45
- 25 D. Abmm, D. Tamma, J. Kirn, S. K. Cullen, *CLSI Suppl. M100* 2020, 30.

- 26 G. Winter, D. G. Waterman, J. M. Parkhurst, A. S. Brewster, R. J. Gildea, M. Gerstel, L. Fuentes-Montero, M. Vollmar, T. Michels-Clark, I. D. Young, et al., *Struct. Biol.* **2018**, *74*, 85–97.
- 27 G. Vonrhein, C.; Tickle, I.J.; Flensburg, C.; Keller, P.; Paciorek, W.; Sharff, A.; Bricogne, *Acta. Cryst.* **2018**, *74*, 43537.
- 28 A. J. McCoy, R. W. Grosse-Kunstleve, P. D. Adams, M. D. Winn, L. C. Storoni, R. J. Read, *J. Appl. Crystallogr.* **2007**, *40*, 658–674.
- 29 L. H. J. Kleijn, H. C. Vlieg, T. M. Wood, J. Sastre Toraño, B. J. C. Janssen, N. I. Martin, *Angew. Chemie - Int. Ed.* **2017**, *56*, 16546–16549.
- 30 P. Emsley, B. Lohkamp, W. G. Scott, K. Cowtan, *Acta Crystallogr. Sect. D Biol. Crystallogr.* **2010**, *66*, 486–501.
- 31 G. N. Murshudov, P. Skubák, A. A. Lebedev, N. S. Pannu, R. A. Steiner, R. A. Nicholls, M. D. Winn, F. Long, A. A. Vagin, *Acta Crystallogr. Sect. D Biol. Crystallogr.* **2011**, *67*, 355–367.
- 32 V. B. Chen, W. B. Arendall, J. J. Headd, D. A. Keedy, R. M. Immormino, G. J. Kapral, L. W. Murray, J. S. Richardson, D. C. Richardson, *Acta Crystallogr. Sect. D Biol. Crystallogr.* **2010**, *66*, 12–21.

# Chapter 3

## The contribution of achiral residues in the laspartomycin family of calcium-dependent lipopeptide antibiotics

*The growing threat of antibacterial resistance is a global concern. The so-called calcium-dependent lipopeptide antibiotics (CDAs) have emerged as a promising source of new antibiotic agents that are rich in structural and mechanistic diversity. Over forty unique CDAs have been identified to date and share a number of common features. Recent efforts in our group have provided new mechanistic and structural insights into the laspartomycin family of CDAs. We here describe investigations aimed at probing the role of the three glycine residues found in the laspartomycin peptide macrocycle. In doing so laspartomycin analogues containing the achiral 2-aminoisobutyric acid (AIB) as well as L- or D-alanine in place of glycine were prepared and their antibacterial activities evaluated*

Published in: Wood, T.M.; Bertheussen, K.; Martin, N.I. *Org. Biomol. Chem.* **2020**, *18*, 514-517

### 3.1 Introduction

The accelerated emergence of multi drug-resistant (MDR) bacteria is now considered a top priority and one of the most urgent global threats to human health.<sup>1</sup> According to a 2017 report from the Center for Disease Control and prevention (CDC) more than 2 million Americans acquire antibiotic-resistant infections each year leading to at least 23,000 deaths in the US alone.<sup>2</sup> Since the so-called “golden age” of antibiotic discovery spanning the 1940s-1960s, very few new antibiotics operating with novel modes of action have been introduced.<sup>3</sup> Notable in this regard is daptomycin, the preeminent calcium-dependent antibiotic (CDA) and the most recent first-in-class antibiotic to have entered the clinic.<sup>4,5</sup> Daptomycin’s precise mechanism of action is a topic of some debate.<sup>6,7</sup> By comparison, the mode of action of the structurally similar CDA laspartomycin C (Fig 1.) is more clearly understood.<sup>8,9</sup> Unlike daptomycin, laspartomycin C specifically targets the essential bacterial phospholipid undecaprenyl phosphate (C<sub>55</sub>-P). C<sub>55</sub>-P represents a novel target and to date there are no clinically approved antibiotics that operate by binding C<sub>55</sub>-P. Our group recently reported the first total synthesis of laspartomycin C<sup>10</sup> as well as the co-crystal structure of laspartomycin C bound to both calcium and a C<sup>10</sup> truncated analogue of C<sub>55</sub>-P.<sup>11</sup>

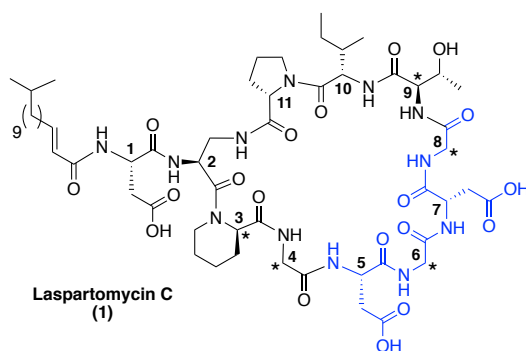


**Figure 1.** Laspartomycin C. Indicated with a star are the achiral or D-amino acids and highlighted in blue is the conserved Asp-X-Asp-Gly calcium binding motif common to the CDAs.

While the CDAs comprise a diverse family of lipopeptide antibiotics with varying mechanisms of action, they share a number of key structural similarities. These include the positioning of key achiral or D-amino acids as well as the highly conserved Asp-X-Asp-Gly motif.<sup>12</sup> This Asp-X-Asp-Gly sequence is essential for the calcium binding that all CDAs utilize in achieving their full antibacterial activity. In the absence of calcium, the activity of the CDAs is significantly reduced or completely lost.<sup>13</sup> Figure 1 presents the structure of laspartomycin C and highlights the structural features common to many CDAs.

At present there are more than 40 unique CDAs known and their structural diversity continues to provide great opportunity for discovery.<sup>14</sup> All CDAs, except for the newly reported malacidins, contain 10 amino acids in their macrocycle. Using the macrocycle of laspartomycin C as a reference point it can be noted that: 1) The majority of CDAs bear an L-amino acid at position 4 (usually an ornithine, alanine, aspartic acid, or  $\beta$ -methyl-aspartic acid) with the exception being the laspartomycins which include a glycine at position 4; 2) position 6 is nearly always a D-amino acid, again with the exception of the laspartomycins (as well as the related friulimicins and amphomycins) which contain glycine at position 6; and 3) 100% of CDAs contain a glycine at position 8.

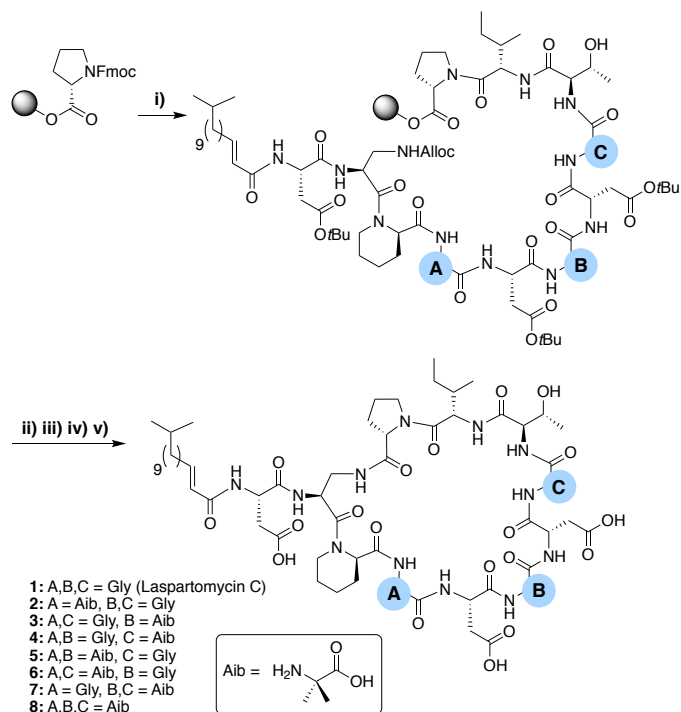
The inclusion of glycine at residues 4, 6, and 8 in the laspartomycin C macrocycle is unique among the CDAs. This observation prompted us to investigate the contribution that the absence of chirality at these positions has on antibacterial activity. To this end we investigated the introduction of the achiral 2-aminoisobutyric acid (Aib) at these positions as well as the introduction of either L- or D-alanine residues. We here describe the preparation and evaluation of a series of novel laspartomycin analogues that provide new stereochemical structure-activity insights at positions 4, 6, and 8.

### 3.2 Results and discussion

To evaluate the role of the three achiral centres in the laspartomycin C macrocycle we began by preparing a series of analogues containing the achiral amino acid 2-aminoisobutyric acid (Aib) at each position. These laspartomycin C variants were prepared using a robust combined solid- and solution-phase approach that our group as well as Payne and co-workers previously described (Scheme 1) and previous chapters.<sup>15,16</sup> The linear lipopeptide precursors were first assembled on solid support using the acid sensitive 2-chlorotrityl (CTC) resin. Starting from C-terminal Pro<sup>11</sup> each peptide was assembled using standard Fluorenylmethyloxycarbonyl (Fmoc)-SPPS strategies with the notable introduction of an allyloxycarbonyl (Alloc)-side chain protected L-diaminopropionic acid (L-Dap) residue at position 2. Also, for analogues containing Gly at positions 6 and/or 8 (compounds **1-6**) 2,4-dimethoxybenzyl (DMB)-Gly was employed to avoid aspartamide formation. Following N-terminal lipidation, the Alloc side chain protecting of L-Dap was removed and the partially protected peptide released from the resin using mildly acidic conditions. The partially protected peptide was then cyclized at high dilution by treatment with (benzotriazol-1-yloxy)tris(dimethylamino)phosphoniumhexafluorophosphate and N,N-diisopropylethylamine (BOP/DiPEA) resulting in the clean formation of the macrocyclic product. Global deprotection followed by RP-HPLC purification provided the various laspartomycin analogues in yields ranging from 5-13%.

To assess the contribution of the achiral positions 4, 6, and 8, analogues **2-8** were prepared wherein one or more of the glycine residues was replaced by the achiral Aib. The rationale for this replacement related to the previously reported ability of the Aib residue to predispose peptides towards their active conformation(s).<sup>17</sup> The antimicrobial activity of analogues **2-8** was compared with that of authentic laspartomycin C (Table 1) using a serial dilution assay employing a clinically relevant strain of Methicillin-resistant *Staphylococcus aureus* (MRSA). Analogues **2** and **3** were found to exhibit calcium-dependent activity, albeit significantly less than laspartomycin C, while analogues **4-8**, were essentially devoid of activity. Interesting, analogues **2** and **3**, both containing a single Aib at position **4** and **6** respectively, maintain some activity. Conversely, Aib substitution at position 8 as in analogue **4** led to complete loss of activity. Notably,

analogue **8** containing Aib at all three positions, exhibits modest activity while showing no  $\text{Ca}^{2+}$  dependency. These results indicate that modification at positions 4 and 6 can compensate for an otherwise detrimental modification at position 8.



**Scheme 1.** i) Fmoc SPPS; ii)  $\text{Pd}[(\text{C}_6\text{H}_5)_3\text{P}]_4$ ,  $\text{C}_6\text{H}_5\text{SiH}_3$ ,  $\text{CH}_2\text{Cl}_2$ , 1h; iii) HFIP,  $\text{CH}_2\text{Cl}_2$ , 1h; (v) BOP, DIPEA,  $\text{CH}_2\text{Cl}_2$ , 16h; v) TFA, TIS,  $\text{H}_2\text{O}$ , 1h (Fmoc-D-Thr was employed without side chain protection and incorporated without incident).

**Table 1.** MIC<sup>a</sup> values for laspartomycin C, compounds 2-8

Compound	[Ca <sup>2+</sup> ] (mM)			
	0	2.5	5	10
1 (LaspC)	>128	8	4	2
2	>128	16	16	16
3	>128	64	32	16
4	>128	>128	>128	>128
5	64	64	64	64
6	>128	>128	>128	>128
7	>128	>128	>128	>128
8	64	64	64	64

<sup>a</sup>Minimum inhibitory concentration reported in µg/mL against MRSA USA 300 at calcium concentration indicated.

All compounds tested in triplicate

All known CDAs contain a glycine at position 8 which is part of the Asp-X<sub>6</sub>-Asp-Gly<sub>8</sub> calcium binding region. It therefore stands to reason that changes at position 8 significantly impact in the peptide's ability to chelate calcium and bind to its bacterial target. In this regard it is notable that position 6, also part of the CDA calcium binding region, is more amenable to variation. In the case of the laspatomycins, friulimicins, and amphomycins the inclusion of Gly at position 6 sets them apart from the majority of other CDAs which generally contain a D-amino acid at this site. In the case of daptomycin D-alanine is found at position 6 while in the A54145 class it is D-lysine and in the confusingly named "CDA-class" it is D-phenylglycine.<sup>18</sup> With this in mind we prepared four additional analogues examining the effect in introducing L- or D-alanine at positions 4 and 6 (Fig 2).



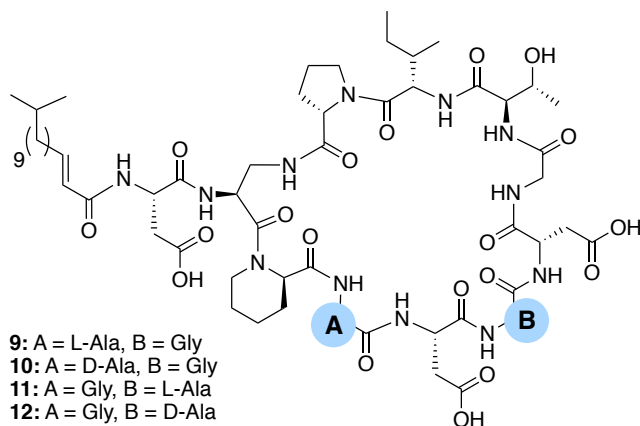


**Figure 2.** Laspartomycin C analogues prepared to investigate the effect of introducing L- or D-alanine at positions 4 and 6.

The antimicrobial activity of analogues **9-12** was compared with that of authentic laspartomycin C (Table 2). Using the same activity assay employing MRSA USA300 as an indicator strain, all four analogues were found to be more active than their Aib containing counterparts with analogues **10** and **12** showing activity on par with that of laspartomycin itself. Interesting, the introduction of L- or D-alanine at position 4 yields compounds of similar activity while at position 6 the D-Ala variant was 16-fold more active than the L-analogue. These findings further demonstrate the importance of a D-stereocenter at position 6 of the CDA calcium-binding motif.

**Table 2.** MIC<sup>a</sup> values for laspartomycin C, compounds **9-12**

Compound	[Ca <sup>2+</sup> ]			
	0	2.5	5	10
<b>1</b> (LaspC)	>128	8	4	2
<b>9</b>	>128	16	8	4
<b>10</b>	>128	16	8	2
<b>11</b>	>128	64	32	16
<b>12</b>	64	16	8	1

<sup>a</sup>Minimum inhibitory concentration reported in µg/mL against MRSA USA 300 at calcium concentration indicated. All compounds tested in triplicate

### 3.3 Conclusion

In summary, we have generated a focused library of laspartomycin C analogues designed to explore the contribution of the achiral 4, 6, and 8 positions on antibacterial activity. Using a combined solid- and solution-phase approach (as described in Chapter 2), analogues were first prepared wherein positions 4, 6 and 8 were modified to contain the achiral amino acid Aib. These analogues showed a significant reduction in activity compared to the parent compound. Incorporation of Aib at position 8 led to complete loss of activity while the same modification at positions 4 or 6 led to analogues that retained some activity. A second series of analogues incorporating either D or L-alanine at positions 4 and 6 were also prepared. The introduction of both D- and L-Ala at position 4 led to compounds that showed activity similar to laspartomycin C. However, at position 6 the D-Ala variant is 16-times more active than the L-Ala and even showed slightly better activity than laspartomycin C.

While the various members of the CDA family contain diverse amino acids at position 4 they are always either glycine or a L-amino acid. Our findings indicate that the incorporation of D-Ala at position 4 does not negatively affect activity. Position 6 plays a key role in the calcium-binding motif (Asp-X<sub>6</sub>-Asp-Gly<sub>8</sub>) and is always either a glycine or a D-amino acid. Our findings demonstrate that positions 4 and 6 of Laspartomycin C are amenable to substitution provided the correct stereochemical constraints are respected. To this end ongoing studies in our laboratory are aimed at establishing whether the antibacterial activity of the laspartomycins can be enhanced by structural variation at these positions.

## 3.4 Experimental

### 3.4.1 Reagents and General Methods

All reagents employed were of American Chemical Society (ACS) grade or finer and were used without further purification unless otherwise stated. D-amino acids and 2-chlorotrityl resin was obtained from Iris Biotech GmbH, Egg PG and 0:6 PA was obtained from INStruChemie BV. C<sub>10</sub>-P lithium salt was obtained from Sigma Aldrich and lyophilized from warm <sup>t</sup>BuOH:H<sub>2</sub>O (1:1) to obtain a white powder with increased aqueous solubility.

### 3.4.2 Instrumentation for Compound Characterization

HRMS analysis was performed on a Shimadzu Nexera X2 UHPLC system with a Waters Acquity HSS C18 column (2.1 × 100 mm, 1.8 μm) at 30 °C and equipped with a diode array detector. The following solvent system, at a flow rate of 0.5 mL/min, was used: solvent A, 0.1 % formic acid in water; solvent B, 0.1 % formic acid in acetonitrile. Gradient elution was as follows: 95:5 (A/B) for 1 min, 95:5 to 15:85 (A/B) over 6 min, 15:85 to 0:100 (A/B) over 1 min, 0:100 (A/B) for 3 min, then reversion back to 95:5 (A/B) for 3 min. This system was connected to a Shimadzu 9030 QTOF mass spectrometer (ESI ionisation) calibrated internally with Agilent's API-TOF reference mass solution kit (5.0 mM purine, 100.0 mM ammonium trifluoroacetate and 2.5 mM hexakis(1H,1H,3H-tetrafluoropropoxy)phosphazine) diluted to achieve a mass count of 10000.

Purity of the peptides was confirmed to be ≥ 95% by analytical RP-HPLC using a Shimadzu Prominence-i LC-2030 system with a Dr. Maisch Reprosil Gold 120 C18 column (4.6 × 250 mm, 5 μm) at 30 °C and equipped with a UV detector monitoring at 214 nm. The following solvent system, at a flow rate of 1 mL/min, was used: solvent A, 0.1 % TFA in water/acetonitrile, 95/5; solvent B, 0.1 % TFA in water/acetonitrile, 5/95. Gradient elution was as follows: 95:5 (A/B) for 2 min, 95:5 to 0:100 (A/B) over 55 min, 0:100 (A/B) for 2 min, then reversion back to 95:5 (A/B) over 1 min, 95:5 (A/B) for 2 min.

The compounds were purified *via* preparative HPLC using a BESTA-Technik system with a Dr. Maisch Reprosil Gold 120 C18 column (25 × 250 mm, 10 μm) and equipped with an ECOM Flash UV detector monitoring at 214 nm. The following solvent system, at a flow rate of 12 mL/min, was

used: solvent A, 0.1 % TFA in water/acetonitrile 95/5; solvent B, 0.1 % TFA in water/acetonitrile 5/95. Gradient elution was as follows: 95:5 (A/B) for 2 min, 95:5 to 0:100 (A/B) over 55 min, 0:100 (A/B) for 2 min, then reversion back to 95:5 (A/B) over 1 min, 95:5 (A/B) for 2 min.

### 3.4.2 Solid Phase Peptide Synthesis

Chlorotrityl resin (5.0 g, 1.60 mmol/g) was loaded with Fmoc-Pro-OH. Resin loading was determined to be 0.41-0.62 mmol.g<sup>-1</sup>. Linear peptide encompassing Pro<sup>11</sup> to Asp<sup>1</sup> were assembled manually *via* standard Fmoc solid-phase peptide synthesis (SPPS) (resin bound AA:Fmoc-AA:BOP:DiPEA, 1:4:4:8 molar eq.) on a 0.1 mmol scale. DMF was used as solvent and Fmoc deprotections were carried out with piperidine:DMF (1:4 v:v). Amino acid side chains were protected as follows: tBu for Asp, Alloc for DAP, and DMB for Gly<sup>6</sup> and Gly<sup>8</sup>. D-allo-Thr was introduced without side chain protection. Following coupling and Fmoc deprotection of Asp<sup>1</sup>, N-terminal acylation was achieved by coupling (E)-13-methyltetradec-2-enoic acid using the same coupling conditions used for SPPS. The resin-bound, Alloc protected intermediate was next washed with CH<sub>2</sub>Cl<sub>2</sub> and treated with Pd(PPh<sub>3</sub>)<sub>4</sub> (30mg, 0.03 mmol) and PhSiH<sub>3</sub> (0.30 mL, 3.0 mmol) in CH<sub>2</sub>Cl<sub>2</sub> (*ca.* 7 mL) under argon for 1 hour. The resin was subsequently washed with CH<sub>2</sub>Cl<sub>2</sub> (5x10 mL), followed by a solution of diethyldithiocarbamic acid trihydrate sodium salt (5 mg mL<sup>-1</sup> in DMF, 5x10 mL), and DMF (5x10 mL). The resin was treated with (CF<sub>3</sub>)<sub>2</sub>CHOH:CH<sub>2</sub>Cl<sub>2</sub> (1:4, 10 mL) for 1 hour and rinsed with additional (CF<sub>3</sub>)<sub>2</sub>CHOH:CH<sub>2</sub>Cl<sub>2</sub> and CH<sub>2</sub>Cl<sub>2</sub>. The combined washings were then evaporated to yield the linear protected peptide with free C- and N-termini. The residue was dissolved in CH<sub>2</sub>Cl<sub>2</sub> (150 mL) and treated with BOP (0.22 g, 0.5 mmol) and DiPEA (0.17 mL, 1.0 mmol) and the solution was stirred overnight after which TLC indicated complete cyclization. The reaction mixture was concentrated and directly treated with TFA:TIS:H<sub>2</sub>O (95:2.5:2.5, 10 mL) for 90 minutes. The reaction mixture was added to MTBE:hexanes (1:1) and the resulting precipitate washed once more with MTBE:hexanes (1:1). The crude cyclic peptide was lyophilized from <sup>t</sup>BuOH:H<sub>2</sub>O (1:1) and purified with reverse phase HPLC. Pure fractions were pooled and lyophilized to yield the

desired cyclic lipopeptide products in >95% purity as white powders, typically in 10-45 mg quantities (4.2-30 % yield based on resin loading).

### 3.4.3 Antibacterial Assays

Minimum inhibitory concentrations (MICs) were determined by broth microdilution according to CLSI guidelines.<sup>19</sup> Blood agar plates were inoculated with glycerol stocks of MRSA and *S. simulans* 22 followed by incubation for 16 hours at 37 °C and 30 °C respectively. Cation adjusted Mueller-Hinton broth (MHB) containing 10 mg L<sup>-1</sup> Mg<sup>2+</sup> was inoculated with individual colonies of MRSA and *S. simulans* and incubated for 16 hours at 220 RPM. The peptides were dissolved in MHB (10 mg L<sup>-1</sup> Mg<sup>2+</sup>) and serially diluted on polypropylene microtiter plates with a volume of 50 µL per well. Inoculated MHB (2x10<sup>5</sup> CFU.mL<sup>-1</sup>) containing 10 mg L<sup>-1</sup> Mg<sup>2+</sup> and varying concentrations of Ca<sup>2+</sup> was added to reach a total volume of 100 µL per well. The microtiter plates were sealed with an adhesive membrane and after 16 hours of incubation at 37 °C or 30 °C and 220 RPM the wells were visually inspected for bacterial growth. All reported MIC values result from three or more measurements.

## References

- 1 J. O'Neill, *Rev. Antimicrob. Resist.*, **2014**, 1-16.
- 2 CDC Antibiotic use in the United States, **2017**: Progress and Opportunities. Atlanta, GA: US Department of Health and Human Services, CDC; 2017
- 3 M. N. Gwynn, A. Portnoy, S. F. Rittenhouse and D. J. Payne, *Ann. N. Y. Acad. Sci.*, **2010**, 1213, 5-19.
- 4 A. E. Muller and I. C. Gyssens, *Kucers Use Antibiot. A Clin. Rev. Antibacterial, Antifung. Antiparasit. Antivir. Drugs*, Seventh Ed., **2017**, 2, 866-907.
- 5 R. Sauer mann, M. Rothenburger, W. Graninger and C. Joukhadar, *Pharmacology*, **2008**, 81, 79-91.
- 6 R. H. Baltz, *Curr. Opin. Chem. Biol.*, **2009**, 13, 144-151.
- 7 G. Seydlová, A. Sokol, P. Lišková, I. Konopásek and R. Fišer, *Antimicrob. Agents Chemother.*, **2019**, 63, 1-14.
- 8 H. Naganawa, M. Hamada, K. Maeda, Y. Okami, T. Takeuchi and H. Umezawa, *J. Antibiot. (Tokyo)*, **1968**, XXI, 55-62.
- 9 D. B. Borders, R. A. Leese, H. Jarolmen, N. D. Francis, A. A. Fantini, T. Falla, J. C. Fiddes and A. Aumelas, *J. Nat. Prod.*, **2007**, 70, 443-446.
- 10 L. H. J. Kleijn, S. F. Oppedijk, P. T Hart, R. M. Van Harten, L. A. Martin-Visscher, J. Kemmink, E. Breukink and N. I. Martin, *J. Med. Chem.*, **2016**, 59, 3569-3574.
- 11 L. H. J. Kleijn, H. C. Vlieg, T. M. Wood, J. Sastre Toraño, B. J. C. Janssen and N. I. Martin, *Angew. Chemie - Int. Ed.*, **2017**, 56, 16546-16549.
- 12 R. H. Baltz, V. Miao, S. K. Wrigley and V. Miao, *Nat. Prod. Rep.*, **2005**, 717-741.
- 13 M. Strieker and M. A. Marahiel, *ChemBioChem*, **2009**, 10, 607-616.
- 14 T. M. Wood and N. I. Martin, *Medchemcomm*, **2019**, 10, 643-646
- 15 L. H. Kleijn, S. F. Oppedijk, P. 't Hart, R. M. van Harten, L. A. Martin-Visscher, J. Kemmink, E. Breukink and N. I. Martin, *J. Med. Chem.*, **2016**, 7, 3569-3574.
- 16 L. Corcilius, N. T. Elias, J. L. Ochoa, R. G. Linington and R. J. Payne, *J. Org. Chem.*, **2017**, 82, 12778-12785.
- 17 J. Michael Conlon, R. Al-Kharrge, E. Ahmed, H. Raza, S. Galadari and E. Condamine, *Peptides*, **2007**, 28, 2075-2080.
- 18 T. M. Wood and N. I. Martin, *Medchemcomm*, **2019**, 10, 634-646.
- 19 Clinical Laboratory Standard Institute, *Methods for Dilution Antimicrobial Susceptibility Tests for Bacteria That Grow Aerobically; Approved Standard – Ninth Edition Performance Standards for Antimicrobial Susceptibility Testing; Twenty-Second Informational Supplement*, **2012**, vol. 32.

# Chapter 4

## A convenient chemoenzymatic preparation of chimeric macrocyclic peptide antibiotics with potent activity against Gram-negative pathogens

*The continuing rise of antibiotic resistance is a global concern and threatens to undermine many aspects of modern medical practice. This threat recently led the World Health Organization (WHO) to announce a list of priority pathogens against which current antibiotics are increasingly ineffective. Among these pathogens, it is exclusively the Gram-negative species that are labelled as “critical”, the highest threat level on the WHO list. Most notable are drug-resistant strains of Acinetobacter, Pseudomonas, and various Enterobacteriaceae (including Klebsiella and E. coli) causing severe and often deadly bloodstream and pulmonary infections. To address this threat, novel antibiotics that utilize unexploited bacterial targets are urgently needed. Over the past decade a number of reports have highlighted the antibacterial potential of macrocyclic peptides that target outer membrane (OM) proteins essential for Gram-negative bacterial cell viability. Such OM targets include  $\beta$ -barrel proteins such as LptD and BamA. In a recent development it was found that the antibacterial activity of macrocyclic peptidomimetics of the antimicrobial peptide protegrin I are dramatically enhanced upon covalently linking to the polymyxin E nonapeptide (PMEN) motif. In this study we describe a convergent, chemoenzymatic route that allows for the convenient preparation of such conjugates. Specifically, we investigated the use of both amide bond formation and the azide-alkyne “click” ligation for connecting a BamA targeting macrocyclic peptide to a PMEN building block (obtained by enzymatic degradation of the full length polymyxin antibiotic). The conjugates obtained via both approaches display potent antibacterial activity against a range of Gram-negative pathogens including a number of multi-drug resistant isolates.*

Published in: †Wood, T. M.; †Slingerland, C. J.; Martin, N. I. *J. Med. Chem.* **2021**, *64*, 15, 10890-10899

†Indicates equal contribution.

## 4.1 Introduction

While the rate at which multi- and pan-drug resistant bacterial infections climb worldwide, the antibiotic development pipeline offers little reason for optimism.<sup>1</sup> Most notable in this regard is the lack of effective antibiotic therapies available for the treatment of infections due to Gram-negative pathogens.<sup>2,3</sup> To address this shortfall, antibiotics that operate *via* unique and unexploited mechanisms are desperately needed. While in recent years there has been some progress made in the development of novel treatments for Gram-positive infections, the same cannot be said for anti-Gram-negative agents with the last major advancement coming nearly four decades ago with the clinical introduction of the carbapenems.<sup>2,4,5</sup> The development of antibiotics for Gram-negative bacteria is particularly challenging given the presence of their outer membrane (OM) which is composed of an inner phospholipid leaflet and a lipopolysaccharide (LPS) decorated outer leaflet.<sup>6</sup> This OM provides an effective barrier, shielding the bacterial cell from many antibiotics. Notably, the polymyxin antibiotics, typified by the clinically used polymyxin E, more commonly known as colistin 1 (Fig. 1A), are cyclic lipopeptides that act specifically against Gram-negative bacteria *via* a mode of action involving binding to Lipid A, the lipid membrane anchor of LPS.<sup>7-9</sup> Despite colistin's inherent (nephro)toxicity, its use has been revived in recent years due to the lack of effective alternative treatments.<sup>10,11</sup> Interestingly, polymyxin derivatives that lack the lipophilic fatty acyl chain are devoid of antimicrobial activity but can in some cases potentiate the action of other antibiotics by permeabilizing the Gram-negative OM.<sup>12-14</sup> Best studied in this regard are the cyclic nonapeptide fragments of polymyxin B and E (PMBN and PMEN) which have also been investigated as leads for the development of antibiotic adjuvants.<sup>12,15-17</sup>

The Gram-negative OM contains a select number of surface-exposed  $\beta$ -barrel outer membrane proteins (OMPs) that are essential for bacterial viability. In recent years increasing efforts have been made to identify novel antibiotics that operate by targeting Gram-negative OMPs. In principle, such antibiotics would circumvent two of the main impediments presented by Gram-negative bacterial cells, namely OM penetration and efflux-pump mediated export. Most notable among OMP-targeting antibiotics is the  $\beta$ -hairpin peptidomimetic Murepavadin 2 (Fig. 1B) first



reported by Robinson and co-workers and subsequently taken into clinical development by Polyphor for the treatment of *P. aeruginosa* infections.<sup>18</sup> Murepavadin specifically targets the OMP LptD, and in doing so interferes with OM biogenesis leading to selective killing of *Pseudomonas* spp.<sup>18,19</sup> In a recent study the same group described a new series of  $\beta$ -hairpin peptidomimetics of the antimicrobial peptide protegrin I that demonstrated a moderate but broader Gram-negative specific antibacterial effect.<sup>20</sup> More notable, however, was the finding that when covalently linked to the PMEN, the antibacterial activity of these macrocyclic peptides is enhanced by many orders of magnitude.<sup>20,21</sup> Interestingly, mechanistic studies revealed that these bicyclic conjugates, including compound 3 illustrated in Figure 1C, function by targeting another OMP, namely BamA, a key component of the  $\beta$ -barrel assembly machine (BAM) that plays an essential role in OMP folding in Gram-negative bacteria.<sup>22-25</sup> Importantly, these new BamA-targeting macrocyclic peptide conjugates were found to retain their potent activity *in vivo*<sup>20</sup> and represent a promising new class of antimicrobials for further development

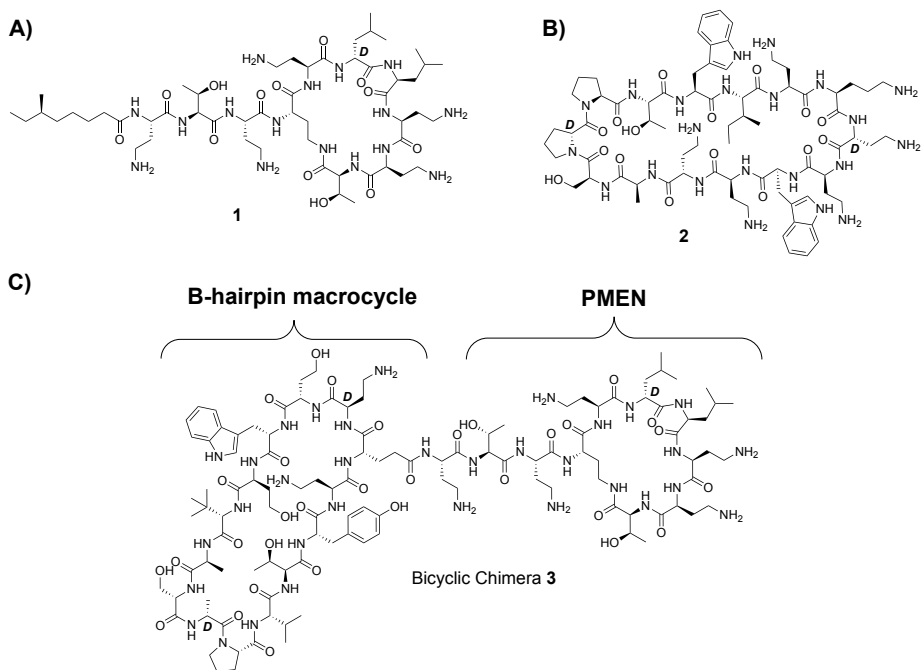
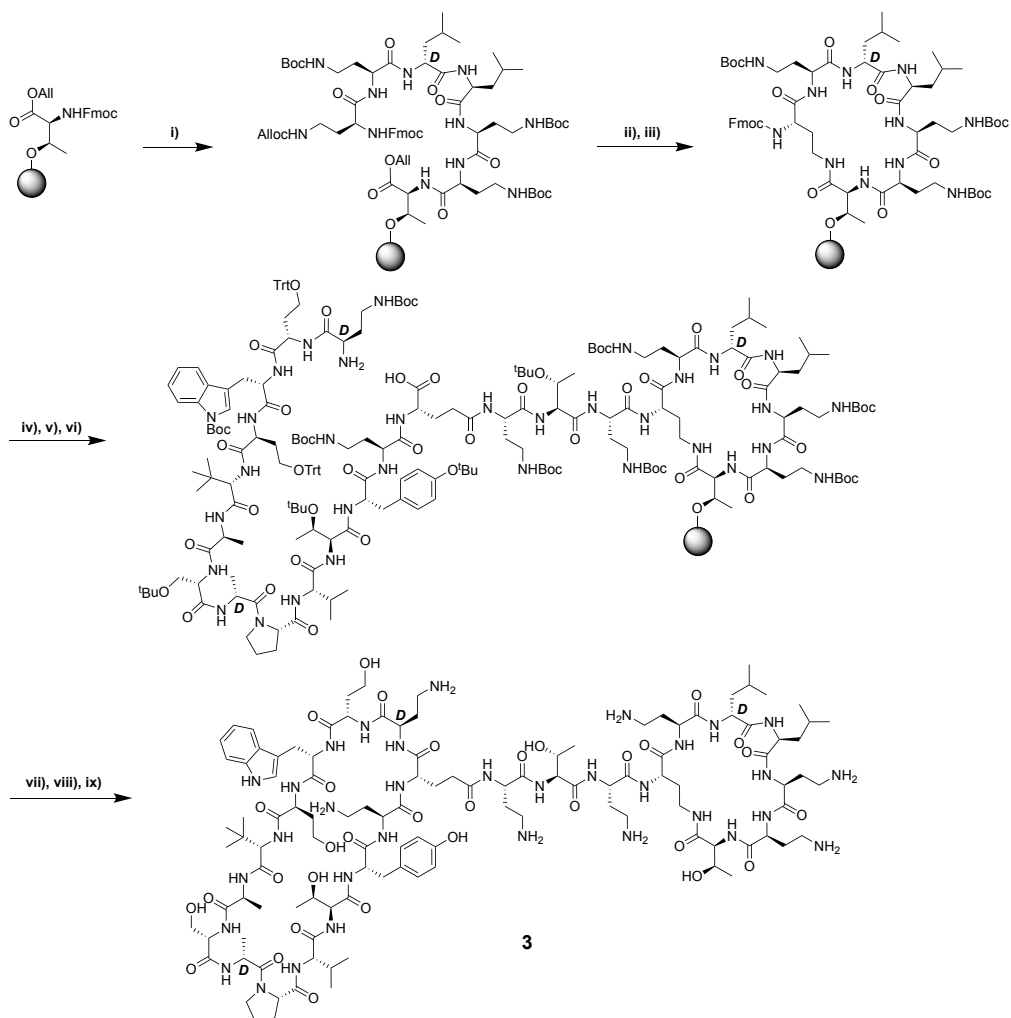


**Figure 1.** Macrocyclic peptide antibiotics targeting the Gram-negative OM. **A)** Structure of clinically used colistin; **B)** Structure of the protegrin I  $\beta$ -hairpin peptidomimetic murepavadin; **C)** Representative structure of recently reported chimeric antibiotics consisting of  $\beta$ -hairpin mimetic ligated to the nonapeptide derived from colistin.

The synthesis reported for the preparation of the PMEN-conjugated BamA targeting macrocyclic peptides relies completely upon a linear SPPS approach (Scheme 1). The PMEN macrocycle is first assembled on resin after which the remaining seventeen amino acids are sequentially added. Following a selective allyl ester removal and cleavage from the resin, the BamA targeting macrocycle is subsequently formed in solution followed by global deprotection to yield the desired bicyclic conjugate. Given our interest in macrocyclic peptide antibiotics and semisynthesis<sup>26-29</sup> we were drawn to explore alternative strategies for the preparation of these constructs. Specifically, rather than synthesizing the PMEN motif “from scratch” we considered a chemoenzymatic approach involving degradation of readily available colistin followed by coupling to the BamA targeting

macrocycle. In addition, as a means of further simplifying both the synthesis of the BamA targeting macrocycle and subsequent assembly of the bicyclic constructs, we also explored the application of the well-established azide-alkyne ligation.<sup>30,31</sup> We here report the applicability of these alternative synthetic approaches to provide convenient access to both the original class of BamA targeting conjugates as well as new triazole linked variants with varying spacer lengths. The antibacterial activity of these constructs was evaluated against a panel of Gram-negative bacteria, including several drug-resistant isolates, confirming the activity of the parent compound as well as revealing new analogues of similar potency.

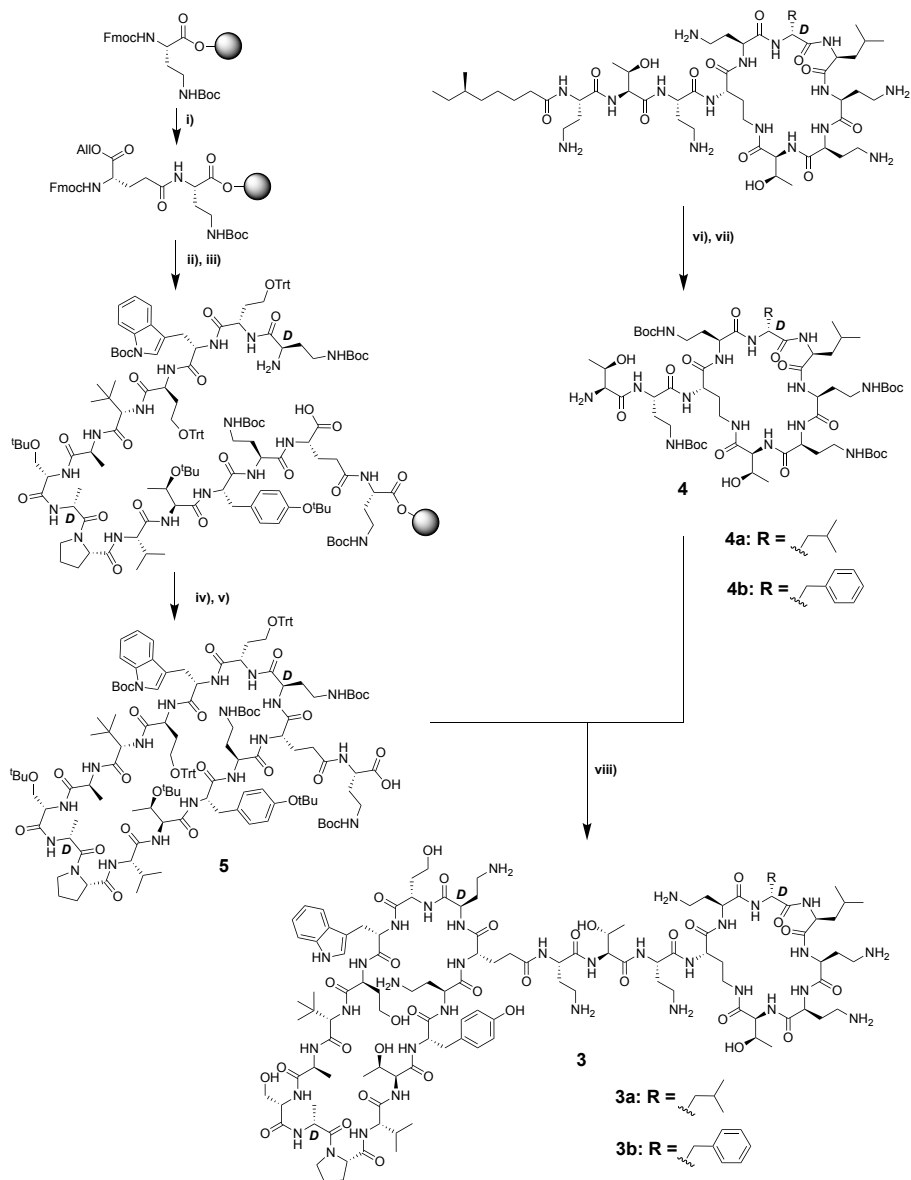


**Scheme 1.** Published synthesis of bicyclic chimera **3**. i) Fmoc SPPS on CTC resin till Fmoc-Dab(Alloc)-OH; ii) Alloc/Allyl deprotection iii) ring closing on resin; iv) Fmoc SPPS till Fmoc-Glu-Oallyl; v) Fmoc SPPS till final Fmoc-D-Dab(Boc)-OH + removal of final Fmoc; vi) Glu-Oallyl deprotection; vii) Cleavage from resin; viii) solution phase cyclization; ix) TFA deprotection and RP-HPLC purification.

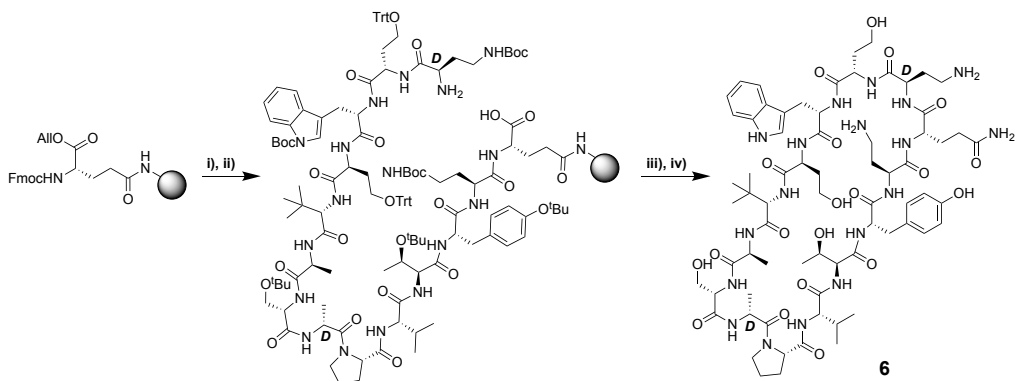
## 4.2 Results and Discussion

As illustrated in Scheme 1, the published synthesis of the bicyclic peptides was accomplished completely by use of SPPS. As an alternative, we were interested in examining whether the PMEN fragment could instead be sourced by degradation of the readily available parent colistin (polymyxin E) and then coupled to the second macrocycle (Scheme 2). As a proof of concept for this approach we selected bicyclic chimera **3**, previously identified as a lead compound by the Polyphor group.<sup>20</sup> To begin, PMEN was obtained by following a previously described protocol of an enzymatic degradation of the parent polymyxin using readily available ficin.<sup>32,33</sup> The crude PMEN thus obtained was then selectively protected at the four Dab side chains by treating with 1-(Boc-oxyimino)-2-phenylacetonitrile (Boc-ON) in water/dioxane/NEt<sub>3</sub> (1:1:1) to yield PMEN-Boc4 (**4a**).<sup>33</sup> In parallel, the protected  $\beta$ -hairpin macrocyclic peptide (**5**) was obtained by SPPS starting from Fmoc-Dab(Boc)-OH loaded onto CTC resin. The next amino acid to be added was the orthogonally protected Fmoc-Glu(OH)-OAll which was coupled *via* its free sidechain carboxylate. The remaining residues were added in linear fashion followed by allyl ester cleavage using Pd(0). Subsequent on-resin cyclization was found to proceed cleanly after which the protected peptide macrocycle was detached from the resin using mild acid conditions to yield protected intermediate **5**. Analysis of crude **5** indicated that the desired product was the major species in good purity, and it was therefore used directly in the subsequent coupling with PMEN-Boc4 (**4a**). The solution phase coupling of fragments **4a** and **5** was accomplished by stirring overnight in DCM with activation using BOP/DiPEA. The following morning LC-MS analysis indicated clean formation of the bicyclic conjugate after which TFA deprotection and HPLC purification provided compound **3a**. Using the same approach, the corresponding conjugate incorporating the PMBN macrocycle, compound **3b**, was also successfully prepared by starting from PMBN-Boc4 **4b**. In addition, the 14-mer monocyclic  $\beta$ -hairpin peptidomimetic (**6**) was prepared to serve as a reference compound. Briefly, Rink amide resin was loaded with the free sidechain of Fmoc-Glu(OH)-OAll followed by coupling of the next 13 amino acids (essentially following the same steps as in scheme 2). Subsequent allyl ester removal and on-resin cyclization followed by strong

acid cleavage/deprotection then provided compound **6**, terminated as an amide at the glutamic acid side chain position (Scheme 3).



**Scheme 2. Convergent, chemoenzymatic synthesis of bicyclic chimera 3.** i) Fmoc SPPS starting on CTC resin and coupling to the free sidechain of Fmoc-Glu-OAllyl (BOP/DIPEA); ii) SPPS till D-Dab(Boc) + removal of final Fmoc; iii) Allyl deprotection with Pd; iv) On resin cyclization (BOP/DIPEA); v) Resin cleavage (HFIP/DCM); vi) Enzymatic digestion by ficin; vii) Site-selective bocylation by Boc-ON; viii) Solution phase coupling, using BOP/DIPEA; HPLC purification.



**Scheme 3. Synthesis of monocyclic peptide 6.** i) Fmoc SPPS starting from Rink amide resin loaded with Fmoc-Glu-OAll *via* carboxyl side chain; ii) Allyl ester deprotection with Pd; iii) On resin cyclization (BOP/DIPEA); iv) TFA deprotection + resin cleavage followed by RP-HPLC purification.

The antibacterial activity of bicyclic constructs **3a** and **3b** was assessed against a range of Gram-negative pathogens including several drug-resistant isolates (Table 1). For comparison, colistin, PMEN, and monocyclic  $\beta$ -hairpin mimetic **6** were also tested. As reported in the literature, **3a** was found to exhibit potent antibacterial activity, on par or superior to that of colistin, among the strains tested. In addition, the activity of PMBN conjugate **3b** was found to largely mirror that of the PMEN conjugate **3a**. Also, of note was the confirmation that activity of bicyclic constructs was not diminished against colistin-resistant strains possessing *mcr*-type plasmids that encode for phosphoethanolamine transferases that modify the structure of lipid A. Both PMEN and the monocyclic  $\beta$ -hairpin mimetic **6** were also assessed, neither of which demonstrated appreciable antibacterial activity. Furthermore, none of the compounds tested showed any activity against a representative Gram-positive strain (MRSA USA300).

**Table 1.** MIC<sup>a</sup> values compounds **3a**, **3b**, **6**, colistin and PMEN

	<b>3a</b>	<b>3b</b>	Colistin	<b>6</b>	PMEN
<i>A. baumannii</i> ATCC 9955	0.2	0.2	0.4	>64	>64
<i>A. baumannii</i> ATCC	0.4	0.4	0.4	>64	>64
<i>A. baumannii</i> NDM2	0.1	0.2	0.2	>64	>64
<i>A. baumannii</i> MDR	0.2	0.4	0.4	>64	>64
<i>K. pneumoniae</i> ATCC	0.2	0.2	0.1	>64	>64
<i>K. pneumoniae</i> NDM1	0.8	0.4	1.6	>64	>64
<i>P. aeruginosa</i> ATCC	0.8	1.6	1.6	>64	>64
<i>P. aeruginosa</i> NRZ	0.8	0.8	0.8	>64	>64
<i>P. aeruginosa</i> NDM1	0.4	0.8	0.4	>64	>64
<i>P. aeruginosa</i> M-120	1.6	1.6	0.8	>64	32
<i>E. coli</i> ATCC 35218	0.2	0.1	0.1	>64	>64
<i>E. coli</i> NDM1	0.1	0.1	0.1	>64	>64
<i>E. coli</i> MCR1	0.2	0.4	3.2	>64	>64
<i>E. coli</i> MCR2	0.2	0.4	>6.4	>64	>64
<i>E. coli</i> MCR3	0.2	0.4	3.2	>64	>64
MRSA USA 300	>64	>64	>64	>64	>64

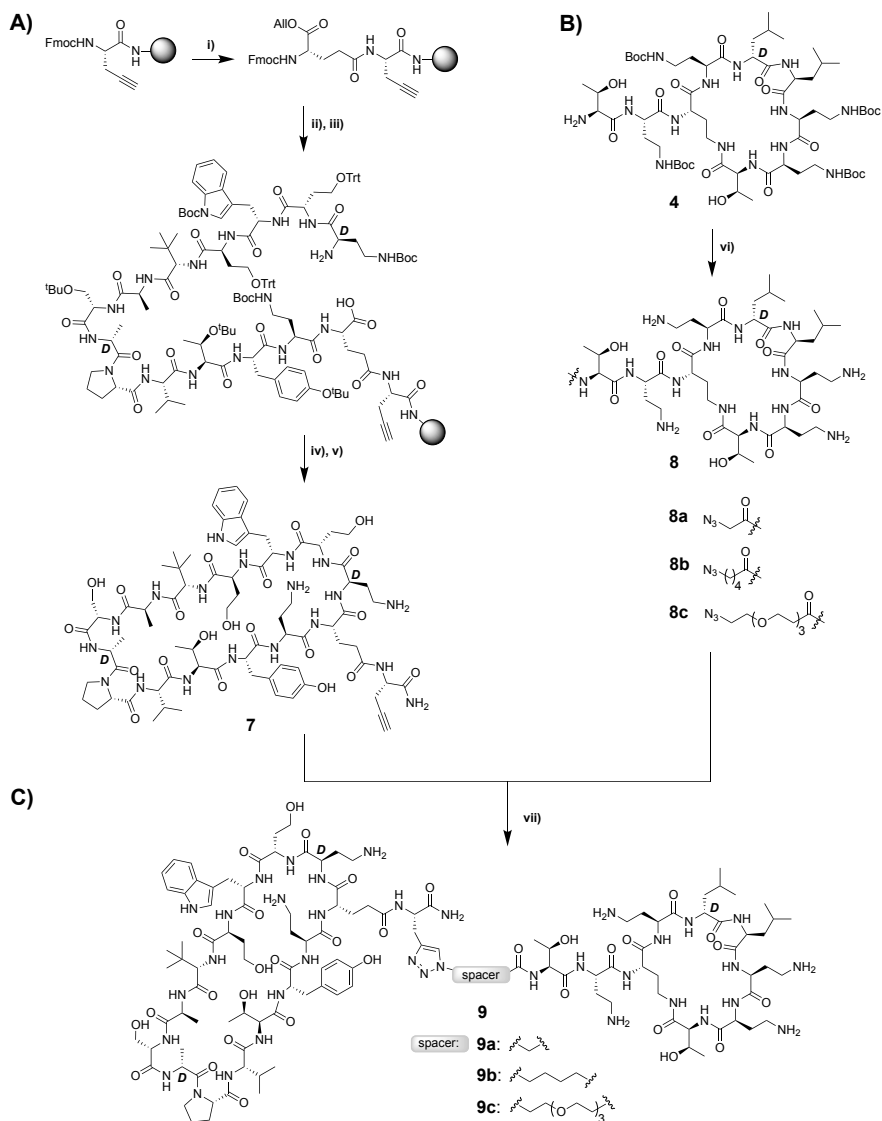
<sup>a</sup>Minimum inhibitory concentration reported in µg/mL

All compounds tested in triplicate

Upon confirming the potent anti-Gram-negative activity of conjugates **3a** and **3b** we next considered other options for the preparation of similar bicyclic constructs. The use of the well-established copper-catalyzed azide-alkyne cycloaddition (“click chemistry”) was deemed particularly attractive.<sup>34</sup> To this end we envisioned a convenient approach whereby the monocyclic β-hairpin mimetic, modified to bear an appropriately placed alkyne moiety, could be ligated to the PMEN moiety containing a complementary azide group. The preparation of each fragment was achieved by extension of the methods used to access the building blocks employed in the synthesis of compounds **3a** and **3b**. The alkyne modified peptidomimetic β-hairpin **7** was conveniently synthesized completely on resin (Scheme 4A). To begin, Rink amide resin was loaded with Fmoc-propargyl-glycine followed by addition of the orthogonally protected Fmoc-Glu(OH)-OAll *via* its free side chain carboxylate. The remaining 13 amino acids were then added and, following final Fmoc removal and Pd(0) catalyzed allyl ester removal, the macrocycle was cleanly formed on resin. Strong acid cleavage/deprotection, then provided



compound **7**. Notably, the use of microwave assisted SPPS enabled the convenient preparation of **7** in as little as four hours including cyclization and cleavage/deprotection. When it came to preparing the azide-modified PMEN fragment, we elected to incorporate azido-carboxylic acids of varying lengths to also assess how the distance between the two peptide macrocycles might impact antibacterial activity. To this end we generated azido PMEN analogues **8a-c** containing a short spacer based on azido glycine, a medium-length C5 spacer, and a longer PEG3-based spacer (Scheme 4B). With these azido-PMEN building blocks in hand, ligation with alkyne **7** was accomplished by treatment with CuSO<sub>4</sub> and ascorbic acid to yield the expected triazole linked conjugates **9a-c**, overall yields ranging from 55%-71% after RP-HPLC (Scheme 4C).



**Scheme 4. Synthesis of triazole linked bicyclic conjugates 9a-c.** i) Starting from Fmoc-propargyl-Gly loaded Rink resin, Fmoc-Glu-OAll was coupled *via* its carboxyl side chain; ii) Fmoc SPPS till the final Fmoc-D-Dab(Boc)-OH + removal of final Fmoc; iii) Glu-OAll deprotection with Pd; iv) On resin cyclization (BOP/DiPEA); v) TFA deprotection + resin cleavage followed by RP-HPLC purification; vi) Coupling of azido carboxylic acids conjugation (BOP/DIPEA); vii) triazole formation with  $\text{CuSO}_4$  and sodium ascorbate followed by RP-HPLC purification.

The antibacterial activities of triazole conjugates **9a-c** were assessed against the same panel of Gram-negative bacteria revealing a clear trend (Table 2). Conjugate **9a**, containing the shortest linker consistently demonstrated potent antibacterial activity with MIC values ranging from 0.25 – 2.0 µg/mL. By comparison, **9b** and **9c**, containing the C5 and PEG3 spacers respectively, exhibited progressively weaker activities. These findings indicate that the proximity of the two monocyclic peptides to each other is an important factor in achieving maximal activity.

Based on the trend revealed by conjugates **9a-c**, we were also curious to know how bringing the two macrocycles even closer together might impact activity. To address this question, we employed polymyxin E heptapeptide (PMEH) building block **10**, a more truncated fragment of colistin lacking the exocyclic amino acids present in the corresponding PMEN. It is known that polymyxin-derived heptapeptides can also bind LPS<sup>35</sup> and permeabilize the Gram-negative OM in a manner similar to polymyxin nonapeptides.<sup>12</sup> In addition, the polymyxin B heptapeptide has also been shown to potentiate various antibiotics against Gram-negative bacteria albeit at 3-fold higher concentrations than required for the corresponding nonapeptide.<sup>12</sup>

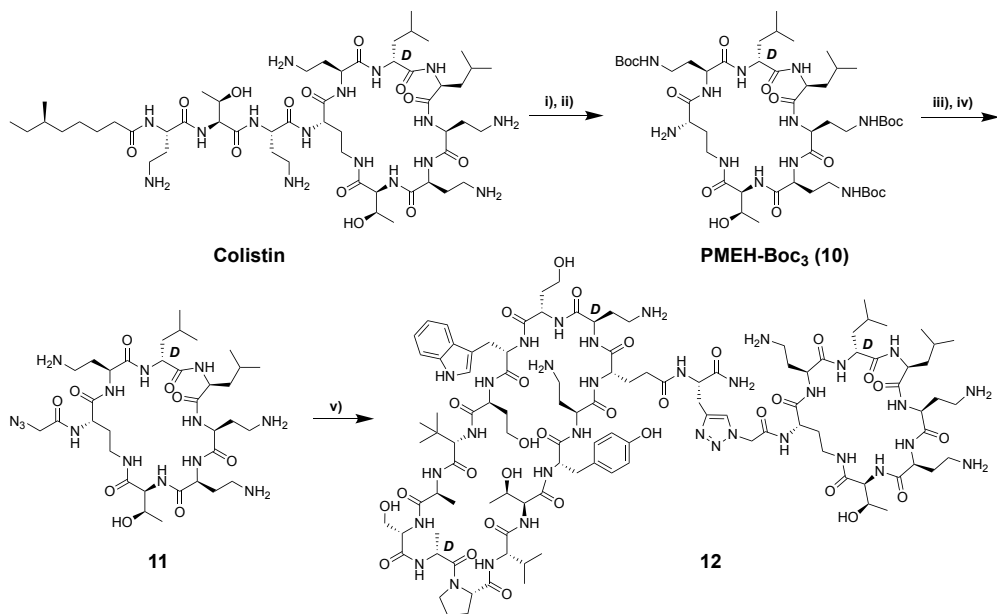
**Table 1.** MIC<sup>a</sup> values compounds **3a**, **3b**, **6**, colistin and PMEN

	<b>9a</b>	<b>9b</b>	<b>9c</b>	<b>12</b>	Colistin
<i>A. baumannii</i> ATTC 9955	2	2	8	64	0.4
<i>A. baumannii</i> ATTC	0.5	1	4	64	0.4
<i>A. baumannii</i> NDM2	0.5	1	2	64	0.2
<i>A. baumannii</i> MDR	1	2	4	32	0.4
<i>K. pneumoniae</i> ATTC	1	2	8	16	0.1
<i>K. pneumoniae</i> NDM1	2	4	16	32	1.6
<i>P. aeruginosa</i> ATCC	1	2	4	64	1.6
<i>P. aeruginosa</i> NRZ	2	4	8	64	0.8
<i>P. aeruginosa</i> NDM1	2	2	4	32	0.4
<i>P. aeruginosa</i> M-120	4	4	8	64	0.8
<i>E. coli</i> ATCC 35218	0.5	1	2	8	0.1
<i>E. coli</i> NDM1	0.25	0.5	2	2	0.1
<i>E. coli</i> MCR1	2	4	16	16	3.2
<i>E. coli</i> MCR2	2	4	16	32	>6.4
<i>E. coli</i> MCR3	4	8	32	64	3.2
MRSA USA 300	>64	>64	>64	64	>64

<sup>a</sup>Minimum inhibitory concentration reported in µg/mL

All compounds tested in triplicate

The preparation of **10** (Scheme 5) followed a literature protocol whereby colistin was first converted to the penta-Boc protected species following by enzymatic degradation with savinase to yield the tri-Boc protected polymyxin E heptapeptide (PMEH-Boc<sub>3</sub>) **10**.<sup>36</sup> Attempts at directly coupling the free N-terminal amine of **10** to the free carboxylic acid of protected peptide **5**, as in the synthesis of conjugates **3a/b**, in this case failed to yield any of the expected bicyclic conjugate, presumably due to increased steric demands introduced by bringing the large macrocycles closer together. As an alternative, we then coupled azido glycine to **10**, which, following deprotection, provided the N-terminally azide-modified PME<sub>H</sub> species **11**. As for azido-PMEN analogues **8a-c**, the ligation of **11** with alkyne modified **7** proceeded smoothly upon treatment with CuSO<sub>4</sub> and ascorbic acid to yield conjugate **12**. Interestingly, the antibacterial activity of **12** was found to be much lower than for the PMEN conjugates **9a-c** containing the longer linkers (Table 2). This finding indicates that there is an optimal spacer length for the conjugation of BamA targeting  $\beta$ -hairpin peptidomimetics to the cyclic polymyxin fragment. Additionally, the reduced activity of compound **12** may point to a role for the exocyclic amino acids Thr and Dab (missing in **12** but present in **3a,b** and **9a-c**) for achieving potent antibacterial activity.



**Scheme 5. Synthesis of triazole linked bicyclic conjugates 12.** i) (Boc)<sub>2</sub>O, Et<sub>3</sub>N; ii) Savinase; iii) 2-Azidoacetic acid, HCTU, HOBt, 2,4,6-trimethylpyridine; iv) TFA deprotection and HPLC purification, v) alkyne containing peptide macrocycle 7, CuSO<sub>4</sub>, sodium ascorbate, followed by RP-HPLC purification.

### 4.3 Conclusion

While peptide-based therapeutics often face specific hurdles in drug development, their success in the field of antibacterials demonstrates that such compounds have potential. Specially, peptide antibiotics that operate *via* exploiting targets on the bacterial cell surface offer much promise. In this regard a new class of Gram-negative-specific macrocyclic peptide antibiotics that target the OMP BamA have recently gained attention.<sup>18-20</sup> Essential to the activity of these BamA targeting antibiotics is ligation to the polymyxin nonapeptide which is known to bind the lipid A component of LPS. In this study we developed a convenient convergent, chemoenzymatic synthesis of these chimeric bicyclic peptide antibiotics. The antibacterial activities of the compounds prepared by our route compare well with MIC

values previously reported. Notably, we also confirmed the potent activity of these compounds against colistin-resistant mcr-positive strains of *E. coli*. Furthermore, a new series of chimeric peptides were readily assembled using copper-catalyzed azide-alkyne cycloaddition ("click chemistry") *via* the ligation of various PMEN building blocks bearing an N-terminal azide ranging in size from a simple azido glycine spacer, to a C5 spacer and a (PEG)<sub>3</sub> spacer. The  $\beta$ -hairpin macrocycle containing a propargyl-glycine was readily prepared entirely on solid support and cleanly conjugated to the different azide containing PMEN units. The resulting triazole linked bicyclic peptides demonstrated a range of antibacterial activities with the azido-glycine linked conjugate demonstrating the most potent activity. Interestingly, conjugates containing either longer or shorter linkers between the  $\beta$ -hairpin macrocycle and PMEN moiety were significantly less active. These findings point to the importance of identifying the optimal linker properties to achieve potent antibacterial activity. In summary, the chemoenzymatic routes here reported for the preparation of BamA-targeting bicyclic peptide antibiotics simplify the synthetic effort required to do so and enable the convenient preparation of new analogues to further evaluate the potential of this exciting new class of anti-Gram-negative agents.

## 4.4 Experimental Section

### 4.4.1 General Procedures

All reagents employed were of American Chemical Society (ACS) grade or finer and were used without further purification unless otherwise stated. For compound characterization HRMS analysis was performed on a Shimadzu Nexera X2 UHPLC system with a Waters Acquity HSS C18 column (2.1 × 100 mm, 1.8 μm) at 30 °C and equipped with a diode array detector. The following solvent system, at a flow rate of 0.5 mL/min, was used: solvent A, 0.1 % formic acid in water; solvent B, 0.1 % formic acid in acetonitrile. Gradient elution was as follows: 95:5 (A/B) for 1 min, 95:5 to 15:85 (A/B) over 6 min, 15:85 to 0:100 (A/B) over 1 min, 0:100 (A/B) for 3 min, then reversion back to 95:5 (A/B) for 3 min. This system was connected to a Shimadzu 9030 QTOF mass spectrometer (ESI ionisation) calibrated internally with Agilent's API-TOF reference mass solution kit (5.0 mM purine, 100.0 mM ammonium trifluoroacetate and 2.5 mM hexakis(1H,1H,3H-tetrafluoropropoxy)phosphazine) diluted to achieve a mass count of 10000.

Purity of the peptides was confirmed to be ≥ 95% by analytical RP-HPLC using a Shimadzu Prominence-i LC-2030 system with a Dr. Maisch Reprosil Gold 120 C18 column (4.6 × 250 mm, 5 μm) at 30 °C and equipped with a UV detector monitoring at 214 nm. The following solvent system, at a flow rate of 1 mL/min, was used: solvent A, 0.1 % TFA in water/acetonitrile, 95/5; solvent B, 0.1 % TFA in water/acetonitrile, 5/95. Gradient elution was as follows: 95:5 (A/B) for 2 min, 95:5 to 0:100 (A/B) over 13 min, 0:100 (A/B) for 2 min, then reversion back to 95:5 (A/B) over 1 min, 95:5 (A/B) for 2 min.

The compounds were purified *via* preparative HPLC using a BESTA-Technik system with a Dr. Maisch Reprosil Gold 120 C18 column (25 × 250 mm, 10 μm) and equipped with an ECOM Flash UV detector monitoring at 214 nm. The following solvent system, at a flow rate of 12 mL/min, was used: solvent A, 0.1 % TFA in water/acetonitrile 95/5; solvent B, 0.1 % TFA in water/acetonitrile 5/95. Gradient elution was as follows: 95:5 (A/B) for 2 min, 95:5 to 0:100 (A/B) over 45 min, 0:100 (A/B) for 2 min, then reversion back to 95:5 (A/B) over 1 min, 95:5 (A/B) for 2 min.

#### 4.4.2 Peptide Synthesis

Chlorotrityl (CTC) resin (5.0 g, 1.60 mmol.g<sup>-1</sup>) was loaded with Fmoc-Dab(Boc)-OH. Resin loading was determined to be 0.477 mmol.g<sup>-1</sup>. Linear peptide encompassing AA-1 to AA-15 were assembled manually *via* standard Fmoc solid-phase peptide synthesis (SPPS) (resin bound AA:Fmoc-AA:BOP:DiPEA, 1:4:4:8 molar eq.) on a 0.1 mmol scale. DMF was used as solvent and Fmoc deprotections were carried out with piperidine:DMF (1:4 v:v). Amino acid side chains were protected as follows: tBu for Tyr, Allyl for Glu C-terminus, Trt for homoserine (Hse), and Boc for Trp/Dab. Following coupling and Fmoc deprotection of the final Fmoc-D-Dab(Boc)-OH the resin-bound, Allyl protected intermediate was next washed with CH<sub>2</sub>Cl<sub>2</sub> and treated with Pd(PPh<sub>3</sub>)<sub>4</sub> (30mg, 0.03 mmol) and PhSiH<sub>3</sub> (0.30 mL, 3.0 mmol) in CH<sub>2</sub>Cl<sub>2</sub> (*ca.* 7 mL) under argon for 1 hour. The resin was subsequently washed with CH<sub>2</sub>Cl<sub>2</sub> (5x10 mL), followed by a solution of diethyldithiocarbamic acid trihydrate sodium salt (5 mg mL<sup>-1</sup> in DMF, 5x10 mL), and DMF (5x10 mL). The linear side chain protected peptide with free C- and N-termini resin was subjected to on-resin cyclization conditions for 1 hour (BOP/DIPEA, 4:8 molar eq.) The cyclic peptide still on resin was treated with (CF<sub>3</sub>)<sub>2</sub>CHOH:CH<sub>2</sub>Cl<sub>2</sub> (1:4, 10 mL) for 1 hour and rinsed with additional (CF<sub>3</sub>)<sub>2</sub>CHOH:CH<sub>2</sub>Cl<sub>2</sub> and CH<sub>2</sub>Cl<sub>2</sub>. The combined washings were then evaporated to yield the side chain protected cyclic peptide 5 with a free C-terminus for use in subsequent couplings.

#### Coupling of protected peptide 5 and tetra-Boc protected PMEN

The protected cyclic peptide 5 and the PMEN-Boc<sub>4</sub> were dissolved in CH<sub>2</sub>Cl<sub>2</sub> (150 mL) and treated with BOP (0.22 g, 0.5 mmol) and DiPEA (0.17 mL, 1.0 mmol) and the solution was stirred overnight. The reaction mixture was concentrated and directly treated with TFA:TIS:H<sub>2</sub>O (95:2.5:2.5, 10 mL) for 90 minutes. The reaction mixture was added to cold MTBE:hexanes (1:1), spun down at 4500 RPM for 5 minutes and the resulting precipitate washed once more with MTBE:hexanes (1:1). The crude peptide was lyophilized from <sup>t</sup>BuOH:H<sub>2</sub>O (1:1) and purified with reverse phase HPLC. Pure fractions were pooled and lyophilized to yield the desired cyclic lipopeptide products in >95% purity as white powders, in 22-62 mg quantities (8-23% yield based on the resin loading used in the preparation of peptide 5).



Rink Amide resin (150 mg, 0.684 mmol.g<sup>-1</sup>) was loaded into a CEM Liberty Blue  $\mu$ wave peptide synthesizer at a 0.1 mmol scale. Linear peptide encompassing AA-1 to AA-15 were assembled using microwave irradiation at 90 °C (resin bound AA:Fmoc-AA:DIC:Oxyma, 1:5:5:5 molar eq.). DMF was used as solvent and Fmoc deprotections were carried out with piperidine:DMF (1:4, v:v). Amino acid side chains were protected as follows: tBu for Tyr, Allyl for Glu C-terminus, Trt for homoserine (Hse), and Boc for Trp/Dab. Following coupling and Fmoc deprotection of the final Fmoc-D-Dab(Boc)-OH the linear peptide was removed from the synthesizer, washed with DCM, and the Allyl protected intermediate was treated with Pd(PPh<sub>3</sub>)<sub>4</sub> (30mg, 0.03 mmol) and PhSiH<sub>3</sub> (0.30 mL, 3.0 mmol) in CH<sub>2</sub>Cl<sub>2</sub> (ca. 7 mL) under argon for 1 hour. The resin was subsequently washed with CH<sub>2</sub>Cl<sub>2</sub> (5x10 mL), followed by a solution of diethyldithiocarbamic acid trihydrate sodium salt (5 mg mL<sup>-1</sup> in DMF, 5x10 mL), and DMF (5x10 mL). The protected, resin-bound peptide was next subjected to on-resin cyclization conditions for 1 hour (BOP/DIPEA, 4:8 molar eq.), washed with DCM, and directly treated with TFA:TIS:H<sub>2</sub>O (95:2.5:2.5, 10 mL) for 90 minutes. The reaction mixture was added to cold MTBE:hexanes (1:1), spun down at 4500 RPM for 5 minutes, and the resulting precipitate washed once more with MTBE:hexanes (1:1). The crude cyclic peptide was lyophilized from <sup>t</sup>BuOH:H<sub>2</sub>O (1:1) and purified with reverse phase HPLC. Pure fractions were pooled and lyophilized to yield the desired cyclic lipopeptide products in >95% purity as white powders, typically in 30-70 mg quantities (11-26% yield based on resin loading).

#### 4.4.3 Antibacterial Assays

Minimum inhibitory concentrations (MICs) were determined by broth microdilution according to CLSI guidelines.<sup>37</sup> Blood agar plates were inoculated with glycerol stocks of the chosen bacteria strains, followed by incubation for 16 hours at 37 °C. Cation adjusted Mueller-Hinton broth (CAMHB) containing 10 mg L<sup>-1</sup> Mg<sup>2+</sup> and 25 mg L<sup>-1</sup> Ca<sup>2+</sup> was inoculated with individual colonies of the chosen bacteria. The peptides were dissolved in CAMHB, supplemented with polysorbate-80 (P-80 or Tween-80, sterile-filtered) at 0.002% v/v final concentration and serially diluted on

polypropylene microtiter plates with a volume of 50  $\mu\text{L}$  per well. Inoculated CAMHB ( $5 \times 10^5 \text{ CFU mL}^{-1}$ ) was added to reach a total volume of 100  $\mu\text{L}$  per well. The microtiter plates were sealed with an adhesive membrane and after 16 hours of incubation at 37 °C. The wells were visually inspected for bacterial growth. All reported MIC values result from three or more measurements performed on multiple days.

## References

- 1 Roope, L. S. J.; Smith, R. D.; Pouwels, K. B.; Buchanan, J.; Abel, L.; Eibich, P.; Butler, C. C.; Tan, P. S.; Sarah Walker, A.; Robotham, J. V. *Sci.* **2019**, 364, 1–8.
- 2 MacNair, C. R.; Tsai, C. N.; Brown, E. D. *Ann. N. Y. Acad. Sci.* **2020**, 1459, 69–85.
- 3 Årdal, C.; Balasegaram, M.; Laxminarayan, R.; McAdams, D.; Outtersen, K.; Rex, J. H.; Sumpradit, N. *Nat. Rev. Microbiol.* **2020**, 18, 267–274.
- 4 Codjoe, F.; Donkor, E. *Med. Sci.* **2017**, 6, 1–28.
- 5 Peri, A. M.; Doi, Y.; Potoski, B. A.; Harris, P. N. A.; Paterson, D. L.; Righi, E. *Diagn. Microbiol. Infect. Dis.* **2019**, 94, 413–425.
- 6 Henderson, J. C.; Zimmerman, S. M.; Crofts, A. A.; Boll, J. M.; Kuhns, L. G.; Herrera, C. M.; Trent, M. S. *Annu. Rev. Microbiol.* **2016**, 70, 255–278.
- 7 Stojanoski, V.; Sankaran, B.; Prasad, B. V. V.; Poirel, L.; Nordmann, P.; Palzkill, T. *BMC Biol.* **2016**, 14, 1–10.
- 8 Tsubery, H.; Ofek, I.; Cohen, S.; Fridkin, M. *Biochemistry* **2000**, 39, 11837–11844.
- 9 Moore, R.; Bates, N. C.; Hancock, R. E. W. *Antimicrob. Agents Chemother.* **1986**, 29, 496–500.
- 10 Falagas, M. E.; Kasiakou, S. K. *Clin. Infect. Dis.* **2005**, 40, 1333–1341.
- 11 T. Velkov; P.E. Thompson; R.L. Nation; J. Li. *J. Med. Chem.* **2010**, 53, 1898–1916.
- 12 Kimura, Y.; Matsunaga, H.; Vaara, M. J. *Antibiot. (Tokyo)*. **1992**, 45, 742–749.
- 13 Zabawa, T. P.; Pucci, M. J.; Parr, T. R.; Lister, T. *Curr. Opin. Microbiol.* **2016**, 33, 7–12.
- 14 French, S.; Farha, M.; Ellis, M. J.; Sameer, Z.; Côté, J. P.; Cotroneo, N.; Lister, T.; Rubio, A.; Brown, E. D. *Infect. Dis.* **2020**, 6, 1405–1412.
- 15 Ofek, I.; Cohen, S.; Rahmani, R.; Kabha, K.; Tamarkin, D.; Herzig, Y.; Rubinstein, E. *Antimicrob. Agents Chemother.* **1994**, 38, 374–377.
- 16 Vaara, M.; Siikanen, O.; Apajalahti, J.; Fox, J.; Frimodt-Møller, N.; He, H.; Poudyal, A.; Li, J.; Nation, R. L.; Vaara, T. *Antimicrob. Agents Chemother.* **2010**, 54, 3341–3346.
- 17 Ferrer-Espada, R.; Sánchez-Gómez, S.; Pitts, B.; Stewart, P. S.; Martínez-de-Tejada, G. *Int. J. Antimicrob. Agents* **2020**, 56, 1–10.
- 18 Zerbe, K.; Steinmann, J.; Meijden, B. Van Der; Bernardini, F.; Lederer, A.; Dias, R. L. A.; Misson, P. E.; Henze, H.; Zumbunn, J.; Käch, A. *Sci.* **2010**, 327, 1010–1013.
- 19 Martin-Loeches, I.; Dale, G. E.; Torres, A. *Expert Rev. Anti. Infect. Ther.* **2018**, 16, 259–268.
- 20 Luther, A.; Urfer, M.; Zahn, M.; Müller, M.; Wang, S. Y.; Mondal, M.; Vitale, A.; Hartmann, J. B.; Sharpe, T.; Monte, F. Lo. *Nature.* **2019**, 576, 452–458.
- 21 McLaughlin, M. I.; Van Der Donk, W. A. *Biochemistry* **2020**, 59, 343–345.
- 22 Hagan, C. L.; Wzorek, J. S.; Kahne, D.; Sauer, R. T. *Proc. Natl. Acad. Sci. U. S. A.* **2015**, 112, 2011–2016.
- 23 Hagan, C. L.; Silhavy, T. J.; Kahne, D. *Annu. Rev. Biochem.* **2011**, 80, 189–210.
- 24 Tomasek, D.; Rawson, S.; Lee, J.; Wzorek, J. S.; Harrison, S. C.; Li, Z.; Kahne, D. *Nature* **2020**, 583, 473–478.
- 25 Robinson, J. A. *Front. Chem.* **2019**, 7, 1–11.
- 26 Koopmans, T.; Wood, T. M.; 't Hart, P.; Kleijn, L. H. J.; Hendrickx, A. P. A.; Willems, R. J. L.; Breukink, E.; Martin, N. I. J. *Am. Chem. Soc.* **2015**, 137, 9382–9389.

- 27 t'Hart, P.; Wood, T. M.; Tehrani, K. H. M. E.; Van Harten, R. M.; Śleszyńska,  
M.; Rentero Rebollo, I.; Hendrickx, A. P. A.; Willems, R. J. L.; Breukink, E.;  
Martin, N. I. *Chem. Sci.* **2017**, *8*, 7991-7997.
- 28 Kleijn, L. H. J.; Oppedijk, S. F.; T Hart, P.; Van Harten, R. M.; Martin-Visscher,  
L. A.; Kemmink, J.; Breukink, E.; Martin, N. I. *J. Med. Chem.* **2016**, *59*, 3569-  
3574.
- 29 Wood, T. M.; Bertheussen, K.; Martin, N. I. *Org. Biomol. Chem.* **2020**, *18*, 514-  
517.
- 30 Silverman, S. M.; Moses, J. E.; Sharpless, K. B. *Chem. - A Eur. J.* **2017**, *23*, 79-83.
- 31 Meyer, J. P.; Adumeau, P.; Lewis, J. S.; Zeglis, B. M. *Bioconjug. Chem.* **2016**, *27*,  
2791-2807.
- 32 Danner, R. L.; Joiner, K. A.; Rubin, M.; Patterson, W. H.; Johnson, N.; Ayers, K.  
M.; Parillo, J. E. *Antimicrob. Agents Chemother.* **1989**, *33*, 1428-1434.
- 33 O'Dowd, H.; Kim, B.; Margolis, P.; Wang, W.; Wu, C.; Lopez, S. L.; Blais, J.  
*Tetrahedron Lett.* **2007**, *48*, 2003-2005.
- 34 Kolb, H. C.; Finn, M. G.; Sharpless, K. B. *Angew. Chemie - Int. Ed.* **2001**, *40*,  
2004-2021.
- 35 Thomas, C. J.; Surolia, A. *FEBS Lett.* **1999**, *445*, 420-424.
- 36 Li, B.; Akin, A.; Magee, T. V.; Martinez, C.; Szeliga, J.; Vuong, D. V. *Synth.*  
**2015**, *47*, 2088-2092.
- 37 Abmm, D.; Tamma, D.; Kirn, J.; Cullen, S. K. Clinical and laboratory standards  
institute (clsi). performance standards for antimicrobial susceptibility Testing,  
30th Ed. CLSI Suppl. M100 **2020**, 30

# Chapter 5

## A $\beta$ -hairpin peptide as the structural requirement for protein arginine rhamnosylation

*The recently discovered bacterial enzyme EarP, that transfers rhamnose to a specific arginine residue in its acceptor protein EF-P, specifically recognizes a  $\beta$ -hairpin loop. Notably, while the in vitro rhamnosyltransferase activity of EarP is abolished when presented with linear substrate peptide sequences derived from EF-P, the enzyme readily glycosylates the same sequence in a cyclized  $\beta$ -hairpin mimic. Additional studies with other substrate-mimicking cyclic peptides revealed that EarP activity is sensitive to the method used to induce cyclization and in some cases is tolerant to amino acid sequence variation. Using detailed NMR approaches, we established that the active peptide substrates all share some degree of  $\beta$ -hairpin formation, and therefore conclude that the  $\beta$ -hairpin epitope is the major determinant of arginine-rhamnosylation by EarP.*

**Collaboration statement:** *The contents of this chapter are the result of a collaboration with the group of Marthe Walvoort (University of Groningen). All peptide synthesis was performed by T. Wood and all biochemical and biophysical experiments were conducted by collaborators.*

Published in: †Yakovlieva, L.; †Wood, T.M.; Kemmink, J.; Kotsogianni, I.; Koller, F.; Lassak, J.; Martin, N.I.; Walvoort, M.T.C. *Chem. Sci.* **2021**, *12*, 1560-1567.

†Indicates equal contribution.

## 5.1 Introduction

Protein glycosylation, an enzymatic process in which a carbohydrate or glycan is covalently added to a specific amino acid residue, is one of the most ubiquitous post-translational modifications in nature.<sup>1</sup> Glycosylation confers specific properties on the acceptor protein, such as increased solubility, protection from degradation, tagging for transport or destruction, interaction with receptors, or functional activation. As a result, protein glycosylation influences a myriad of biological processes in all kingdoms of life.

In addition to the well-established forms of protein glycosylation, novel glycosylation systems have been discovered that are unique to bacteria.<sup>15</sup> Recently, arginine rhamnosylation was identified as a novel type of *N*-glycosylation.<sup>2,3</sup> Here the enzyme EarP transfers a rhamnose moiety from dTDP- $\beta$ -L-rhamnose (TDP-Rha) to a specific arginine residue in the acceptor translation elongation factor P (EF-P) (Figure 1).<sup>2,4</sup> Arginine glycosylation is a rare modification with only two other examples reported to date, *i.e.* autocatalytic modification of Arg with glucose (Glc) of sweet corn amygdalin,<sup>5</sup> and with *N*-acetylglucosamine (GlcNAc) of human death receptor domains by the bacterial effector protein NleB.<sup>6</sup>

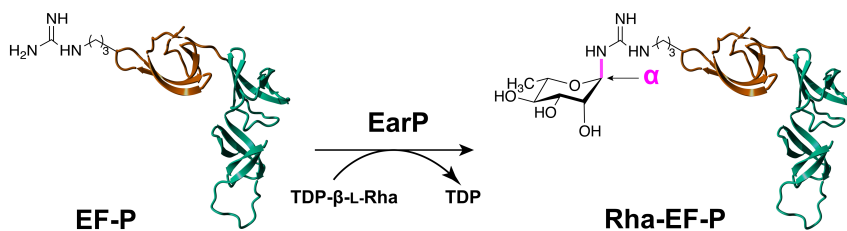


**Figure 1:** Rhamnosylation of EF-P by EarP. Domain I of EF-P (amino acids 1-65) is shown in orange.

Genes associated with the newly discovered EF-P rhamnosylation (*earP*, *efp*, and *rmlABCD* genes for TDP-Rha donor synthesis) have been identified predominantly in beta- and gamma-proteobacteria, including multiple clinically relevant pathogens, *e.g.* *Pseudomonas aeruginosa*, *Neisseria*

*meningitidis*, and *Bordetella pertussis*.<sup>2</sup> The rhamnose modification has been shown to activate EF-P which alleviates ribosomal stalling during the synthesis of poly-proline stretches in nascent polypeptides.<sup>7-9</sup> Abolishing rhamnosylation of EF-P in *P. aeruginosa* and *N. meningitidis* led to cellular effects that were detrimental to bacterial fitness and increased susceptibility to antibiotics.<sup>4,10</sup> It is hypothesized that these severe effects are associated with the importance of polyPro-containing proteins and virulence factors for bacterial survival.<sup>4,10</sup>

Since the discovery of EF-P rhamnosylation in 2015, several studies have contributed to an increased understanding of this unique system. The stereochemistry of the  $\alpha$ -glycosidic linkage between Arg and Rha was shown by two research groups independently,<sup>11,12</sup> proving that EarP is an inverting glycosyltransferase. An anti-Arg<sup>Rha</sup> antibody has also been developed, allowing for facile (*in vitro*) monitoring of arginine rhamnosylation.<sup>11,13</sup> Several (co)-crystal structures have been reported for EarP (from *P. putida*,<sup>13</sup> *N. meningitidis*<sup>14</sup> and *P. aeruginosa*<sup>15</sup>), also in complex with its EF-P substrate, providing insight into the specific amino acid interactions and the catalytic mechanism of rhamnosylation. As only a single Arg residue in EF-P is modified, an important yet unexplored aspect of this novel glycosylation system is the basis for the observed specificity in recognizing this arginine residue. Previous reports indicate that domain I of EF-P (aa 1-65, Figure 2) is sufficient for recognition and rhamnosylation by EarP.<sup>13</sup> Domain I, commonly referred to as a “KOW-domain”,<sup>13</sup> is a conserved domain in various ribosome-associated proteins involved in transcription and translation,<sup>16</sup> and it appears to contain all recognition elements necessary to promote Arg rhamnosylation.<sup>13-15</sup> A recent study indicates that structural elements are more important than a specific sequon to promote EarP-mediated rhamnosylation.<sup>17</sup> However, the precise determinants for recognition by EarP had not been investigated. Elucidating the necessary substrate recognition elements allows to better understand this unique bacterial system, an important step towards exploiting bacterial glycosylation systems for the development of novel anti-virulence strategies.<sup>18</sup>

In this Chapter the discovery of a novel  $\beta$ -hairpin recognition element in arginine rhamnosylation of EF-P from *P. aeruginosa* is described. Using *in vitro* rhamnosylation assays and in-depth NMR studies the

importance of this key structural motif in acceptor substrate recognition by EarP is demonstrated. Moreover, the shortest peptide fragment known to date to be rhamnosylated by EarP is identified. Next to expanding the current knowledge on structural requirements of protein glycosyltransferases, these results have the potential to inform the development of inhibitors and activity assays to screen for inhibitors for EarP based upon the  $\beta$ -hairpin motif of the EF-P KOW domain

## 5.2 Results

A common strategy for studying the activity of *N*-glycosyltransferases *in vitro* is using linear peptide fragments corresponding to their protein substrate. The rhamnosyltransferase EarP from *P. aeruginosa* was heterologously expressed using a previously described procedure,<sup>15</sup> and natural substrate EF-P<sub>Pa</sub> was used in the studies. As a first step in deciphering the determinants of substrate recognition in arginine rhamnosylation, linear peptide fragment comprised of eight amino acids was investigated. Unexpectedly, this linear peptide did not prove to be a suitable substrate for EarP as no conversion was observed under *in vitro* rhamnosylation conditions (analysis with RP-LCMS). These results suggest that EarP does not rely exclusively on a specific amino acid sequence (primary structure) in the protein substrate for recognition, suggesting that there may be secondary structure requirements involved

As revealed in various structural studies,<sup>13-15</sup> the acceptor binding site of EarP is unusually large and multiple contacts between active site residues of EarP and amino acids of domain I of EF-P are necessary for protein substrate recognition. Upon examining the co-crystal structure of EarP and domain I of EF-P from *P. aeruginosa*<sup>15</sup> (PDB 6J7M) it is evident that the majority of EF-P residues involved in binding to EarP are located in the  $\beta$ -hairpin with Arg32 at its tip (Figure 2). Multiple EarP active site residues are involved in acceptor protein recognition and form both main-chain and side-chain promoted H-bonds, salt bridges, and hydrophobic interactions. As can be seen from Figure 3, a selected number of EF-P residues (Arg32, Lys29, Ser30, Asn28, Val36, Phe54, Val53, Lys55) are involved in binding to EarP suggesting that both sequence and shape of the bound motif are



recognized, rather than just the target arginine. The  $\beta$ -hairpin secondary structure appears to optimally position Arg32 for binding in the EarP active site. Based on this interaction profile, the importance of secondary structure in Arg-rhamnosylation was explored by preparing peptide mimics of the  $\beta$ -hairpin containing Arg32. Various mimics of the  $\beta$ -hairpin secondary structure have been extensively studied over the years, and many structure-inducing templates have been developed.<sup>19</sup> One of the most widely used methods to nucleate a  $\beta$ -hairpin structure is the introduction of an L-Pro-D-Pro motif.<sup>19</sup> This motif leads to a “kink” in the sequence and brings the strands in close proximity to allow the formation of secondary structure-stabilizing H-bonds between the antiparallel strands.

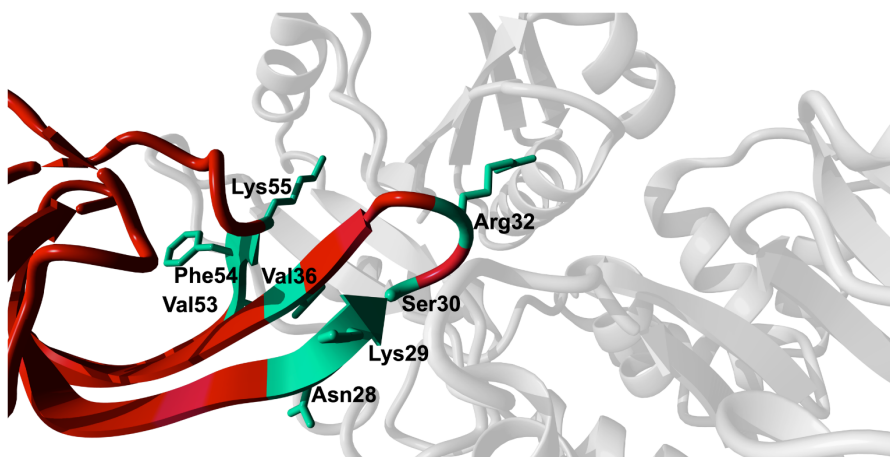


**Figure 2.** EarP-EF-P complex from *P. aeruginosa* (generated with YASARA, PDB 6J7M). EarP is depicted in grey, domain I of EF-P is colored red, EF-P residues involved in binding with EarP are in green.

Based on the sequences of EF-P proteins from *P. aeruginosa*, *Ralstonia solanacearum* (a Gram-negative plant pathogen) and *N. meningitidis*, the corresponding cyclic 11mer peptides depicted in Figure 3A and Figure 4 were prepared using solid-phase peptide synthesis (SPPS). The peptides were tested in the *in vitro* rhamnosylation reaction with EarP<sub>Pa</sub> and TDP-Rha, and the rhamnosylated products were identified by an increase in the mass of +146 Da with RP-LCMS. Gratifyingly, the prepared cyclic peptides revealed successful modification by EarP, albeit to varying extents. The best substrate identified was the L-Pro-D-Pro-cyclized 11mer

fragment of EF-P from *P. aeruginosa* (11mer\_*Pa*, 85% conversion overnight) (Fig 3A). The extent of rhamnosylation was calculated from ion intensities in the MS spectra and corrected for the relative ionization factor (RIF) values,<sup>20</sup> as described in the Experimental Procedures. A detailed kinetic analysis of the rhamnosylation of 11mer\_*Pa* and native protein substrate EF-P was obtained through a time course study. This analysis revealed that the cyclic 11-mer is indeed rhamnosylated in a time-dependent manner albeit with a lower rate of conversion relative to EF-P (Fig 3B).

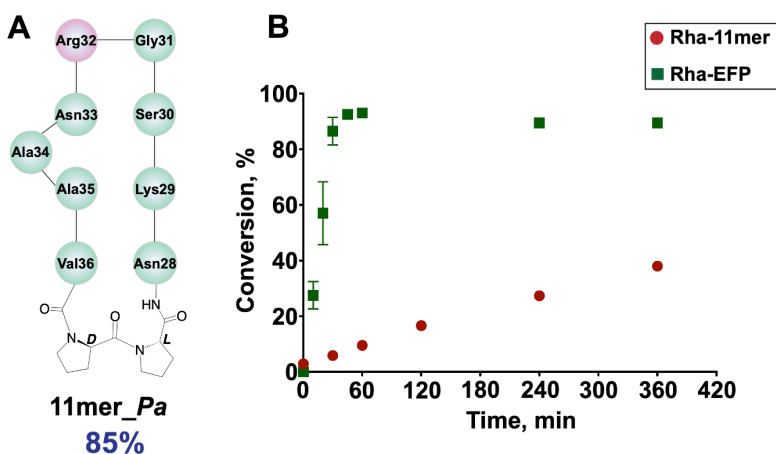


**Figure 3 A:** Cyclic 11mer peptide mimic of the EF-P\_*Pa*  $\beta$ -hairpin. **B:** Time-course experiment of the EarP-catalyzed conversion of 11mer\_*Pa* and EF-P\_*Pa* to the respective rhamnosylated products. Rhamnosylation of 11mer\_*Pa* was performed with a ratio of enzyme : acceptor substrate of 1:2.5 (40  $\mu$ M EarP, 100  $\mu$ M peptide). Rhamnosylation of EFP was performed with a ratio of enzyme : acceptor substrate of 1:250 (0.4  $\mu$ M EarP, 100  $\mu$ M protein). The reactions were monitored by LC-MS (peptide) and q-TOF-LC-MS (protein), and % conversion was corrected using the RIF factor. Time course studies performed by Liubov Yakovlieva (PhD candidate in the group of Marthe Walvoort).

Interestingly, follow-up experiments with both shorter and longer cyclic peptides inspired by the successful 11mer\_*Pa* peptide, revealed that the 11mer peptide (nine native amino acids, plus the L-Pro-D-Pro motif) was favored as a substrate, as EarP exhibited no activity towards the shorter (7mer\_*Pa*) and only low levels of conversion (14%) were achieved with the longer (15mer\_*Pa*) fragment (Table S1).

After successful rhamnosylation of 11mer\_*Pa* was achieved, the promiscuity of EarP for the amino acid sequence surrounding Arg32 was investigated next. To this end, the 11mer fragments of EF-P sequences from *R. solanacearum* and *N. meningitidis* were tested in the rhamnosylation reaction with EarP from *P. aeruginosa* (Fig 4). Interestingly, the 11mer\_*Rso* peptide with two amino acid mutations compared to 11mer\_*Pa* showed low levels of conversion (14% overnight), whereas the 11mer\_*Nm* peptide bearing five mutations was not accepted as a substrate. While these cyclic 11mer peptides do not show high conversion with EarP\_*Pa*, this does not exclude the possibility that they may be substrates for their associated native enzymes EarP\_*Rso* and EarP\_*Nm*, respectively.

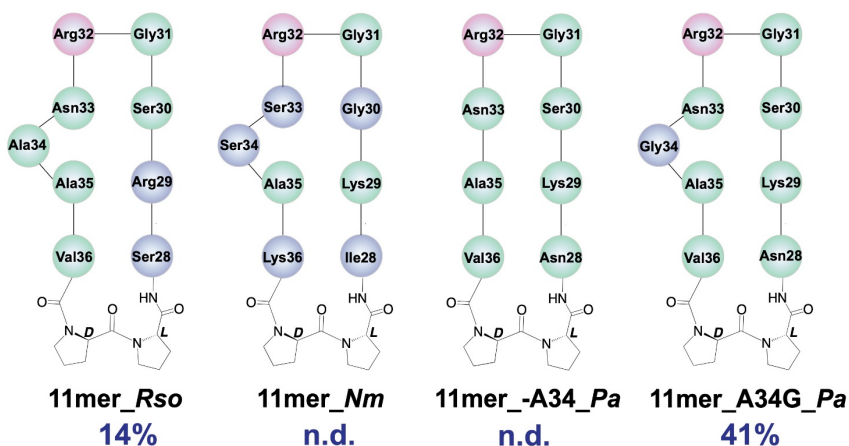


**Figure 4.** Cyclic peptide mimics of the EF-P  $\beta$ -hairpin. Arg32 is shown in pink, altered residues (with respect to 11mer\_*Pa*) are shown in blue.

The co-crystal structure of EF-P bound to EarP revealed that Ala34 in EF-P undergoes a significant conformational change.<sup>15</sup> It appears that upon binding to EarP, the “bulge” formed by Ala34 is significantly reduced, leading to a more narrowly shaped and structured loop than that in free EF-P. To investigate whether Ala34 and the concomitant conformational movement are important for binding, the residue was completely removed in peptide 11mer\_*A34\_Pa*. Interestingly, this substrate was not rhamnosylated by EarP, suggesting that the Ala34 bulge is important for recognition. Whereas the co-crystal structure suggests that Ala34 is not

directly involved in binding to EarP,<sup>15</sup> it is reasonable to assume that this residue contributes to shaping the  $\beta$ -hairpin, which in turn positions Arg32 in the active site. This was further corroborated by substituting Ala34 with glycine (11mer\_A34G\_Pa), a smaller and more flexible amino acid. This mutant retained its role as a substrate for EarP, albeit with reduced efficiency (41% conversion).

Next, alternate cyclization strategies were compared to assess their impact on recognition by EarP (Table S1, Figure 5). Specifically, peptides of varying lengths, based upon the same key EF-P amino acid substrate sequence were synthesized and cyclized using CLIPS (Chemical Linkage of Peptides onto Scaffolds)<sup>21</sup> and disulfide strategies<sup>22</sup> to introduce conformational rigidity and flexibility, respectively. In addition, linear peptides containing the same EF\_P sequence with Trp and Phe residues were prepared to introduce a so-called “tryptophan zipper” motif known to promote interstrand H-bonding as another means of generating a  $\beta$ -turn mimic.<sup>23</sup> Despite the diversity of designs (length and placement of the template, Table S1), only a few of the new peptides bearing the key EF-P substrate sequence were recognized as substrates by EarP with low to moderate yields of conversion (disulfide-cyclized 11mer (~6%) and 15mer (~17%); trp-zips 9mer\_WK (~6%), 18mer\_WKWF (~22%), and 18mer\_2WW (~13%). Notably, the majority of the trp-zip designs (especially longer sequences of 13mers, 17mers and 18mers) led to almost immediate precipitation when incubated with EarP, indicating that the hydrophobicity of these substrate mimics is not compatible with forming and maintaining a soluble complex with the enzyme.

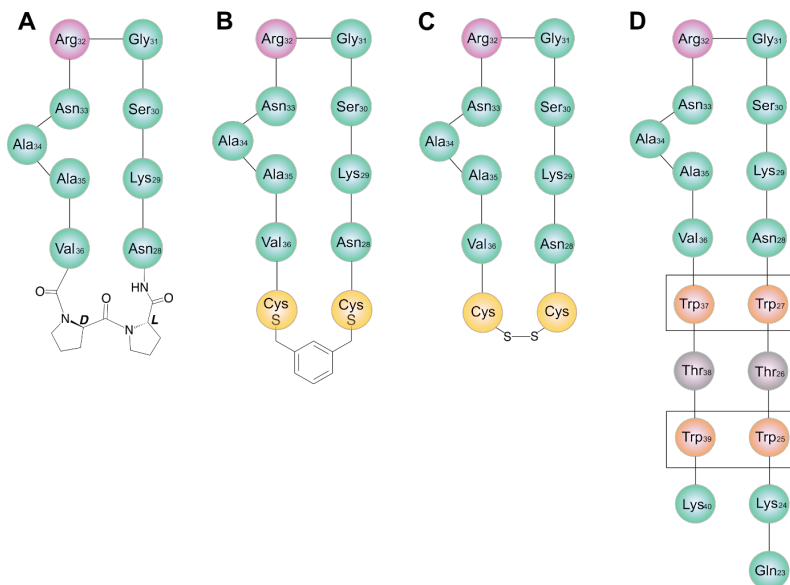


**Figure 5.** Stabilization strategies used in this Chapter to induce the  $\beta$ -hairpin. **A:** L-Pro-D-Pro cyclization strategy. **B:** CLIPS cyclization. **C:** Disulfide cyclization. **D:** Trp-zip stabilization.

Suitable EarP substrates were further investigated with several NMR techniques to gain understanding of the secondary structure, with the most pronounced effects depicted in the Figure 6. By performing temperature studies of the chemical shift of amide-hydrogens, two NH groups (Asn28 and Asn33) with low temperature coefficients were identified, indicative of the  $\beta$ -hairpin-forming interstrand hydrogen bonds (dashed lines). Interestingly, the majority of the observed NOE signals that are characteristic of a  $\beta$ -hairpin structure (Asn28NH-Val36NH, Lys29HA-Val36NH, Lys29HA-Ala35HA, Ser30NH-Ala35HA) are clustered in close proximity to the L-Pro-D-Pro motif, which supports the ability of this template to induce the twist of the peptide structure and consequently bring the strands together for H-bonding. As can be seen from the Figure 8 this structure-inducing effect of the L-Pro-D-Pro template tapers off towards the Ala35 residue, as the bulge most likely does not allow strands to come close together. Finally, the NOE signals and another H-bond (Asn33) re-appear around Arg32, presumably induced by the Gly31-Arg32  $\beta$ -turn.

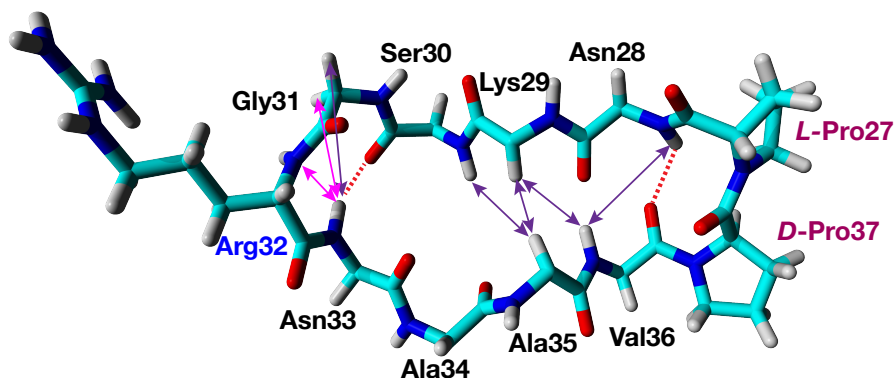


**Figure 6.** Experimentally determined NOE signals that are indicative of a  $\beta$ -hairpin structure are mapped on the 11mer L-Pro-D-Pro<sub>Pa</sub> fragment (from 3OYY crystal structure). Hydrogen bonds inferred from the NH temperature studies are shown as red dashed lines. NOE signals are shown as double-ended arrows (magenta: medium NOE; purple: weak NOE). NMR studies performed by Johan Kemmink (NMR group RuG).

Compared to the original 11mer<sub>Pa</sub> peptide, the 11mer<sub>A34G</sub><sub>Pa</sub> variant features only one of the two H-bonds (NH of Asn28) and several NOE signals are missing (K29HA-V36NH, S30NH-A35HA, Table S4). It was also shown to exhibit more flexibility, presumably due to the inclusion of the inherently more flexible glycine in the loop. In the case of 11mer<sub>A34</sub><sub>Pa</sub>, that showed no conversion to product, only very few structural elements were preserved (sequential NOE signals of P27HA-N28NH and R32NH-N33NH, and the structure was found to lack one of the two H-bonds (NH of Asn33) present in the 11mer<sub>Pa</sub> that enable the formation of the  $\beta$ -hairpin structure. The 11mer<sub>Rso</sub> variant structure has both H-bonds found in 11mer<sub>Pa</sub> (NH of Ser28 and Asn33) and more of  $\beta$ -hairpin characteristic NOEs, although S28NH-V36NH was absent. On the other hand, it was not possible to determine the structure of the 11mer<sub>Nm</sub> peptide, as it appears to be a mixture of several structures due to *cis/trans* isomerization of Pro residues. It is therefore difficult to conclude whether absence of conversion for 11mer<sub>Nm</sub> peptide stems from the sequence variation or lack of structure. NMR analysis of the structures of the linear peptide, CLIPS-, disulfide- and Trp-rich peptides showed that these

peptides tend to form disordered structures and show close to none of the  $\beta$ -sheet structure.

In order to study the binding between EarP and the 11mer\_*Pa* peptide, different experimental methods were employed. Saturation-transfer difference (STD) NMR is a widely employed strategy to observe binding between proteins and ligands, even at low binding affinities.<sup>24</sup> However, several attempts at measuring STD-NMR for the EarP-11mer\_*Pa* peptide complex, in the presence and absence of TDP, provided no definitive proof of binding affinity (data not shown). Similarly, attempts with (TR)-NOE measurements to identify the amino acid residues of 11mer\_*Pa* that are involved in binding to EarP proved unsuccessful (data not shown), presumably due to the low affinity between the protein and the peptide substrate. In a final attempt to quantify the binding affinity of EarP for the best substrate 11mer\_*Pa*, isothermal titration calorimetry (ITC) studies were performed. Tight binding of the native protein substrate EF-P was measured with a binding constant  $K_d$  of  $473 \pm 94$  nM for EarP (Figure 7A), in agreement with reported values.<sup>15</sup> Conversely, binding of 11mer\_*Pa* to EarP could not be detected by ITC using a range of increasing concentrations (Figure 7B). Even a displacement experiment, in which EF-P was titrated into a solution of pre-formed 11mer\_*Pa*-EarP-TDP complex, did not reveal binding of 11mer-*Pa* to EarP (data not shown). The absence of clear results from the STD-NMR and ITC suggests that the binding affinity of EarP for 11mer\_*Pa* is too low (mM range or higher) to clearly visualize and quantify using such techniques.

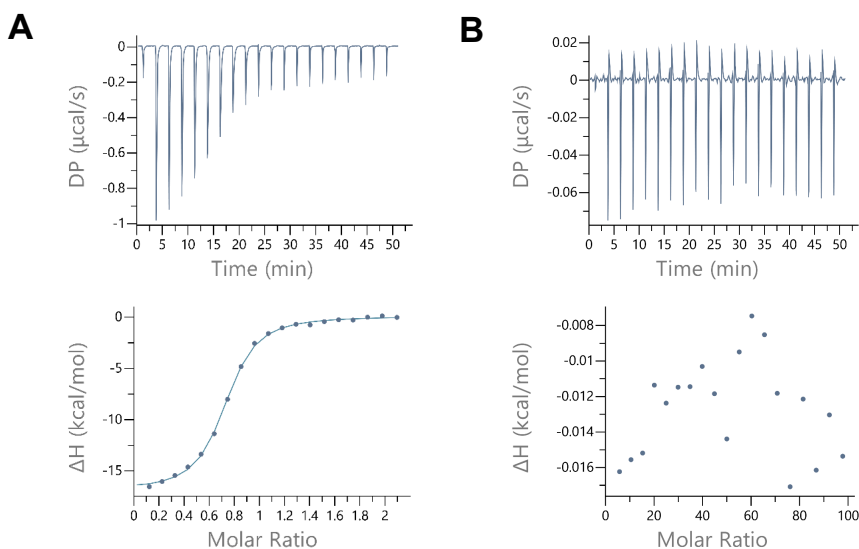


**Figure 7. A:** ITC studies reveal strong binding between EF-P (233  $\mu\text{M}$ ) and EarP (20  $\mu\text{M}$ ) in the presence of 60  $\mu\text{M}$  TDP. **B:** No apparent binding was observed between 11mer\_Pa (10 mM) and EarP (20  $\mu\text{M}$ ) with ITC in the presence of 60  $\mu\text{M}$  TDP. ITC studies performed by Ioli Kotsogianni (PhD candidate in the group of Nathaniel Martin).

Finally, the structural similarity between rhamnosylated EF-P (Rha-EF-P), and the *in vitro* rhamnosylated cyclic peptide (Rha-11mer\_Pa) was investigated. In previous studies, antibodies against the Rha-Arg modification were raised using synthesized linear Rha-peptide coupled to BSA.<sup>27</sup> To determine binding of the anti-Arg<sup>Rha</sup> antibodies to the rhamnosylated cyclic peptide, a dot blot affinity assay was performed using freshly rhamnosylated 11mer\_Pa (Rha-11mer\_Pa) and Rha-EF-P as a control. As can be seen in Figure 8B, a clear fluorescent signal belonging to the formation of Rha-11mer\_Pa was observed well into low micromolar concentrations (up to 4  $\mu\text{M}$ ). As can be seen from the Figure 8A, a similar, albeit more intense signal was obtained for the native substrate (Rha-EFP). At the same time, identical concentrations of non-modified substrates were not detected in this assay (Figure 8C, D). Interestingly, a similar dot blot affinity study with the  $\beta$ -linked Rha-11mer\_Pa product, serendipitously obtained after complete anomerization during anion exchange chromatography under basic conditions (*vide supra*), revealed very little



binding to anti-Arg<sup>Rha</sup> antibodies (Figure 8E). This establishes the selectivity of the antibodies for the  $\alpha$ -anomeric linkage in the Arg-Rha glycosidic bond.

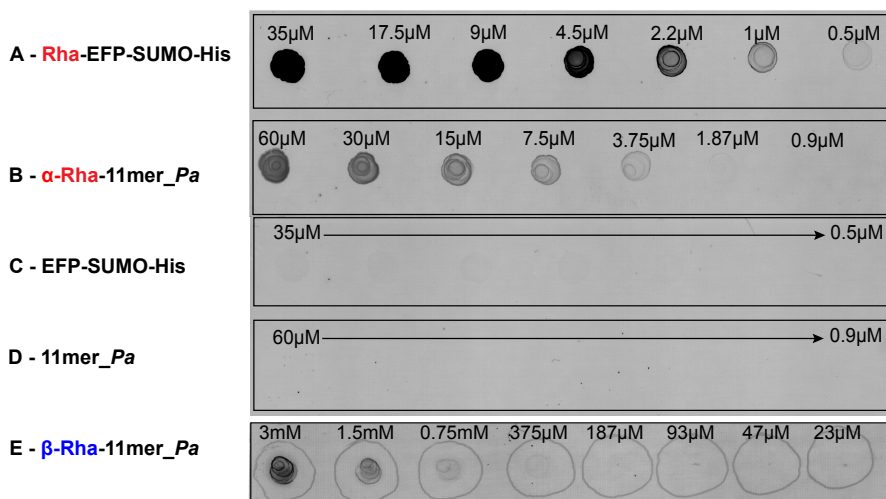


**Figure 8.** A: Dot blot affinity assay of a two-fold serial dilution of 35  $\mu$ M Rha-EFP and B: 60  $\mu$ M Rha-11mer\_Pa binding to the anti-Arg<sup>Rha</sup> antibody and visualized using anti-rabbit Alexa488 secondary antibody. Non-rhamnosylated substrates are not recognized by the anti-Arg<sup>Rha</sup> antibody (C and D). E: Dot blot affinity assay of a two-fold serial dilution of 3 mM  $\beta$ -Rha-11mer. Dot blot studies performed by Liubov Yakovlieva (PhD candidate in the group of Marthe Walvoort).

### 5.3 Conclusion

Whereas the structural determinants for asparagine-linked protein glycosylation are largely based on the primary sequence (consensus sequence), the results described in this Chapter suggest that for bacterial arginine-rhamnosylation a specific secondary structural motif is required. The clear importance of secondary structure, and more specifically a  $\beta$ -hairpin motif, as the minimal structural epitope for protein glycosylation may be a unique characteristic of this class of enzymes. Taken together these findings show that the propensity of the (cyclic) peptides to form a  $\beta$ -hairpin structure is an important substrate prerequisite for EarP rhamnosyltransferase and can be directly correlated to activity of the enzyme towards various peptide substrates. This Chapter provides

important insights into the recognition motifs for bacterial arginine rhamnosylation which will be useful for the development of future substrate mimics or structure-guided design of peptide inhibitors.

## 5.4 Experimental Section

### 5.4.1 General Procedures

All chemicals were purchased from Sigma Aldrich unless otherwise stated. dTDP- $\beta$ -Rha was purchased from Carbosynth. All reagents employed were of American Chemical Society (ACS) grade or higher and were used without further purification unless otherwise stated.

#### Preparative HPLC

Preparative HPLC runs were performed on a BESTA-Technik system with a Dr. Maisch Reprosil Gold 120 C18 column (25 × 250 mm, 10  $\mu$ m) and equipped with an ECOM Flash UV detector monitoring at 214 nm. The following solvent system, at a flow rate of 12 mL/min, was used: solvent A, 0.1% TFA in water/acetonitrile 95/5; solvent B, 0.1% TFA in water/acetonitrile 5/95. Gradient elution was as follows: 70:30 (A:B) for 2 min, 70:30 to 0:100 (A:B) over 60 min, 0:100 (A:B) for 3 min, then reversion back to 70:30 (A:B) over 1 min, 70:30 (A:B) for 2min.

#### Analytical HPLC

HPLC analyses were performed on a Shimadzu Prominence-i LC-2030 system with a Dr. Maisch ReproSil Gold 120 C18 column (4.6 × 250 mm, 5  $\mu$ m) at 30 °C and equipped with a UV detector monitoring 214 nm. The following solvent system, at a flow rate of 1 mL/min, was used: solvent A, 0.1% TFA in water/acetonitrile 95/5; solvent B, 0.1% TFA in water/acetonitrile 5/95. Gradient elution was as follows: 95:5 (A:B) for 1 min, 95:5 to 0:100 (A:B) over 25 min, 0:100 (A:B) for 2 min, then reversion back to 95:5 (A:B) over 1min, 95:5 (A/B) 1min.

#### HRMS

HRMS analyses were performed on a Thermo Scientific Dionex UltiMate 3000 HPLC system with a Phenomenex Kinetex C18 column (2.1 × 150 mm, 2.6  $\mu$ m) at 35 °C and equipped with a diode array detector. The following solvent system, at a flow rate of 0.3 mL/min, was used: solvent A, 0.1% formic acid in water; solvent B, 0.1% formic acid in acetonitrile. Gradient elution was as follows: 95:5 (A:B) for 1 min, 95:5 to 5:95 (A:B) over 9 min, 5:95 to 2:98 (A:B) over 1 min, 2:98 (A:B) for 1 min, then reversion back to 95:5 (A:B) over 2 min, 95:5 (A:B) for 1 min. This system was connected to a

Bruker micrOTOF-Q II mass spectrometer (ESI ionization) calibrated internally with sodium formate.

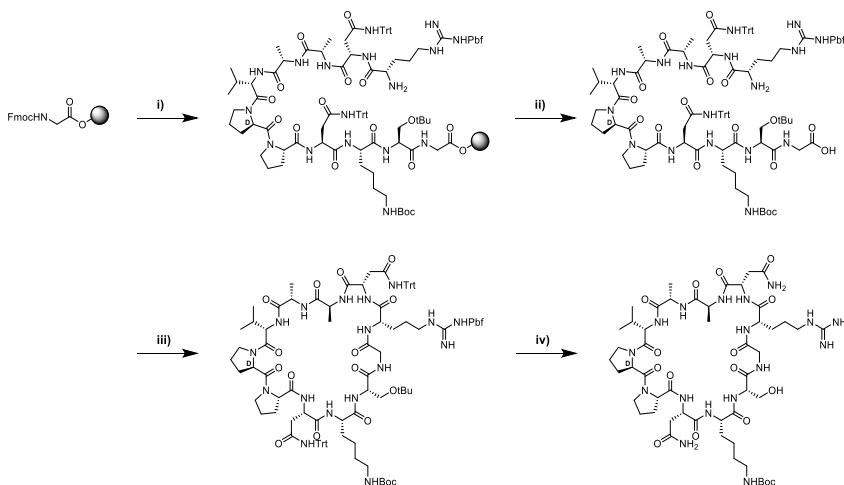
### 5.4.2 Automated peptide synthesis

Peptides were synthesized by a microwave-assisted peptide synthesizer (Liberty Blue HT-12, CEM) using the following cycles of deprotection and coupling.

1) Fmoc deprotection: 90 °C, 80 W, 65 s with 20% piperidine in DMF, 3 mL/deprotection

2) AA coupling: Fmoc-AA-OH (0.2 M in 2.5 mL DMF, 5 eq), DIC (1 M in 1 mL DM, 10 eq) and Oxyma (1 M in 0.5 mL DMF, 5 eq) at 76 °C, 80 W, 15 s before the temperature was increased to 90 °C, 80 W for 110 s.

**General SPPS route employed for the synthesis of all L-Pro-D-Pro cyclized peptides:** i) Fmoc SPPS; ii) HFIP, CH<sub>2</sub>Cl<sub>2</sub>, 1h; iii) BOP, DIPEA, CH<sub>2</sub>Cl<sub>2</sub>, 16h; iv) TFA, TIS, H<sub>2</sub>O, 1h.

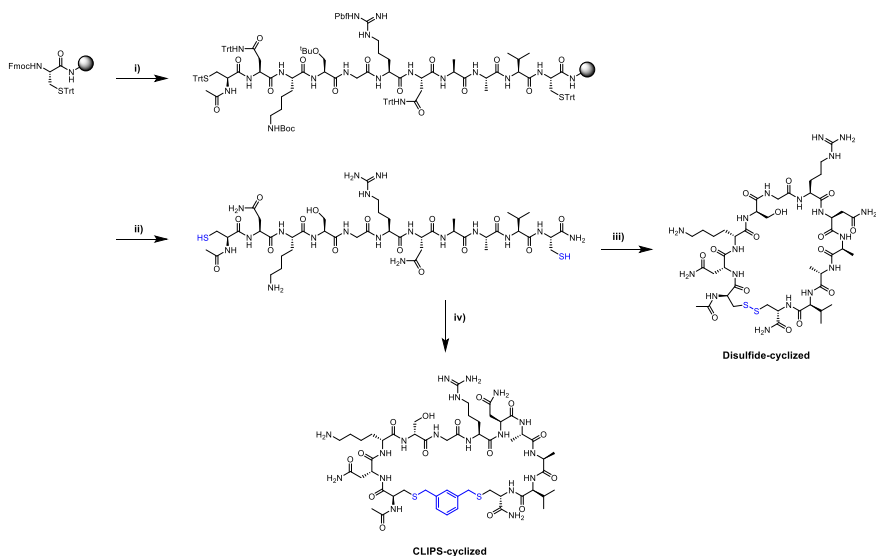


### Synthesis of L-Pro-D-Pro peptides

Chlorotrityl resin (5.0 g, 1.60 mmol.g<sup>-1</sup>) was loaded with Fmoc-Gly-OH. Resin loading was determined to be 0.63 mmol.g<sup>-1</sup>. Linear peptide encompassing Gly31 to Arg32 (numbering based on the EF-P sequence) was assembled manually *via* standard Fmoc solid-phase peptide synthesis

(SPPS) (resin bound AA:Fmoc-AA:BOP:DIPEA, 1:4:4:8 molar eq.) on a 0.25 mmol scale. DMF was used as solvent and Fmoc deprotections were carried out with piperidine:DMF (1:4 v:v). Amino acid side chains were protected as follows: <sup>t</sup>Bu for Ser, Trt for Asn, Boc for Lys, and Pbf for Arg. Following coupling and Fmoc deprotection of the final Arg32, the resin was washed with CH<sub>2</sub>Cl<sub>2</sub> and treated with (CF<sub>3</sub>)<sub>2</sub>CHOH:CH<sub>2</sub>Cl<sub>2</sub> (1:4, 10 mL) for 1 h and rinsed with additional (CF<sub>3</sub>)<sub>2</sub>CHOH:CH<sub>2</sub>Cl<sub>2</sub> and CH<sub>2</sub>Cl<sub>2</sub>. The combined washings were then evaporated to yield the linear protected peptide with free C- and N-termini. The residue was dissolved in CH<sub>2</sub>Cl<sub>2</sub> (150 mL) and treated with BOP (0.22 g, 0.5 mmol) and DIPEA (0.17 mL, 1.0 mmol) and the solution was stirred overnight after which TLC indicated complete cyclization. The reaction mixture was concentrated and directly treated with TFA:TIS:H<sub>2</sub>O (95:2.5:2.5, 10 mL) for 90 min. The reaction mixture was added to cold MTBE:hexanes (1:1) and the resulting precipitate was centrifuged at 3500 rpm for 5 min, washed once more with MTBE:hexanes (1:1) and centrifuged at 3500 rpm for 5 min. The crude cyclic peptide was lyophilized from <sup>t</sup>BuOH:H<sub>2</sub>O (1:1) and purified with reverse phase HPLC. Pure fractions were pooled and lyophilized to yield the desired cyclic peptide products in >95% purity as white powders, typically in 20-70 mg quantities (18-27 % yield based on resin loading).

**General SPPS route employed for the synthesis of all disulfide and CLIPS peptides:** i)  $\mu$ W Fmoc SPPS, 90°C; ii) TFA, TIS, H<sub>2</sub>O, 1h; iii) 100 mM NH<sub>4</sub>HCO<sub>3</sub>, bubble air, 16h; iv) 100mM NH<sub>4</sub>HCO<sub>3</sub>, MeCN,  $\alpha,\alpha'$ -Dibromo-m-xylene, 1h.



## Synthesis of CLIPS- and disulfide-cyclized peptides

Rink Amide resin (150 mg, 0.684 mmol.g<sup>-1</sup>) was loaded into the CEM Liberty Blue peptide synthesizer for a 0.1 mmol scale. Linear peptide encompassing Cys1 to Cys11 were assembled using microwave irradiation (resin bound AA:Fmoc-AA:DIC:Oxyma, 1:5:5:5 molar eq.). DMF was used as solvent and Fmoc deprotections were carried out with piperidine:DMF (1:4, v:v). Amino acid side chains were protected as follows: <sup>t</sup>Bu for Ser, Trt for Asn/Cys, Boc for Lys, and Pbf for Arg. Following coupling, Fmoc deprotection and acetylation of the final Cys11, the linear peptide was removed from the peptide synthesizer, washed with DCM and directly treated with TFA:H<sub>2</sub>O:TIS:EDT (90:5:2.5:2.5, 10 mL) for 90 min. The reaction mixture was added to cold MTBE:hexanes (1:1) and the resulting precipitate washed once more with MTBE:hexanes (1:1) and the resulting precipitate was centrifuged at 3500 rpm for 5 min, washed once more with MTBE:hexanes (1:1) and centrifuged at 3500 rpm for 5 min. The obtained pellet was split into two and dissolved in a mixture of 20 mM NH<sub>4</sub>HCO<sub>3</sub> and MeCN (typically 3:1 but ratio can be varied depending on peptide solubility, total volume should be 90 mL per 0.05 mmol).

*To make the disulfide peptide:* the peptide solution was stirred for 1 h at room temperature while bubbling oxygen through the mixture.

*To make the CLIPS peptide:* A solution 1,3-bis(bromomethyl)benzene (0.075 mmol; 19.7 mg) in MeCN (5 mL) was added to the peptide solution and stirred for 1 h at room temperature. Once the peptide reactions were completed MeCN was evaporated and the crude peptides were lyophilized from <sup>t</sup>BuOH:H<sub>2</sub>O (1:1) and purified with reverse phase HPLC. Pure fractions were pooled and lyophilized to yield the desired disulfide or CLIPS products in >95% purity as white powders, typically in 10-40 mg quantities (18-30 % yield based on resin loading).

### **Synthesis of the trp-zip peptides**

Rink Amide resin (150 mg, 0.684 mmol.g<sup>-1</sup>) was loaded into the CEM Liberty Blue peptide synthesizer for a 0.1mmol scale. Linear peptide encompassing the first amino acid to the last amino acid were assembled using microwave irradiation (resin bound AA:Fmoc-AA:DIC:Oxyma, 1:5:5:5 molar eq.). DMF was used as solvent and Fmoc deprotections were carried out with piperidine:DMF (1:4, v:v). Amino acid side chains were protected as follows: <sup>t</sup>Bu for Ser/Thr/Asp/Glu, Trt for Asn/Cys/Gln, Boc for Lys/Trp, and Pbf for Arg. Following coupling, Fmoc deprotection and acetylation of the final amino acid the linear peptide was removed from the peptide synthesizer, washed with DCM and directly treated with TFA:H<sub>2</sub>O:TIS:EDT (90:5:2.5:2.5, 10 mL) for 90 min. The reaction mixture was added to cold MTBE:hexanes (1:1) and the resulting precipitate washed once more with MTBE:hexanes (1:1) and the resulting precipitate was centrifuged at 3500 rpm for 5 min, washed once more with MTBE:hexanes (1:1) and centrifuged at 3500 rpm for 5 min. The crude peptides were lyophilized from <sup>t</sup>BuOH:H<sub>2</sub>O (1:1) and purified with reverse phase HPLC. Pure fractions were pooled and lyophilized to yield the desired peptide products in >95% purity as white powders, typically in 20-70 mg quantities (20-30 % yield based on resin loading).

### **5.4.3 Protein expression and purification**

pBADSUMO plasmids harbouring *earp* or *efp* gene (from *Pseudomonas aeruginosa* PAO1, synthesized and cloned by GenScript) were used to transform chemically competent *E. coli* TOP10 cells (standard heat-shock

protocol) and plated on LB-agar plates containing an appropriate antibiotic (ampicillin). A single colony was selected from the plate and used to prepare glycerol stock. To express the protein on large scale, a preculture (10 mL) in LB (100 µg/mL ampicillin) was prepared from the appropriate glycerol stock and grown at 37 °C with shaking (200 rpm) for 16-18 h. It was then used to inoculate 500 mL of Terrific Broth (TB) (100 µg/mL ampicillin) at 1:200 dilution ratio and incubated at 37 °C with shaking until OD<sub>600</sub> reached values of 0.6-0.7. Protein expression was induced by addition of 0.05% L-Ara (w/v, final concentration) and further incubation for 16-18 hours at 18 °C with shaking (EarP) or 4 h at 37 °C with shaking (EF-P). Cells were harvested by centrifugation at 5000 rpm for 15 min (Sorvall centrifuge, F-12 6x500 LEX fixed angle rotor, Thermo Scientific). The supernatant was discarded and cell pellets were resuspended in ice-cold lysis buffer (20 mM Tris, 100 mM NaCl, pH 8) in the presence of the protease inhibitor cocktail (Roche, complete, EDTA-free). Cells were lysed by sonication (Branson Sonifier 450, output control 30%, 2 min) and subsequently spun down at 7000 rpm at 4 °C for 1 hour. For His<sub>6</sub>-tag protein purification, the cell-free extract was incubated with Ni-NTA resins (Qiagen) for 1.5 h at 4 °C with gentle shaking. The mixture was loaded on a gravity column and the lysate was allowed to flow through, followed by a washing step (twice) with washing buffer (20 mM Tris, 100 mM NaCl, 15 mM imidazole, pH 8). The protein of interest was eluted with elution buffer (20 mM Tris, 100 mM NaCl, 400 mM imidazole, pH 8) in three steps. Column fractions were analyzed by 12% SDS-PAGE analysis and the resulting gels were stained using Instant Blue protein stain. Fractions containing protein of interest were pooled and desalted using midi PD-10 desalting columns (GE Healthcare). Proteins were routinely obtained in the yields of 20-40 mg per 1 L of culture.

#### **5.4.4 *In vitro* rhamnosylation of Arg-containing peptides**

Reaction mixtures routinely consisted of 100 µM peptide (from 10 mM DMSO stock to keep DMSO content low) and 1 mM TDP-Rha. Reactions were generally initiated by the addition of 20 µM EarP (usually from freshly concentrated 200-300 µM stock) and incubated at 30 °C overnight. For experiments where peptide substrates were pushed to conversion, 200 µM of peptide substrate and 70 µM of EarP were used. To prepare the sample for LCMS analysis, the reaction mixture was spun down in the table top



centrifuge (Eppendorf) and an aliquot was taken for RP-LCMS analysis (1  $\mu$ L injection, Acquity UPLC HSS T3 column (Waters, 2.1 $\times$ 150 mm, 1.8  $\mu$ m) was used in combination with eluents A (0.1% formic acid in H<sub>2</sub>O) and B (0.1% formic acid in acetonitrile), 20 min run (flow rate 0.3 mL/min) with a linear gradient from 5% to 50% of B in 10min with subsequent increase to 95% B for 3 min).

#### **5.4.5 Time course of rhamnosylation**

To visualize the progress of rhamnosylation of 11mer\_*Pa* and EF-P\_*Pa*, the rhamnosylation reaction with respective acceptor substrates was monitored over time. For the 11mer\_*Pa* reaction: mixtures containing 40  $\mu$ M EarP, 100  $\mu$ M peptide and 1 mM TDP-Rha were incubated at 30  $^{\circ}$ C. For EFP\_*Pa* reaction: mixtures containing 0.4  $\mu$ M EarP, 100  $\mu$ M peptide and 1 mM TDP-Rha were incubated at 30  $^{\circ}$ C. At certain time points aliquots were withdrawn and quenched either by diluting the reaction fourfold and removing the EarP enzyme by centrifugation through a 10 kDa MWCO spin filter (for 11mer\_*Pa* reaction) or by diluting threefold and heating at 100  $^{\circ}$ C for 10 min (EF-P\_*Pa* reaction). For the 11mer\_*Pa* reaction the aliquots were analyzed with RP-LCMS as described above. For the EF-P\_*Pa* reaction, aliquots were further diluted tenfold with 2% ACN, 0.1% FA solution (aq.) and analyzed with q-TOF LCMS (Waters). A BEH300 C4 column was used (Waters, 2.1 $\times$ 150 mm, 1.7  $\mu$ m) in combination with eluents A (0.1% formic acid in H<sub>2</sub>O) and B (0.1% formic acid in acetonitrile), 20 min run (flow rate 0.3 mL/min) with a linear gradient from 5% to 50% of B in 10 min with subsequent increase to 95% B in 1 min and isocratic flow of 95% B for 2 min). Deconvolution was performed with an open access UniDec software. Graphs were prepared using GraphPad Prism 8. Reactions were performed in duplicates.

#### **5.4.6 Large-scale rhamnosylation and purification of the 11mer\_*Pa* peptide**

To scale up the enzymatic rhamnosylation of 11mer-L-Pro-D-Pro\_*Pa* for NMR studies, 1.8 mM 11mer\_*Pa* (5 mg), 3.5 mM TDP-Rha (5.17 mg) and 26.4  $\mu$ M EarP (3.7 mg) were incubated overnight at 30  $^{\circ}$ C. Reaction was pushed to full conversion over two days by addition of extra 10  $\mu$ M EarP and extra 0.625 mM TDP-Rha after 16 h and 48 h. Subsequently, the reaction mixture was applied to an Amicon spin filter (MWCO 10 kDa, 15 mL,

Millipore) and centrifuged at  $5000 \times g$  to remove the enzyme. The resulting solution was further purified from TDP and TDP-Rha by strong anion exchange on FPLC ÄKTA system (GE Healthcare). For this, 0.25 mL of the reaction mixture (approx. 1 mM peptide concentration) was applied on Q FF column (5 mL, GE Healthcare) with flow rate 1 mL/min in 5 column volumes (CV). The column was eluted with the linear gradient from 0 to 10% Buffer B in two CV with subsequent increase to 100% in four CV (Buffer B: 1M  $\text{NH}_4\text{HCO}_3$ ). Elution was monitored with UV (214 nm - peptide and 280 nm - TDP, TDP-Rha). After 14 runs, the fractions containing rhamnosylated 11mer\_*Pa* peptide were pooled and freeze-dried. Residual buffer salts were removed by desalting with PD10 desalting columns (GE Healthcare). The Rha-11mer\_*Pa* peptide was eluted in pure  $\text{H}_2\text{O}$  and freeze-dried to yield 1.5 mg of material for NMR studies.

#### **5.4.7 Isothermal titration calorimetry (ITC) experiments**

All binding experiments were performed using a MicroCal PEAQ-ITC Automated microcalorimeter (Malvern). The samples were equilibrated at 20 °C prior to the measurement. The solution of ligand in 20 mM Tris-HCl, 100 mM NaCl, pH 8, was titrated into a solution of EarP:TDP (1:3) in the same buffer. The titrations were conducted at 20 °C under constant stirring at 750 rpm. Each binding experiment consisted of an initial injection of 0.3  $\mu\text{L}$  followed by 19 separate injections of 2.0  $\mu\text{L}$  into the sample cell of 200  $\mu\text{L}$ . The time between each injection was 150 s, the measurements were performed with the reference power set at 5  $\mu\text{cal s}^{-1}$  and the feedback mode set at "high". The calorimetric data obtained was analyzed using MicroCal PEAQ-ITC Analysis Software Version 1.20. ITC data fitting was made based on the "One set of sites" fitting model of the software. The best fit was defined by chi-square minimization. The thermodynamic parameters are reported as the average of three independent experiments.

#### **5.4.8 Preparation of crude reaction mixture for HSQC experiments (glycosidic linkage determination)**

To prepare the crude reaction mixture of Rha-11mer\_*Pa* for glycosidic linkage determination, 1.4 mg of TDP-Rha (in  $\text{D}_2\text{O}$ ), 1 mg of 11mer\_*Pa* (in  $\text{D}_2\text{O}$ ) and 50  $\mu\text{M}$  EarP (exchanged into  $\text{D}_2\text{O}$  by diafiltration) were mixed in a total volume of 600  $\mu\text{L}$  (in  $\text{D}_2\text{O}$ ) and incubated overnight at 30 °C. The next

day, conversion was checked by LCMS and determined to be about 78%. To push conversion further, an additional 0.6 mg of TDP-Rha (in D<sub>2</sub>O) and 14 μM of EarP (exchanged into D<sub>2</sub>O) were added and the reaction mixture was incubated overnight at 30 °C. LCMS analysis determined the conversion to be about 88%. The resulting crude sample was used for the NMR analysis of the glycosidic linkage.

#### 5.4.9 Antibody-based dot blot assay

Typically, 4 μL of mixture of interest was spotted on the nitrocellulose membrane and let dry for 1 h. Subsequently, the membrane was blocked in 3% BSA in TBS buffer (Tris buffer saline, 20 mM Tris, 150 mM NaCl, pH 7.5), followed by incubation with anti-Arg<sup>Rha</sup> antibody (1:1000 in 3% BSA-TBS) for 2 h while shaking. Consequently, the membrane was washed with TBS three times (5 min each) and incubated with the secondary Alexa488 coupled Anti-rabbit antibody (Abcam, 1:7500 in 3% BSA-TBS) for 30 min. After three washes with TBS (5 min each), the membrane was dried and visualized with Typhoon fluorescent scanner (Typhoon FLA 9500, GE Healthcare) using Alexa488 settings.

#### 5.4.10 RIF values determination

An experiment to determine relative ionization factor values for rhamnosylated *vs* non-rhamnosylated peptides was adopted from [34]. Briefly, reaction mixtures containing 100 μM peptide (11mer\_*Pa*, 11mer\_*Rso*, 11mer\_*Pa*\_A34G), 1 mM TDP-Rha and 40 μM EarP were prepared and incubated overnight at 30 °C. Alongside, identical mixtures where TDP-Rha was omitted (blank) were prepared and incubated overnight at 30 °C. To prepare LCMS samples, either the reaction sample or a 1:1 mixture of reaction and blank sample were filtered through the 10 kDa MWCO Amicon filter and analyzed by LCMS. RIF values were calculated according to the formulae from [34]:

$$(1) \%I(Re) = \frac{I(P)}{I(P)+I(S)} \times 100\%$$

$$(2) \%I(mix) = \frac{I(Pm)}{I(Pm)+I(Sm)} \times 100\%$$

$$(3) RIF(P \text{ to } S) = \frac{\%I(Re) \times \%I(mix)}{\%I(Re) \times \%I(mix) + I(Re) - 2 \times \%I(mix)}$$

$$(4) \%conversion = \frac{I(P)/RIF}{\frac{I(P)}{RIF} + I(S)} \times 100\%$$

$I(P)$  - intensity of the product ion in the reaction sample;  $I(S)$  - intensity of the substrate ion in the reaction sample;  $I(P_m)$  - intensity of the product ion in the 1:1 mixed sample;  $I(S_m)$  - intensity of the substrate in the 1:1 mixed sample.

#### 5.4.11 NMR spectroscopy

All NMR spectra were recorded on a Varian Inova 500 MHz NMR spectrometer equipped with an HCN triple resonance probe or on a Bruker Avance NEO 600 MHz spectrometer equipped with either a broadband Prodigy CryoProbe or a SmartProbe. The peptides were dissolved in a mixture of H<sub>2</sub>O/D<sub>2</sub>O (9:1 v/v) with 15 mM phosphate buffer at pH = 4.7. Spectral assignments and structural analyses were accomplished by recording TOCSY spectra (mixing time 80 ms) and NOESY spectra (mixing times 300 or 500 ms) at 278 K using a spectral width of 10 ppm in both dimensions and the excitation sculpting solvent suppression scheme.<sup>41</sup> <sup>1</sup>H-<sup>13</sup>C HSQC spectra were recorded at 278 K with a spectral width of 10 ppm in the <sup>1</sup>H- and 115 ppm in the <sup>13</sup>C-dimension. All data were processed with NMRPipe<sup>42</sup> and analyzed using Sparky.<sup>43</sup> Chemical shifts were referenced with respect to internal dioxane ( $\delta_{1H} = 3.750$  ppm/  $\delta_{13C} = 69.3$  ppm).

Temperature coefficients of the amide protons of selected peptides were determined by measuring 1D <sup>1</sup>H experiments in a temperature series between 273 and 303 K with 5 K intervals. The <sup>1</sup>J-coupling constant of the anomeric proton and carbon was determined by recording a <sup>1</sup>H-<sup>13</sup>C HSQC at 298 K without carbon decoupling during acquisition on a crude mixture of glycosylated substrate, EarP and dTDP-Rha. Diffusion ordered NMR spectroscopy (DOSY) measurements were performed on the same crude mixture using a stimulated spin-echo bipolar gradient pulse sequence.<sup>44</sup> 16 experiments of 16 scans each were recorded with gradient strengths increasing linearly between 0 and 42 G/cm with a pulse length of 1 ms ( $\delta = 2$  ms). A diffusion delay of  $\Delta = 200$  ms was used. Saturation transfer difference NMR (STD-NMR)<sup>45</sup> experiments were performed on samples containing mixtures of EarP, peptide and dTDP plus controls without EarP present. Saturation of the protein resonances was accomplished by a 2 s pulse train of 50 ms Gaussian pulses applied at a frequency corresponding

to -0.5 ppm (on resonance) and 30 ppm (off resonance). Protein background signals were suppressed by a  $T_{1\rho}$  purge pulse before data acquisition. These data were processed and analyzed using Mnova (Mestrelab Research S.L., Spain).

## References

1. Khoury, G.A.; Baliban, R.C.; Floudas, C.A. *Sci. Rep.* **2011**, *1*, 90.
2. Kelleher, D. J.; Gilmore, R. *Glycobiology* **2006**, *16*, 47-62.
3. Szymanski, C.M.; Yao, R.; Ewing, C.P.; Trust, T.J.; Guerry, P. *Mol. Microbiol.* **1999**, *32*, 1022-1030.
4. Dell, A.; Galadari, A.; Sastre, F.; Hitchen, P. *Int. J. Microbiol.* **2010**, 148178.
5. Yan, A.; Lennarz, W.J. *J. Biol. Chem.* **2005**, *280*, 3121-3124.
6. Lizak, C.; Gerber, S.; Numao, S.; Aebi, M.; Locher, K.P. *Nature* **2011**, *474*, 350-355.
7. Bause, E. *Biochem. Soc. Trans.* **1984**, *12*, 514-517.
8. Imperiali, B.; Shannon, K.L.; Unno, M.; Rickert, K.W. *J. Am. Chem. Soc.* **1992**, *114*, 7944-7945.
9. Lizak, C.; Gerber, S.; Michaud, G.; Schubert, M.; Fan, Y-Y.; Bucher, M.; Darbre, T.; Aebi, M.; Reymond, J-L.; Locher, K.P. *Nat. Commun.* **2013**, *4*, 2627.
10. Imperiali, B. *Acc. Chem. Res.* **1997**, *30*, 452-459.
11. Petrescu, A.J.; Milac, A.L.; Petrescu, S.M.; Dwek, R.A.; Wormland, M.R. *Glycobiology* **2004**, *14*, 103-114.
12. Silverman, J.M.; Imperiali, B. *J. Biol. Chem.* **2016**, *291*, 22001-22010.
13. Z. Li, M. Fischer, M. Satkunarajah, D. Zhou, S. G. Withers and J. M. Rini. *Nat. Commun* **2017**, *8*, 185.
14. Z. Li, K. Han, J. E. Pak, M. Satkunarajah, D. Zhou and J. M. Rini. *Nat. Chem. Biol.* **2017**, *13*, 757-763.
15. Nothhaft, H.; Szymanski, C.M. *Curr. Opin. Chem. Biol.* **2019**, *53*, 16-24.
16. Lassak, J.; Keilhauer, E.C.; Fürst, M.; Wuichet, K.; Gödeke, J.; Starosta, A.L.; Chen, J-M.; Søgaard-Andersen, L.; Rohr, J.; Wilson, D.N.; Häussler, S.; Mann, M.; Jung, K.. *Nat. Chem. Biol.* **2015**, *11*, 266-270.
17. Gast, D.; Koller, F.; Krafczyk, R.; Bauer, L.; Wunder, S.; Lassak, J.; Hoffmann-Röder, A. *Org. Biomol. Chem.* **2020**, *18*, 6823-6828.
18. Rajkovic, A.; Erickson, S.; Witzky, A.; Branson, O.E.; Seo, J.; Gafken, P.R.; Frietas, M.A.; Whitelegge, J.P.; Faull, K.F.; Navarre, W.; Darwin, A.J.; Ibba, M. *mBio*. **2015**, *6*.
19. Singh, D.G.; Lomako, J.; Lomako, W.M.; Whelan, W.J.; Meyer, H.E.; Serwe, M.; Metzger, J.W. *FEBS Lett.* **1995**, *376*, 61-64.
20. Li, S.; Zhang, L.; Yao, Q.; Li, L.; Dong, N.; Rong, J.; Gao, W.; Ding, X.; Sun, L.; Chen, X.; Chen, S.; Shao, F. *Nature* **2013**, *501*, 242-246.
21. Ude, S.; Lassak, J.; Starosta, A.L.; Kraxenberger, T.; Wilson, D.N.; Jung, K. *Science* **2013**, *339*, 82-85.
22. Peil, L.; Starosta, A.L.; Lassak, J.; Atkinson, G.C.; Virumäe, K.; Spitzer, M.; Tenson, T.; Jung, K.; Remme, J.; Wilson, D.N. *Proc. Natl. Acad. Sci. U. S. A.* **2013**, *110*, 15265-15270.
23. Lassak, J.; Wilson, D.N.; Jung, K. *Mol. Microbiol.* **2016**, *99*, 219-235.
24. Yanagisawa, T.; Takahashi, H.; Suzuki, T.; Masuda, A.; Dohmae, N.; Yokoyama, S. *PLoS One*. **2015**, *11*.
25. Li, X.; Krafczyk, R.; Macošek, J.; Li, Y-L.; Zou, Y.; Simon, B.; Pan, X.; Wu, Q-Y.; Yan, F.; Li, S.; Hennig, J.; Jung, K.; Lassak, J.; Hu, H-G. *Chem. Sci.* **2016**, *7*, 6995-7001.
26. Wang, S.; Corcilus, L.; Sharp, P.P.; Rajkovic, A.; Ibba, M.; Parker, B.L.; Payne, R.J. *Chem. Sci.* **2017**, *8*, 2296-2302.
27. Krafczyk, R.; Macošek, J.; Jagtap, P.K.A.; Gast, D.; Wunder, S.; Mitra, P.; Jha, A.K.; Rohr, J.; Hoffman-Röder, A.; Jung, K.; Hennig, J.; Lassak, J. *mBio* **2017**, *8*, e014112.
28. Sengoku, T.; Suzuki, T.; Dohmae, N.; Watanabe, C.; Honma, T.; Hikida, Y.; Yamaguchi, Y.; Takahashi, H.; Yokoyama, S.; Yanagisawa, T. *Nat. Chem. Biol.* **2018**, *14*, 368-374.
29. He, C.; Liu, N.; Li, F.; Jia, X.; Peng, H.; Liu, Y.; Xiao, Y. *J. Bacteriol.* **2019**, *201*, e00128.
30. Kyrpides, N.C.; Woese, C.R.; Ouzounis, C.A. *Trends Biochem. Sci.* **1996**, *21*, 425-426.

31. Volkwein, W.; Krafczyk, R.; Jagtap, P.K.A.; Parr, M.; Mankina, E.; Macošek, J.; Guo, Z.; Fürst, M.J.L.J.; Pfab, M.; Frishman, D.; Hennig, J.; Jung, K.; Lassak, J. *Front. Microbiol.* **2019**, *10*.
32. Lu, Q.; Li, S.; Shao, F. *Trends Microbiol.* **2015**, *23*, 630-641.
33. Robinson, J.A. *Acc. Chem. Res.* **2007**, *41*, 1278-1288.
34. Kightlinger, W.; Lin, L.; Rosztoczy, M.; Li, W.; DeLisa, M.P.; Mrksich, M.; Jewett, M.C. *Nat. Chem. Bio.* **2018**, *14*, 627-635.
35. Timmerman, P.; Beld, J.; Puijk, W.C.; Meloen, R.H. *ChemBioChem.* **2005**, *6*, 821-824.
36. Santiveri, C.M.; León, E.; Rico, M.; Jiménez, M.A. *Chem. Eur. J.* **2008**, *14*, 488-499.
37. Cochran, A.G.; Skelton, N.J.; Starovasnik, M.A. *Proc. Natl. Acad. Sci. U. S. A.* **2001**, *98*, 5578-5583.
38. Viegas, A.; Manso, J.; Nobrega, F.L.; Cabrita, E.J. *J. Chem. Educ.* **2011**, *88*, 990-994.
39. Robinson, J.A. *Chimia.* **2013**, *67*, 885-890.
40. Gimeno, M.P.; Glas, A.; Koch, O.; Grossman, T.N. *Angew. Chem. Int. Ed.* **2015**, *54*, 8896-8927.
41. Hwang, T. L.; Shaka, A. J. *J. Magn. Reson. Ser. A* **1995**, *112*, 275-279.
42. Delaglio, F.; Grzesiek, S.; Vuister, G. W.; Zhu, G.; Pfeifer, J.; Bax, A. *J. Biomol. NMR* **1995**, *6*, 277-293.
43. Lee, W.; Tonelli, M.; Markley, J. L. *Bioinformatics* **2015**, *31*, 1325-1327.
44. Cotts, R. M.; Hoch, M. J. R.; Sun, T.; Markert, J. T. *J. Magn. Reson.* **1989**, *83*, 252-266.





# Chapter 6

## Summary and Outlook

The work described in this thesis focuses on the development and elucidation of cyclic antimicrobial peptides that operate *via* novel modes of action. With the accelerated appearance of multi-drug resistant bacterial pathogens, we may be on the brink of a “post-antibiotic” era and new antibiotics that operate *via* novel modes of action are desperately needed.

In **Chapter 1** a general introduction was given to the main classes of cyclic lipopeptide antibiotics with a focus on their unique structural features, mode of actions, and clinical development. These natural products are produced by soil organisms and consist of a peptide macrocycle that is decorated with a lipid. There is great structural diversity in this class with over 40 known lipopeptides.

Laspartomycin, Friulimicin and Amphomycin are all lipopeptides that belong to the family of calcium dependant antibiotics (CDAs), of which Daptomycin is also member. It is known that their molecular target is C<sub>55</sub>-P and to gain a better understanding of the interplay and binding we obtained crystal structures of these antibiotics bound to both calcium and C<sub>10</sub>-P, truncated variant of C<sub>55</sub>-P (**Chapter 2**). The complex showed us that Friulimicin and Amphomycin form a “higher ordered” structure that is not seen with Laspartomycin. This higher ordered structure arises from subtle changes in the macrocyclic portion of these peptides. Namely, the inclusion of a carboxylate and amino containing amino acid allows these peptides to form inter-molecular salt bridges that is not possible in the case of Laspartomycin. From the crystal structure it was revealed that the hydrophobic amino acid Valine at position 10 occupies this space in the case of Friulimicin and Amphomycin. To further explore this analogue, Amphomycin and Laspartomycin were synthesized with various branched, hydrophobic amino acids in position 10. It was found that the parent amino acid (Valine for Amphomycin and Isoleucine for Laspartomycin) is the most well-tolerated one.

Next the contribution of achiral residues in laspartomycin was explored (**Chapter 3**). It is known that all CDAs contain the calcium binding motif (Asp-X<sub>6</sub>-Asp-Gly<sub>8</sub>), and using the newly reported synthesis route a series of analogues were prepared that introduced the achiral Aminoisobutyric acid (Aib) into the achiral 4, 6 and 8 positions of Laspartomycin. All these analogues showed very poor activity compared to

the patent compound and incorporation of Aib at position 8 led to complete loss of activity. A second series of compounds incorporating either D or L-alanine at positions 4 and 6 were prepared. The introduction of both D- and L-Ala at position 4 led to compounds that showed activity similar to laspatpomcyin. However, at position 6 the D-Ala variant is 16-times more active than the L-Ala and even showed slightly better activity than laspartomycin C.

**Chapter 4** switches focus to Gram-negative bacteria and focuses on the newly reported macrocyclic peptide antibiotics that target the outer membrane protein BamA. We developed a convent strategy to easily ligate the polymyxin nonapeptide to the  $\beta$ -hairpin peptide using a chemoenzymatic approach. These antibiotics have potent activity against colistin resistant mcr-positive strains of *E. coli*. Furthermore, we prepared a series of chimeric peptides that were assembled using copper-catalyzed azide-alkyne cycloadditions. The  $\beta$ -hairpin macrocycle containing a propargyl-glycine was readily prepared entirely on solid support and cleanly conjugated to the different azide containing PMEN units. The resulting triazole linked bicyclic peptides demonstrated a range of antibacterial activities with the azido-glycine linked conjugate demonstrating the most potent activity. Interestingly, conjugates containing either longer or shorter linkers between the  $\beta$ -hairpin macrocycle and PMEN moiety were significantly less active. These findings point to the importance of identifying the optimal linker properties to achieve potent antibacterial activity. Ongoing work is still being done to evaluate the potential of this exciting new class of anti-Gram-negative agents.

**Chapter 5** focusses on the substrate recognition specificity of the bacterial arginine rhamnosyltransferase EarP. The enzyme is responsible for arginine glycosylation which is exceedingly rate. EF-P rhamnosylation is crucial for bacterial fitness and when abolished in *Pseudomonas aeruginosa* led to multiple detrimental effects, including greater susceptibility to antibiotics. In this chapter a series of short peptide mimics were prepared that contained a  $\beta$ -hairpin secondary structure. It was revealed that this secondary structural unit plays a crucial role in recognition. Through screening several secondary structure stabilizing templates and various peptide lengths, the smallest EF-P fragment to be rhamnosylated to date was identified, which is a cyclic 11mer peptide. Several mutants of this

peptide were tested to screen the promiscuity of EarP and revealed that EarP had a greater tolerance towards amino acid sequence variation than the absence of secondary structure elements. This is especially important for the rational design of inhibitors as well as for developing tools for the identification of other bacterial arginine rhamnosylation systems.

# **Nederlandse Samenvatting**

Het in dit proefschrift beschreven werk richt zich op de ontwikkeling en opheldering van cyclische antimicrobiële peptiden die werken via nieuwe mechanismen. Met de versnelde opkomst van multiresistente bacteriële pathogenen, staan we misschien aan de vooravond van een "post-antibioticum"-tijdperk en zijn nieuwe antibiotica die werken *via* nieuwe mechanismen hard nodig.

In **Hoofdstuk 1** is een algemene introductie en samenvatting gewijd aan de belangrijkste klassen van cyclische lipopeptide antibiotica met een focus op hun unieke structurele kenmerken, werkingsmechanisme en klinische ontwikkeling. Deze natuurlijke producten worden geproduceerd door bodemorganismen en bestaan uit een peptide-macrocyclus, gekoppeld aan een lipide. Er is een grote structurele diversiteit in deze klasse met meer dan 40 bekende lipopeptiden.

Laspertomycine, Friulimicin en Amphomycin zijn allemaal lipopeptiden die behoren tot de familie van calciumafhankelijke antibiotica (CDA's), waar ook daptomycine onder valt. Het is bekend dat hun moleculaire doelwit C<sub>55</sub>-P is en om een beter begrip te krijgen van het samenspel en de binding hebben we kristalstructuren verkregen van deze antibiotica gebonden aan zowel calcium als C<sub>10</sub>-P, een afgeknotte variant van C<sub>55</sub>-P (**Hoofdstuk 2**). Het complex liet zien dat Friulimicin en Amphomycin een "hogere geordende" structuur vormen, wat niet het geval is bij Laspertomycine. Deze hoger geordende structuur komt voort uit subtiele veranderingen in het macrocyclische deel van deze peptiden. De opname van een carboxylaat en amino-bevattend aminozuur maakt het namelijk mogelijk dat deze peptiden intermoleculaire zoutbruggen vormen, wat in het geval is van Laspertomycine niet mogelijk is. Uit de kristalstructuur bleek dat het hydrofobe aminozuur Valine op positie 10 deze ruimte inneemt in het geval van Friulimicin en Amphomycin. Om dit analoog van Amphomycin en Laspertomycine verder te onderzoeken werd het gesynthetiseerd met verschillende vertakte, hydrofobe aminozuren op positie 10. Het bleek dat het bron-aminozuur (Valine voor Amphomycin en Isoleucine voor Laspertomycine) het best verdragen wordt.

Vervolgens werd de bijdrage van achirale residuen in laspartomycine onderzocht (**Hoofdstuk 3**). Zoals bekend bevatten alle CDA's het calciumbindende motief (Asp-X6-Asp-Gly8) bevatten, en met behulp

van de nieuw gerapporteerde synthesroute werd een reeks analogen bereid die het achirale amino-isoboterzuur (Aib) in de achirale 4, 6 en 8 posities van laspartomycine inbouwden. Al deze analogen vertoonden een zeer slechte activiteit in vergelijking met de octrooiverbinding; opname van Aib op positie 8 veroorzaakte een volledig verlies van activiteit. Een tweede reeks verbindingen waarin ofwel D ofwel L-alanine op posities 4 en 6 was opgenomen, werd bereid. De introductie van zowel D- als L-Ala op positie 4 leidde tot verbindingen die een vergelijkbare activiteit vertoonden als laspartomycine. Op positie 6 is de D-Ala-variant echter 16 keer actiever dan de L-Ala en vertoonde zelfs een iets betere activiteit dan laspartomycine C.

**Hoofdstuk 4** verlegt de focus naar Gram-negatieve bacteriën en focust op de nieuw gerapporteerde macrocyclische peptide antibiotica die zich richten op het buitenmembraaneiwit BamA. We ontwikkelden een handig strategie om, met behulp van een chemo-enzymatische benadering, het polymyxine nonapeptide gemakkelijk te ligeren aan het  $\beta$ -haarspeldpeptid. Deze antibiotica vertonen een krachtige activiteit tegen colistine-resistente mcr-positieve stammen van *E. coli*. Verder hebben we een reeks chimere peptiden bereid die werden geassembleerd met behulp van door koper gekatalyzeerde azide-alkynycycloaddities. De  $\beta$ -haarspeld-macrocyclus die een propargyl-glycine bevatte, werd zonder problemen volledig bereid op een vaste drager en netjes geconjugeerd aan de verschillende azidebevattende PMEN-eenheden. De resulterende triazolgekoppelde bicyclische peptiden vertoonden een reeks antibacteriële activiteiten, waarbij het azido-glycine-gekoppelde conjugaat de meest krachtige activiteit liet zien. Interessant is dat conjugaten die ofwel langere of kortere linkers bevatten tussen de  $\beta$ -haarspeld-macrocyclus en de PMEN-groep significant minder actief waren. Deze bevindingen wijzen op het belang van het identificeren van de optimale linkereigenschappen om krachtige antibacteriële activiteit te bereiken. Er wordt nog steeds gewerkt aan het evalueren van het potentieel van deze opwindende nieuwe klasse van anti-Gram-negatieve middelen.

**Hoofdstuk 5** richt zich op de substraatherkennungsspecificiteit van het bacteriële arginine-rhamnosyltransferase EarP. Het enzym is verantwoordelijk voor de glycosylering van arginine, die buitengewoon snel is. EF-P-rhamnosylering is cruciaal voor bacteriële conditie en leidde bij weglating in *Pseudomonas aeruginosa* tot meerdere nadelige effecten,

waaronder een grotere gevoeligheid voor antibiotica. In dit hoofdstuk werd een reeks korte peptide-nabootsers gemaakt die een secundaire  $\beta$ -haarspeldstructuur bevatten. Het bleek dat deze secundaire structurele eenheid een cruciale rol speelt bij de herkenning. Door screening van verschillende secundaire structuurstabiliserende sjablonen en verschillende peptidelengtes, werd het kleinste EF-P-fragment tot nu toe geïdentificeerd, te weten, een cyclisch 11-meer peptide is. Verschillende mutanten van dit peptide werden getest om de gemengdheid van EarP te screenen en dit toonde dat EarP een grotere tolerantie had voor variatie in aminozuursequenties dan de afwezigheid van secundaire structuurelementen. Dit is vooral belangrijk voor het rationele ontwerp van remmers en voor het ontwikkelen van hulpmiddelen voor de identificatie van andere bacteriële arginine-rhamnosyleringssystemen.



## Popular English summary

Bacteria have been on Earth billions of years before humans and will probably be on Earth billions of years after humans. They have found ways to survive in almost any environment. It has recently been reported that there are about 10 times as many bacterial cells in the human body as there are human cells. While the overwhelming majority of bacteria don't cause any harm, there are a few pathogenic bacteria that can absolutely wreak havoc upon us. To help fight against these bacteria we have relied on the use of antibiotics for decades. Unfortunately, these bacteria have developed creative ways to become resistant to these antibiotics. Right now, there isn't a single antibiotic we have left that bacteria haven't developed resistance against. Furthermore, new antibiotics that are developed target already existing pathways and the latest "new" antibiotic to enter the market that had a new mode of action was Daptomycin which was introduced nearly 20 years ago in 2003.

The projects described in thesis focus on new, unexploited targets within bacteria while investigating their working mechanism of action. For example, in one project, it was elucidated with high-resolution crystal structures, that friulimicin/amphomycin pack differently than laspartomycin in a crystal lattice. These antibiotics belong to the unique class known as the calcium-dependent antibiotics (CDAs) and target C<sub>55</sub>-P, which is one the last unexploited targets on the bacteria membrane. In another project a various amino acids substitution on Laspartomycin were made to study structure-activity relationship and the overall impact this had on antibacterial activity.

With these findings our results provide new insights into the mechanisms of action associated with the C<sub>55</sub>-P-targeting subfamily of CDAs and expand our current understanding of this promising class of lipopeptide antibiotics.

## Popular Dutch summary

Bacteriën waren al miljarden jaren op aarde vóór de mens verscheen en zullen waarschijnlijk miljarden jaren na de mens op aarde zijn. Ze hebben creatieve manieren gevonden om in bijna elke omgeving te overleven. Onlangs is bekend gemaakt dat er ongeveer 10 keer zoveel bacteriële cellen als menselijke cellen in het menselijk lichaam aanwezig zijn. Hoewel de overgrote meerderheid van bacteriën onschadelijk is, zijn er een paar pathogene bacteriën die grote schade bij de mens aan kunnen richten. Om deze bacteriën te helpen bestrijden, vertrouwen we al tientallen jaren op het gebruik van antibiotica. Helaas hebben deze bacteriën creatieve manieren ontwikkeld om resistent te worden tegen deze antibiotica. Op dit moment is er geen enkel antibioticum meer waar bacteriën geen resistentie tegen hebben ontwikkeld. Bovendien richten nieuwe antibiotica die worden ontwikkeld zich op reeds bestaande routes en het laatste "nieuwe" antibioticum met een nieuw werkingsmechanisme dat op de markt kwam was daptomycine, dat bijna 20 jaar geleden in 2003 werd geïntroduceerd.

De projecten die in dit proefschrift worden beschreven, richten zich op nieuwe, onbenutte doelwitten in bacteriën terwijl ze hun werkingsmechanisme onderzoeken.

Bij één project werd bijvoorbeeld met behulp van kristalstructuren met een hoge resolutie duidelijk gemaakt dat friulimicine en amfomycine zich anders rangschikken dan laspartomycine in een kristalrooster. Deze antibiotica behoren tot de unieke klasse die bekend staat als de calciumafhankelijke antibiotica (CDA's) en doelwit C<sub>55</sub>-P, een van de laatste onbekende doelwitten op het bacteriemembraan. Bij een ander project werden verschillende aminozuursubstituties op laspartomycine gemaakt om de structuur-activiteitsrelatie en de algehele impact die dit had op de antibacteriële activiteit te bestuderen.

Met deze bevindingen bieden onze resultaten nieuwe inzichten in de werkingsmechanismen geassocieerd met de C<sub>55</sub>-P-targeting subfamilie van CDA's en breiden ze ons huidige begrip van deze veelbelovende klasse van lipopeptide-antibiotica uit.

## List of publications (\* denotes shared authorship)

1. Kotsogianni, I.; **Wood, T.M.**; Alexander, F.M.; Cochrane, S.A.; Martin, N.I. Binding Studies Reveal Phospholipid and Its Role in the Calcium-Dependent Mechanism of Action of Daptomycin. *ACS Infect. Dis.* 2021, 7, 9, 2612-2619
2. **Wood, T.M.\***; Slingerland, C.J.\*; Martin, N.I. A Convenient Chemoenzymatic Preparation of Chimeric Macrocyclic Peptide Antibiotics with Potent Activity against Gram-Negative Pathogens. *J. Med. Chem.* 2021, 64, 15, 10890-10899
3. Wesseling, C.M.J.\*; **Wood, T.M.\***; Martin, N.I. Crossing the barrier: Gram-positive antibiotics kill Gram-negative pathogens by repurposing of anti-inflammatory peptides as potent synergists. *Molecules.* 2021, 26, 1954
4. Cioce, A.; Bineva-Todd, G.; Agbay, A.J.; Choi, J.; **Wood, T.M.**; Debets, M.F.; Browne, W.M.; Douglas, H.L.; Roustan, C.; Tastan, O.Y.; Kjaer, S.; Bush, J.T.; Bertozzi, C.R.; Schumann, B. Optimization of Metabolic Oligosaccharide Engineering with Ac4GalNalk and Ac4GlcNalk by Engineered Pyrophosphorylase. *ACS Chem. Biol.* 2021, 16, 10, 1961-1967
5. Yakovlieva, L.\*; **Wood, T.M.\***; Kemmink, J.; Kotsogianni Teftsoglou, A.I.; Krafczyk, R.; Lassak, J.; Martin, N.I.; Walvoort, M.T.C. A  $\beta$ -hairpin epitope as structural requirement for the recognition of bacterial protein arginine rhmnosylation in *Pseudomonas aeruginosa*. *Chem. Sci.* 2021, 12, 1560-1567
6. Diehl, A.; **Wood, T.M.**; Gebhard, S.; Martin, N.I.; Fritz, G. The Cell Envelope Stress Response of *Bacillus subtilis* towards Laspartomycin C. *Antibiotics*, 2020, 9(11), 729
7. **Wood, T.M.**; Bertheussen, K.; Martin, N.I. The contribution of achiral residues in the laspartomycin family of calcium-dependent lipopeptide antibiotics. *Org. Biomol. Chem.* 2020, 18, 514
8. **Wood, T.M.**; Martin, N.I. The calcium-dependent lipopeptide antibiotics: structure, mechanism, & medicinal chemistry. *Med. Chem. Commun.*, 2019, 10, 634
9. Kleijn, L.H.J.; Vlieg, H.C.; **Wood, T.M.**; Sastre, T.J.; Janssen, B.J.C.; Martin, N.I. A High-Resolution Crystal Structure that Reveals Molecular Details of

Target Recognition by the Calcium-Dependent Lipopeptide Antibiotic Laspartomycin C. *Angew. Chem. Int. Ed.* 2017, 56, 16546-16549

10. 't Hart, P.; **Wood, T.M.**; van Harten, R.; Kleijn, L.H.J.; Hendrickx, A.P.A.; Willems, R.J.L.; Breukink, E.J.; Martin, N.I. De novo identification of lipid II binding lipopeptides with antibacterial activity against vancomycin-resistant bacteria. *Chem. Sci.* 2017, 8, 7991-7997

11. Koopmans, T.; **Wood, T.M.**; 't Hart, P.; Kleijn, L.H.J.; A.P.A.; Willems, R.J.L.; Breukink, E.J.; Martin, N.I. Semisynthetic lipopeptides derived from nisin display antibacterial activity and lipid II-binding on par with that of the parent compound. *J. Am. Chem. Soc.* 2015, 137, 9382-9389

2016 PCT application number PCT/EP2016/050827; Title: Nisin-based compounds and use thereof in the treatment of bacterial infections; Inventors: Martin, N.I.; Koopmans T.; **Wood, T.M.**; Kleijn, L.H.J. Priority date: January 19, 2015.

## **Manuscripts submitted and in preparation**

1. **\*Wood, T.M.**; \*Zeronian, M.R.; Hanieh, Abedian, H.K.; Johnson, A.V.; Kemmink, J.; Hamoen, L.W.; Janssen, B.J.C.; Martin, N.I. New mechanistic insights into the C<sub>55</sub>-P binding family of CDAs provided by structure-activity studies and high-resolution crystal structures.

## *Curriculum vitae*

Thomas Melvin Wood was born in Ogden, Utah, United States of America on the 12<sup>th</sup> of November 1992. He obtained his Bachelor degree in the College of Pharmaceutical Sciences from the Utrecht University in 2014. During the same year he started his Master studies in the Drug Innovation program, also at Utrecht University. During his Master studies he performed a 12-month research project in the group of Prof. N. I. Martin focusing on the design of cyclic peptides to treat bacterial infections. Subsequently, he joined the group of Prof. C. R. Bertozzi at Stanford University for eight months where he worked on metabolic oligosaccharide engineering.

Thomas graduated his Masters with *cum laude* distinction in 2016 and obtained his own funding from the NWO Future Medicines start his PhD research. His work in the Martin group started September 2016 and his primary research focus was development and improvement of Laspartomycin C, a novel antibiotic that belongs to the class of calcium-dependent antibiotics (CDAs). Alongside his main projects, he used solid-phase peptide synthesis (SPPS) to generate a variety of (cyclic) peptides for several other collaborative projects.

During his PhD studies Thomas presented his research in a variety of poster and oral presentations. Poster presentations were delivered at the 101<sup>st</sup> Canadian Chemistry Conference and Exhibition (2018), and the annual Dutch chemistry conference CHAINS (2018). Three research projects were presented during talks at the University of Groningen (visiting researcher), Institute of Biology Leiden (IBL) symposium day (2018) and a conference talk at CHAINS (2019).

As of September 2021, the author of this thesis is employed as a postdoctoral associate in the group of Prof. Bradley Pentelute, in the Department of Chemistry at the Massachusetts Institute of Technology (MIT).

## Acknowledgements

I had some of the best times of my life as a PhD student and it is time to thank all the people without whom this journey would not have been possible or nearly as fun.

First and foremost, Nathaniel – I could not have picked a better supervisor if I tried. I first started working in your group as a Bachelor student in the summer of 2013 and I like to think I have come a long way since then. I learned so much from you and while the research wasn't always easy you were always there to point me in the right direction. Whether we were discussing science or watching hockey I always enjoyed my time with you. I am honored to now be an alumnus and I am proud, not only to call you my supervisor, but a friend as well.

Roland Pieters, thank you for your support and guidance during my time in the group and for being my other main promotor. Many thanks other professors from the UIPS CBDD department as well. Ed, Dirk, John, Tom and Seino you have all been great. I appreciate all the advice and feedback over the years from you all.

A big thanks to the members of the reading committee for your time and effort.

To Timo, Peter, and Laurens – thank you guys for being phenomenal mentors to me over the years. You guys welcomed me into the group way back when and taught me most of the lab skills I know today. Best of luck wherever you guys are.

To Hanieh, Aiden, Kristine and Marcel – thank you for the experimental efforts and for providing a great mentoring experience.

To my many other friends in the CBDD department, namely Ingrid, Yvette, Hanna, and Enrico. It has always been a blast talking, getting frikandelbroodje lunch, going to 90s disco parties, celebrating New Year's, or playing hide and seek with you guys! I hope we can see each other in the future.

To many collaborators without whom I wouldn't know half the things I know now. First off, a big thanks to Prof. Marthe Walvoort for chatting with Nathaniel during CHAINS and getting us to join you and Liubov for the

EarP project. I am honored to be a part of Chapter 5 and it has truly been life changing! To Johan Kemmink, a true master of NMR thank you for teaching me the ways of 2D NMR assignment. To Prof. Bert Janssen and Matthieu Zeronian for working with us on the Laspartomycin work. Your crystal structures are beautiful, and your input has been phenomenal. Chapter 2 is what my PhD research was all about, and it is made even better with your help!

To the other members of the Martin group, you are all special! Paolo, talking with you has always been a pleasure and you really help keep the group running smoothly. You take care of the small (and big) tasks so that we can focus on research. That is very much appreciated, and Nathaniel should honestly give you a raise. Matthijs, your dry humor and dead-pan response to different situations is top tier, never change. Kamal, your expertise, and knowledge in the biolab was super useful and always helpful, best of luck to you in Germany. Yongzhi, the true organic chemist of the group, best of luck to you and your family back home! Charlotte (Charly, Charly, Charly), you have always been so kind and sharing, especially when you give me the Ace of hearts to shoot the moon! I will definitely miss playing hearts with you! Emma, you were a good housemate and fume-hood neighbor, best of luck in the future. Jaco, thank you so much for teaming up with me and making Chapter 4 a success. I'm glad we pushed to get our paper in *J. Med. Chem.* even if it was a harrowing experience! Big Ray! Boi, you are so fengkaung I don't even know what to say. Not only were you my lab buddy but also my gym buddy. We had many great moments in the lab, making peptides, playing hearts, and learning a lot from each other. Never lose your fun-loving personality, you are amazing! Karol, the other lab DJ who knows the sickest tunes to bump during late night peptide synthesis, all the best to you and your young family. Ioli, the real ITC fairy, thank you for joining the project and helping make chapter 5 a success. Hopefully we can share a bag of honey roasted peanuts in the future! Nicola, you were a phenomenal addition to the team, your humor, subway sandwiches and Irn Bru always came in clutch. Ned, it has been a pleasure teaching you the ways of SPPS, I know you'll do great. Thank you for helping last minute with chapter 2, hopefully it gets published soon! Nora, your biological expertise is a great addition to the team, best of luck during your PhD.

Koen and André, my two best friends, you are my paranympths for a reason. You guys have been there for it all. From our gum chewing, oregano cooking, late night gaming days in high school to now we have come a long way. No matter if we are watching the sun rise in Crete drinking a brewski, road tripping through the States, dealing with massive mosquitoes in Sweden or getting locked out of someone's winter house in Zurich, we always have a blast. I can't wait to see where we meet up next. Every once in a while, I think to myself "I don't deserve friends like you" but I just laugh it off because I know we are more than friends, we are brothers.

Minu, you have been my number one supporter since day one, your love and support are more than I could have ever asked for. You helped build the foundation that I stand upon and I don't think I could ever put into words how grateful I am for that. You are the best and I love you.

To Liubov: My life has been so much brighter since you entered it. You truly are amazing, and I appreciate everything you do for me. I can't wait to see what Boston has in store for us! Ya tebe kohayu KH:]